THE UNIVERSITY OF CHICAGO

SENSORIMOTOR CIRCUITS FOR THE CONTROL OF THE FLEXIBLE OCTOPUS ARM

A DISSERTATION SUBMITTED TO

THE FACULTY OF THE DIVISION OF THE BIOLOGICAL SCIENCES

AND THE PRITZKER SCHOOL OF MEDICINE

IN CANDIDACY FOR THE DEGREE OF

DOCTOR OF PHILOSOPHY

COMMITTEE ON COMPUTATIONAL NEUROSCIENCE

BY

CASSADY SUZANNE OLSON

CHICAGO, ILLINOIS

AUGUST 2025

TABLE OF CONTENTS

LIST OF FIGURES

CHAPTER 1

CHAPTER 2

CHAPTER 3

CHAPTER 4

CHAPTER 5

APPENDIX

LIST OF TABLES

ACKNOWLEDGEMENTS

I would first like to thank my advisor, Cliff Ragsdale, for his mentorship throughout my PhD. Thank you for taking a chance on a student who didn't know what an in situ was before stepping foot in your lab and thank you for supporting me as I explored many routes of inquiry into my project. I am especially grateful for your broad knowledge base that has led to many interesting conversations, from the arrangement of chromatin in the nucleus to how different brain areas may function.

Thank you to members of the Ragsdale lab, past and present. My thanks especially goes to Grace Schulz, who was instrumental in teaching me the techniques of the lab and co-managing the lab, and to Aashna Moorjani, whose assistance greatly extended the scope of work I was able to. I was also fortunate to have Jan Kasal, Amelia Cheng, Ellie Khalil-Felbinger, Thea Applebaum-Litch, Caroline Miller and Sofia Collins help me with everything from my tracer studies to imaging and image analysis.

Thank you to the members of my committee: Jason MacLean, Ellie Heckscher, Matthew Kaufman, and Peter Littlewood. Thank you all for the support and encouragement. My thanks especially goes to Peter Littlewood. Thank you for advice and support as I approached modeling the octopus arm. That experience greatly informed the way I think about the octopus motor control problem. I also benefited considerably from the UChicago Imaging Core. I am grateful to Christine Labno, Khalil Rodriguez and Vytas Bindokas for their advice and assistance with imaging.

I would like to thank my parents, Larry and Anna Olson, who encouraged my curiosity for weird critters, and my brother Lucas, the other Dr. Olson, for the advice and support through my PhD.

I am greatly indebted to my grad school support network who got me through my PhD. Special thanks goes to Ben and Charlotte, for the weekly Wednesday night hangs, to Hannah, for the science conversations and fun travel adventures, to James and Sasha, for the silly shenanigans, and to Ross, whose support got me over the finish line. I am also thankful to friends outside of grad school: Marisa, Jeff, Lydia, Reva, Emmy and Louise: you may not have fully understood the research I was doing with the octopuses, but you were always my biggest cheerleaders.

ABSTRACT

Octopuses have the extraordinary ability to control eight prehensile arms with hundreds of suckers. With these highly flexible limbs, they engage in a wide variety of tasks including hunting, grooming, and exploring their environment. While the neural circuitry generating these movements engages every division of the octopus nervous system, much of the control circuitry is found within the arms themselves. The axial nerve cords (ANC), which lie in the center of every arm, are the largest neuronal structures in the octopus, containing four times as many neurons as are found in the central brain. There are also five peripheral nerve centers in the arm: a sucker ganglion in the stalk of every sucker and four intramuscular nerve cords. In this thesis, I explored the structure of the extensive nervous system in the arm of the octopus, focusing on the cellular and molecular composition of the ANCs and sucker ganglia.

I first studied the neuronal organization of the adult axial nerve cord (ANC) of *Octopus bimaculoides*. In transverse cross section, the cell body layer (CBL) of the ANC wraps around its neuropil (NP) with little apparent segregation of sensory and motor neurons or nerve exits. Strikingly, when studied in longitudinal sections, the ANC is segmented. ANC neuronal cell bodies form columns separated by septa, with 15 segments overlying each pair of suckers. The segments underlie a modular organization to the ANC neuropil: neuronal cell bodies within each segment send the bulk of their processes directly into the adjoining neuropil, with some reaching the contralateral side. Cellular analysis establishes that adjoining septa issue nerves with distinct fiber trajectories, which across two segments (or three septa) fully innervate the arm musculature. Sucker nerves also use the septa, setting up a nerve fiber “suckerotopy” in the sucker-side of the ANC. The ANC also contains many longitudinal fiber tracts, well suited for intermediate and long-distance communication. The neural modules described here provide a

new template for understanding the motor control of octopus soft tissues. The segments in the CBL supply the structure for local sensorimotor control, and the longitudinal tracts provide the pathways for coordinating motor acts between suckers and along the arm.

Comparative analysis suggests that arm nervous system structure varies based on appendage morphology, environmental context and behavioral needs. Examination of the axial nerve cord in the arms of the pelagic squid *Doryteuthis pealeii* reveals a reduced complexity, with fewer number of segments and an expansion of longitudinal tracts, compared to *O. bimaculoides*, a benthic animal. Additionally, the ANC in the sucker-poor tentacle stalk in *D. pealeii* is unsegmented, suggesting a strong link between segmentation and suckers.

I next examined the cellular organization and molecular composition of the sucker ganglion in *O. bimaculoides*. The sucker ganglion has an ellipsoid shape and features an unusual organization: the neuropil of the ganglion is distributed as a cap aborally (away from the sucker) and a small pocket orally (towards the sucker), with neuronal cell bodies concentrated in the space between. Using in situ hybridization, we detected positive expression of sensory (*PIEZO*) and motor (*LHX3* and *MNX*) neuron markers in the sucker ganglion cell bodies. Nerve fibers spread out from the sucker ganglion, targeting the surrounding sucker musculature and the oral roots extending to the ANC. These results indicate that the sucker ganglion is composed of both sensory and motor elements and suggest that this ganglion is not a simple relay for the ANC but facilitates local reflexes for each sucker.

CHAPTER 1

Towards an understanding of octopus arm motor control[1]

INTRODUCTION

The motor system enables animals to interact with their environment. How the motor system does this is constrained. The system must reflect the properties of the moving parts which are composed of biological materials. There should be coordination among muscle groups, and in the case of multiple limbs, across limbs. The incorporation of sensory information, including feedback, is necessary for goal-directed actions and behavioral success. The motor system should be well-suited to its environment to improve the chances of survival and reproduction. Finally, the ability to learn new skills and adapt is critical. The nervous system has provided solutions for the motor control problem in many creatures for very different behavioral tasks, body plans and environmental contexts. Current research in the motor field is dominated by vertebrate model systems. In taking a comparative perspective to motor control, however, we would likely find emergent properties or even striking differences that provide deep insight to neural motor control beyond what can be gained through vertebrate models alone. We cannot, for example, now say whether having a skeletal system with defined joints, such as those found in arthropods and vertebrates, makes the motor control problem more or less complex. Thus, it is informative to examine how the motor system must change if there is no rigid skeletal support system.

Octopuses are fascinating creatures with the ability to control and coordinate eight extremely flexible arms, each with hundreds of suckers. They have an incredibly rich behavioral repertoire (Hanlon and Messenger, 2018). They can perform the essential task of prey capture,

[1] Modified from doi.org/10.1093/icb/icad069 published in Integrative Comparative Biology. Referred to as Olson and Ragsdale (2023) in other chapters.

which involves reaching and grasping with a single arm, or the coordinate action of multiple arms, or an all-eight-arm pounce (Gutfreund et al., 1996; Bidel et al., 2022). Each of these methods also engages the suckers, which can, in turn, move independently. Octopuses can walk, swim and hunt in rough terrains. They can build shelters and groom themselves. They can even learn novel tasks, such as unscrewing a jar to obtain a crab. This behavioral repertoire provides a fruitful landscape for the study of motor control. How are they able to walk with flexible arms? How are they able to coordinate all eight arms? How are they able to command a single arm to move in isolation? How are they able to control each sucker? How are they able to learn to use their arms in new tasks?

The octopus relies on its central nervous system to drive this extensive behavioral output. There is a large brain located between the eyes, comprising two optic lobes and a central brain, along with an axial nerve cord (ANC), equivalent to a spinal cord, running down the center of each arm. This nervous system is massive. In *Octopus vulgaris,* the central brain, which wraps around the esophagus, contains 40 million neurons, and the flanking optic lobes contain 130 million neurons, nearly twice as many reported in the mouse brain (Young, 1963, 1971; Herculano-Houzel et al., 2006). In addition, the ANCs collectively contain 350 million neurons (Young, 1963, 1971). Accordingly, we will consider the current state of octopus arm motor control at the level of arm muscles, arm nervous system, and the central brain. Particular emphasis will be given to open questions and challenges.

Arm muscles

In its most basic form, the motor system controls muscle fiber length-tension relationships. For octopus arm motor control, we must account for what the nervous system is trying to control, that is, the arm itself. Indeed, to understand any final control signals, we need

to consider the properties of the muscles. Especially with a limb that can be moved in near infinite degrees of freedom (Kennedy et al., 2020), natural modes of movement could arise from the overall structure of the arm and the biophysical properties of the muscles. Some of these constraints may simplify the control problem.

Each arm is a muscular hydrostat, composed of only muscles, connective tissue, skin, and internal neural tissue. There is no rigid skeleton. The muscles, therefore, provide both structural support and mediate arm movements (Kier and Stella, 2007; Kier, 2016; see also Appendix). Arm movement arises from the brachial musculature, which surrounds the ANC and comprises four muscle groups. In the transverse plane, which is perpendicular to the long axis of the arm, one can readily distinguish these groups (Fig. 1.1a). The longitudinal muscles run the length of the arm and are thought to be involved in shortening the arm (Graziadei, 1971; Kier and Stella, 2007; Kier, 2016). The transverse muscles are oriented perpendicular to the longitudinal muscles and extend anchoring trabeculae to the edges of the arm. Transverse muscle contraction could elongate the arm. A selective combination of longitudinal muscle and transverse muscle activation is thought to cause bending (Graziadei, 1971; Kier and Stella, 2007; Kier, 2016). There are three bilateral sets of oblique muscles: the outer, middle, and inner obliques. These muscles form sheets tilting away from the longitudinal axis. The handedness of the outer oblique is the same as the inner oblique, but opposite that of the middle oblique. With this arrangement, the obliques are likely to mediate torsion of the arm, though they may also help elongate and shorten the arm (Graziadei, 1971; Kier and Stella, 2007; Kier, 2016). The last muscle group of the arm is the circular musculature. This thin sheet surrounds the other muscle groups and is challenging to discern in transverse section. By their location on the outside of the arm, the circular muscles could constrain movement and may have a role in posture (Kier and Stella,

2007; Kier, 2012). Connective tissue also plays a fundamental role in supporting the arm (Kier, 2012; Clemente et al., 2021); at the least, in the absence of a rigid skeleton, it provides insertion sites for the muscle. Studies indicate that connective tissue wraps around the outside of the arm musculature and surrounds the ANC in the center of the arm (Kier & Stella, 2007).

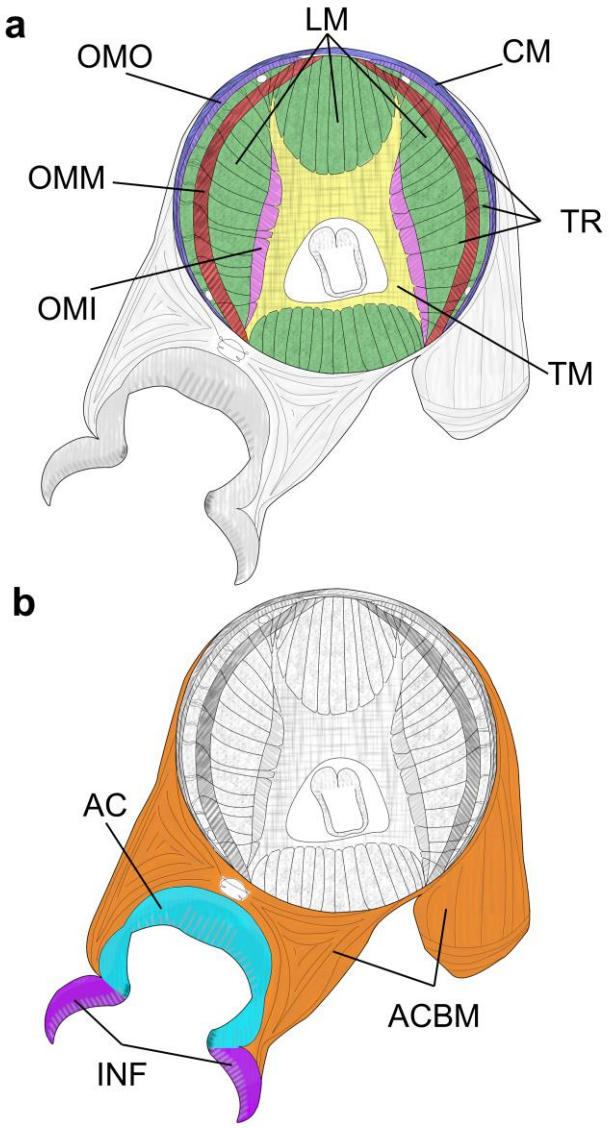

Figure 1.1: Muscles of the arm.
a, Brachial Musculature. LM (green), longitudinal muscles. TM (yellow), transverse muscles. TR, trabeculae. OMO (purple), outer oblique muscle. OMM (red), middle oblique muscle. OMI (pink), inner oblique muscle. CM (blue), circular muscles. **b,** The sucker and its musculature. ACBM (orange), acetabulobrachial muscles. AC (cyan), acetabulum. INF (magenta), infundibulum

Sucker movement arises from both the intrinsic sucker musculature and the acetabulo-brachial muscles (Fig. 1.1b). The sucker musculature, forming the acetabulum and the infundibulum, is responsible for the suction and grasping movements of a single sucker. The acetabulum and infundibulum are composed of a three-dimensional array of muscle fibers (Kier and Smith, 2002). Suction is achieved by thinning the wall of the acetabulum, a consequence of contracting the radial muscles. Engagement of muscles that act in opposition to radial muscles releases suction (meridional and circumferential muscles; Kier and Smith 2002). The acetabulo-brachial muscles enable sucker stalk movements. These muscles originate from the connective tissue surrounding the arm and insert into the acetabulum. Using the acetabulobrachial muscles, the sucker, like the arm itself, can orient in the full range of different directions (Kier and Smith, 2002).

The biophysical and molecular properties of cephalopod muscles are understudied (Appendix). Initial investigations demonstrated that the cells are electrically compact – meaning local input influences the voltage potential of the whole cell – and that their inputs are cholinergic (Matzner et al., 2000; Nesher et al., 2019). Investigations into passive and active contractile properties reveal differences between longitudinal and transverse muscles (Clemente et al., 2021; Zullo et al., 2022). Longitudinal muscles appear to have fast activation properties and may be suited to quick movements. Transverse muscles, on the other hand, exhibit slow activation and thus could help maintain posture (Zullo et al., 2022). Further work is needed to investigate these properties in the other muscle groups. Invertebrate muscles possess unique features when compared to vertebrate muscles. In squid, tentacles display a rapid elongation for prey capture, whereas the arms do not. This difference is not due to differences in myosin

isoforms, which are usually associated with differences in contractile properties, but rather in the ultrastructure of the muscle (Shaffer and Kier, 2016). The transverse muscles in squid tentacles are cross-striated, which allows for rapid elongation, while the transverse muscle mass in squid arm tissue is obliquely striated (Kier, 1985). Octopus transverse muscles are also obliquely striated (Shaffer and Kier, 2016). This indicates that the contractile properties of the transverse muscles may be akin to those of squid arms and therefore could not produce rapid elongation as seen with squid tentacles. Other unique features of invertebrate muscles include a catch mechanism, which enables prolonged muscle contraction without sustained neural activity. This mechanism is found in cuttlefish papillae and bivalve adductor muscles and is mediated by the protein twitchin (Shelud'ko et al., 2004; Gonzalez-Bellido et al., 2018). We do not know if octopus arm muscles have such a catch mechanism, and study of the molecular composition of octopus muscles may divulge many unique properties.

There exists limited experimental evidence for the coordinated activity of muscles, and current theories leave unresolved questions. For example, even though it is hypothesized that the transverse muscles are involved in elongating the arm, the obliques could also mediate elongation (Graziadei, 1971; Kier and Stella, 2007). More generally, do these muscle groups work independently or in concert? In squid arms and tentacles and in elephant trunks, there are two sets of obliques with opposite handedness, whereas octopus arms have three (Kier and Smith, 1985). In each of these cases, it is thought that the obliques facilitate torsion, but why do octopuses have three, with two of the same handedness? Current hypotheses of arm muscle function only describe movement at a single location, with a bend, twist or elongation of the arm able to occur at any point along the arm (Kennedy et al., 2020). By contrast, current descriptions of muscle activity down the length of the arms are limited to a single arm reach and retraction.

During reach, a wave of muscle activity propagates down the arm (Gutfreund et al., 1998), and during retraction, localized collisions of muscle activity create joint-like bends in the arm (Sumbre et al., 2006). While these descriptions capture single arm behavior, they do not provide a basis for generating hypotheses regarding how more complex movements arise. A theoretical framework that could be helpful is that of a long, highly elastic rod. This framework is used in models of octopus arms for application to soft robotics and, more interestingly, perturbations of these models have resulted in movements similar to those of an octopus arm (Chang et al., 2023).

The control system:

The extensive octopus nervous system harbors most of its neurons in the arms (Young, 1963, 1971). As a result, the nervous system is described as more distributed than that of vertebrates. There is, however, a clear hierarchical arrangement of the control system. For arm movements, lower motor control centers originate in the arm itself. Intermediate motor centers are found in the suboesophageal brain, and higher motor centers reside in the supraesophageal brain (Boycott, 1961; Young, 1971). We will explore each level in turn.

Arm nervous system

Much of the control circuitry of the arm appears to be in the arm. Amputated arms will move on their own, grasp and reject food, and stimulation of an amputated arm can give rise to behaviors seen in intact animals, such as a full arm reach or movement of a single sucker (Rowell, 1963; Sumbre et al., 2001). The arrangement of the arm nervous system has not been rigorously studied since the 1960s. From these studies, it is known that the ANC can be divided into two anatomically distinct territories (Altman, 1968; Graziadei, 1971). On the aboral side (the side opposite the suckers) sits the cerebrobrachial tract that interconnects the arms and the brain. On the oral side (the side of the suckers) exists a mass of neurons and their processes arranged

with the cell bodies on the outside and neuropil on the inside, which is characteristic of invertebrate medullary nerve cords (Richter et al., 2010). At the level of gross morphology, the ANC orients in turn to each sucker and, since most octopus suckers are arranged in two offset rows, the ANC snakes from side to side along the length of the arm (Graziadei, 1971). Beyond the ANC, five peripheral nerve centers sit in the arm (Fig. 1.2a). Situated in the acetabulo-brachial musculature is a sucker ganglion for every sucker. Whether this ganglion is a motor center, sensory center or both is contested (Graziadei, 1971; Olson et al., 2021; Rowell, 1963). Located in the four corners of the arm, between the outer and middle obliques, are four intramuscular nerve cords. These intramuscular nerve cords have been described to contain both sensory and motor information for the brachial musculature and may mediate local reflexes (Graziadei, 1965a, 1971).

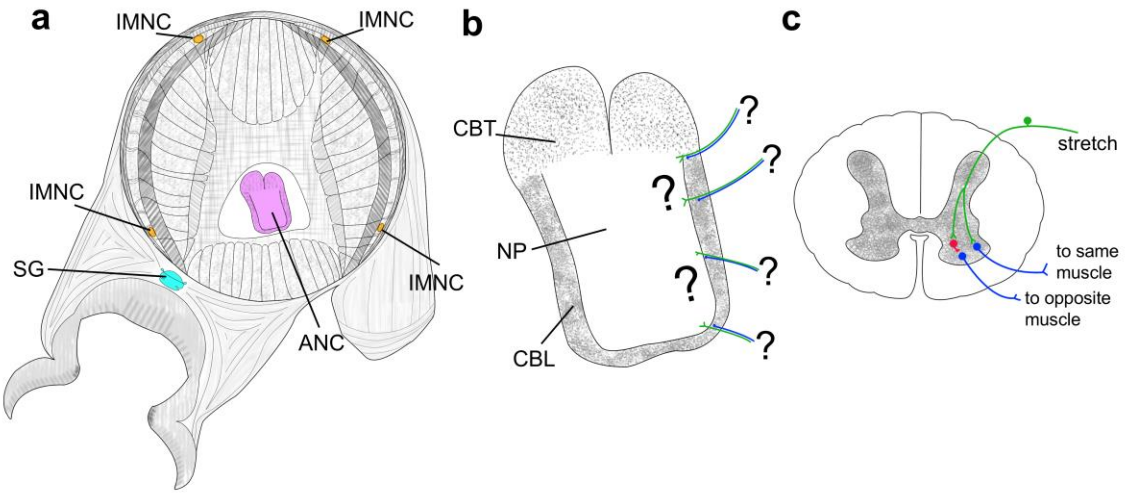

Figure 1.2: Arm Nervous System.
a, Central and peripheral components. ANC (pink), axial nerve cord. IMNC (orange), intramuscular nerve cord. SG (cyan), sucker ganglion **b,** The ANC. Where efferent nerve fibers (blue) travel and where afferent nerve fibers (green) originate, and how both are processed by the ANC, is not known (Indicated by question marks). CBT, cerebrobrachial tract. NP, neuropil. CBL, cell body layer. **c,** Vertebrate spinal cord. Example of the stretch reflex circuit. Afferent fibers (green) carrying stretch information enter the spinal cord from the dorsal side, excite

motor neurons (blue) contracting the agonist muscle and inhibit (red) motor neurons to the antagonist muscle.

Nerve fibers regularly exit the ANC to connect with the skin, suckers and brachial musculature, and the peripheral nerve centers (Fig. 1.2b; Altman 1968; Graziadei 1971; Gutfreund et al. 2006). The oral roots, which are reported to carry both sensory and motor information, connect to the sucker ganglion and sucker musculature. While the aboral roots are also reported to carry both sensory and motor information, how these nerves connect to the intramuscular nerve cords and brachial muscles is unknown (Gutfreund et al., 2006; Rowell, 1963). The location of motor neurons and how they pool into these nerves is also not known. While claims that each muscle group is innervated separately have been offered, limited experimental evidence supports this proposal (Altman, 1968; Graziadei, 1971; Nesher et al., 2019). Simply put, we do not know what the full set of neuromuscular units of the arm are.

An important feature of motor control is sensory feedback. Where and how proprioceptive feedback originates in the arm is unclear, and the extent to which octopuses rely on proprioceptive information for arm movements is debated (Gutnick et al., 2011, 2020; Bidel et al., 2022). Despite this, Graziadei (1965) reported the existence of muscle receptors located between the outer and middle oblique, with indications that these receptors feed into the intramuscular nerve cords. He also describes similar cells embedded into the acetabulobrachial musculature with projections towards the sucker ganglion. The existence of these cells, and their candidate proprioceptive nature, needs further study. Another source of sensory information are the suckers. Sensory receptors receiving chemo-tactile information line the epithelium of the sucker (Graziadei, 1962). This information is useful for determining if an object is food. Recent studies have uncovered the existence of chemoreceptors composed of atypical acetylcholine

receptors (Albertin et al., 2015; van Giesen et al., 2020). Additional study of the chemo-tactile properties of the octopus sucker apparatus could reveal other novelties in sensory transduction.

The ANC exhibits many similarities to a vertebrate spinal cord (Fig. 1.2b, c). In a broad sense, they have similar anatomical features: cell bodies, complex neuropil, fiber tracts relaying connections to and from the brain, and regularly exiting nerve fibers. There are also functional similarities. Like an amputated arm freely moving, animals can walk without input from the brain, relying solely on spinal cord circuits (Kriellaars et al., 1994; Whelan, 2003; Rossignol and Frigon, 2011). This comparison provides a framework to ask questions about the ANC: is there, as in the spinal cord, a loose somatotopic arrangement? Current experiments have shown that the nerve fibers are mixed (Gutfreund et al., 2006), so how is sensory and motor information parsed and integrated? Is there a functional equivalent of the stretch reflex? How are the muscles recruited? Are motor units enlisted incrementally from small to large, as proposed in Henneman's size principle? More broadly, study of how the ANC executes muscle activation and transforms sensory information can inform theories of how the spinal cord might work. Studying the octopus is advantageous as the ANC serves as an easily accessible spinal cord. In a single slice of arm, it is possible to capture the ANC, the full muscle structure, and the sensory afferents. One notable difference, however, is that although the muscles in the arm decrease in size down the length of the arm, their overall structure remain the same (Kier and Stella, 2007). This muscle organization implies a pattern of innervation by the ANC akin to the repeated innervation seen in the body segments of a drosophila larva or annelid worm (Clark et al., 2018). However, no current evidence of a segmental arrangement of muscles in the adult octopus arm exists. Research on the development of the arm musculature could reveal a segmental patterning of muscles that blurs by adulthood, thereby offering insight into patterns of innervation.

Intermediate and higher motor centers

While the arm houses a large portion of the neural real estate, the arm nervous system does not control movement in isolation (Fig. 1.3). The octopus possesses a large, complex brain with more than three dozen lobes and lobules (Young, 1971). The role that the brain plays in motor control has been investigated with Golgi anatomy, electrical stimulations, and lesion studies dating back to the middle of the last century (Wells, 1978). As the ANC ascends to the brain, it first branches into the interbrachial commissure. The interbrachial commissure is composed of two bundles of nerve fibers. The first connects each arm to its nearest neighbors, and the second forms a ring which connects the rest of the arms to each other (Graziadei, 1971). Recent evidence indicates that the oral intramuscular nerve cords also connect between arms (Kuuspalu et al., 2022). The kind of information which passes along the commissure and through the connecting intramuscular nerve cords is not known, though it has been suggested that it could be proprioceptive in nature (Kuuspalu et al., 2022). Beyond the interbrachial commissure, the ANC loses its cell body layer as it approaches the brain and coalesces into a nerve known as the brachial nerve. The brachial nerve enters the brachial lobe located in the anterior suboesophageal brain (Young, 1971). Along with the pedal lobe, the brachial lobe is considered an intermediate motor center for the control of the arms. It is thought that the brachial lobe exhibits afferent and efferent connections with the arm (Young, 1971). Stimulation of the brachial lobe can elicit contraction of multiple arms at once, and stimulation particularly near the site of brachial nerve entry can produce contraction of individual arms (Boycott, 1961; Young, 1971). Cells from the anterior pedal lobe send fibers to the brachial lobe and into the brachial nerves, and most of the connections appear to be efferent. The main sources of input to the anterior pedal lobe are from the basal lobes of the supraesophogeal brain and the lateral pedal lobe. The lateral pedal lobe in

turn accepts afferents from the brachial lobe as well as the basal lobes and the statocysts, which detect vestibular information (Young, 1971). While stimulation of the pedal lobe elicits movements of the arms, the lobe also subserves additional motor roles, such as controlling head, funnel and eye movements (Boycott, 1961). Further work is needed to sort out the roles of these intermediate motor centers in movement of the arms.

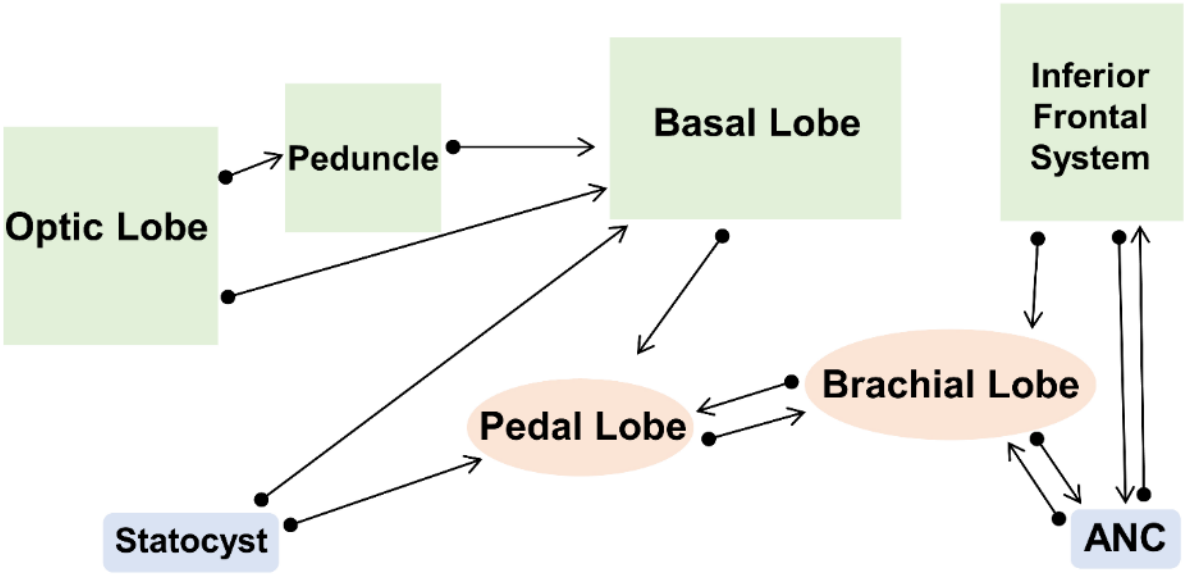

Figure 1.3. Motor pathways in the brain.
Simplified account of motor control pathways in the brain and arms of the octopus, emphasizing major connections and motor hierarchies. Modern evidence for some of these connections, for example, those between the pedal and brachial lobes, is not strong. ANC, axial nerve cord.

The higher motor centers are the basal lobes in the supraesophegeal brain. At this point in the motor hierarchy, stimulation will produce coordinated behaviors. In particular, electrical stimulation of the anterior basal lobe of an octopus produces effective walking movements of the arms, as well as eye and head movements (Young, 1971). If the frontal supraesophogeal brain is removed with the basal lobes still intact, animals can still walk. However, removing the basal lobes will induce the animal to lie in a heap before finally crawling with sucker movements

(Wells, 1959; Altman, 1968). Stimulation of other regions of the basal lobes will also produces changes in chromatophores, skin papillae, and respiration (Boycott, 1961; Young, 1971; Zullo et al., 2009).

The pedal lobes possess both contralateral and ipsilateral connectivity with the higher motor centers (Young, 1971). No other decussations have been reported deeper in the motor pathway, apart from the interbrachial commissure described above. Interestingly, split brained octopuses demonstrated no obvious impairments in behaviors (Muntz, 1961).

Feedforward visual input is vital for orchestrating complex, goal-directed movements. For the octopus, this information has been shown to influence arm choice: when reaching for an object, octopuses most often use the arm that falls in the line of sight between the eye and the object of interest (Byrne et al., 2006). Visual information passes through the optic lobe and then to the peduncle lobe. The anterior basal lobe receives input from both of these lobes, indicating the potential existence of at least two visuomotor pathways (Messenger, 1971). Stimulation of the peduncle can elicit locomotor movements of walking and swimming, and lesions of the peduncle lobe have effects on coordinated locomotive abilities (Messenger, 1967, 1971). Specifically, while a lesioned animal may be able to recognize prey, its locomotor control is compromised and profound deficits in posture arise (Messenger, 1967). However, animals deprived of vision can navigate normally, indicating that visual input is not essential for movement whereas peduncle input is (Messenger, 1967). These findings indicate that one system is critical for maintaining posture, whereas the other is used for visually guided behaviors. Thus, in many ways, the octopus brain contains a parcellation of motor system function not so foreign from that known in vertebrate systems.

The arms receive a plethora of sensory information, and it is expected that by the time that information reaches the brain, it is highly processed (Rowell, 1966). The inferior frontal system (IFS) of the supraesophegeal brain takes in sensory information from the suckers (Young, 1971). Only with an intact IFS can octopuses appropriately distinguish between a food and non-food object, and lesions to the IFS interfere with an octopus's ability to discriminate by touch (Altman, 1971). Additionally, lesions to the IFS render the octopus unable to reject objects, as the suckers become sticky (Wells, 1961). This indicates that the IFS provides some motor control over suckers, possibly of an inhibitory nature. It is not known how or where proprioceptive information is represented in the brain. Current views dictate that this information does not reach the brain (Rowell, 1966). However, given that an octopus can produce coordinated movements in the absence of visual information, proprioceptive input likely reaches the brain in some form.

Aims and results of the current work

Clearly, a modern neuroscience cellular and molecular approach to octopus motor control is needed. Here, by leveraging gene expression experiments, in vitro circuit tracing techniques, and analyses of nerve fiber morphology, I explore sensorimotor circuits in the extensive arm nervous system of *Octopus bimaculoides*. Particular focus is given to the organization of the axial nerve cord (ANC; Chapters 3 and 4) and the structure of the sucker ganglion (Chapter 5).

In Chapter 3, I detail our discovery of segmentation in the cell body layer of the ANC, which constitutes the first description of nervous system segmentation in a mollusc. These neuronal segments underlie a modular organization to the ANC neuropil: neuronal cell bodies within each segment send the bulk of their processes directly into the adjoining neuropil. The septa between each segment contains nerve exits, vasculature and abundant collagen. Nerves exiting from neighboring septa differ in their fiber trajectories indicating that multiple adjoining

segments must cooperate to innervate the arm musculature fully. The nerves for each sucker also exit through septa, radially tiling the sucker to create a spatial topographic map in the ANC. In the squid *Doryteuthis pealeii*, the ANCs in the arms and the sucker-rich club of the tentacles have segments, but the ANC in the sucker-poor stalk of the tentacles does not, suggesting a strong link between segmentation and flexible sucker-laden arms.

Many behaviors require the coordination of sucker and arm movements over a distance (Gutfreund et al., 1998; Sumbre et al., 2006; Kennedy et al., 2020; Bidel et al., 2022). In Chapter 4, I describe the organization of the longitudinal tracts in the ANC. The ANC cerebrobrachial tract (CBT), which interconnects the arms and brain, is located aboral to the cell body layer and neuropil. We found that the CBT can be subdivided into four main bundles: the α, δ, β, and γ tracts. Tract-tracing studies suggest that connections to the brachial musculature and sucker may travel in spatially distinct CBT tracts. We also detected longitudinal fiber tracts within the ANC neuropil. By their positioning and trajectories, these neuropil tracts seem well poised for orchestrating movements involving multiple suckers as well as motor acts coordinating the suckers and brachial musculature.

The octopus sucker is a profoundly complex sensorimotor structure. As shown in Chapter 3 and 4, large portions of the ANC are dedicated to the neural control of each sucker. There is also a sucker ganglion, a peripheral nervous element, situated in the stalk of every sucker. The structure and function of the sucker ganglion, especially in the context of the ANC, remains unclear. In Chapter 5, I report our examination of the cellular organization and molecular composition of the sucker ganglion in *Octopus bimaculoides*. The sucker ganglion features an unusual organization: the neuropil of the ganglion is distributed as a cap aborally (away from the sucker) and a small pocket orally (towards the sucker), with neuronal cell bodies concentrated in

the space between. With gene expression experiments, we determined that the sucker ganglion is composed of sensory and motor elements. Sucker ganglion nerves target the surrounding musculature and the oral roots extending to the ANC, providing pathways for local processing as well as connections to the central nervous system. Thus, the sucker ganglion is well situated for control of sucker reflexes and integrative sensorimotor processing.

On contributions from collaborators

The work presented in Chapter 3 was done in collaboration with Ms. Natalie Grace Schulz and Dr. Clifton W. Ragsdale and was published in Olson et al. (2025). The initial discovery of segmentation in the cell body layer of the ANC was made by Ms. Schulz and me. Ms. Schulz did the vascular injections and Picrosirius Red staining. All other work was done by me.

By my direction and under my supervision, Aashna Moorjani completed the ANC and cerebrobrachial tract measurements reported in Chapter 4. Ms. Moorjani also assisted with determining CBT subdivisions. All other work was done by me.

The work presented in Chapter 5 was done in collaboration with Ms. Moorjani and Dr. Ragsdale and was published in Olson et al. (2025a). Ms. Moorjani completed the sucker ganglion measurements and traced the sucker ganglion nerve fibers, with edits from me. All other work was done by me.

Contributions of other undergraduate research assistants and prior members in the lab are noted throughout the methods.

CHAPTER 2

Materials and methods

These cephalopod experiments were performed in compliance with the EU Directive 2010/63/EU guidelines on cephalopod use, the University of Chicago Animal Resources Center and the MBL and UChicago Institutional Animal Care and Use Committees (Fiorito et al., 2015; Lopes et al., 2017).

Animals

Wild caught adult *Octopus bimaculoides* (*Obi*) of both sexes and at least six months of age were purchased from Aquatic Research Consultants, a field-collection venture operated by Dr. Chuck Winkler, San Pedro, CA. Animals were individually housed in 20-gallon saltwater tanks equipped with a carbon particle filter, aquarium bubbler, and an UV light. Animals were fed daily with fiddler crabs, bivalves or frozen shrimp. The artificial seawater (ASW) was prepared in deionized water from pharmaceutically pure sea salt (33g/liter; Tropic Marin "classic", Wartenberg, Germany). Sex was recorded in sexually mature animals but not studied.

Adults were deeply anesthetized in 4% ethanol/ASW (EtOH/ASW, n = 17) and trans-orbitally perfused with 4% paraformaldehyde/phosphate-buffered saline solution (PFA/PBS, pH 7.4) delivered via a peristaltic pump (Cole Parmer Masterflex) through a 21½ gauge needle (Becton Dickinson). The left and right white bodies, a hematopoietic tissue, were targeted alternately and iteratively throughout the procedure. Arms were dissected and stored in 4% PFA/PBS overnight at 4°C. Specimens were then either cut into 2-4 cm pieces for immediate processing or stored in diethyl pyrocarbonate (DEPC) treated-PBS at 4°C.

Wild caught adult *Doryteuthis pealeii* (*Dpe,* n = 3) were obtained from the Marine Biological Laboratory, Woods Hole, MA. Animals were kept in circulating, filtered containment tanks for several days before being deeply anesthetized in 7.5% $MgCl_2$/ASW and dissected. Arm crowns were immersion fixed in 4% PFA/PBS. Arms and tentacles were dissected and cut into 2-4 cm pieces for further processing.

Tissue Processing

For sections, arm explants were incubated in 30% sucrose/4%PFA/PBS at 4°C for three to five days until saturated, rinsed with 30% sucrose/PBS, and infiltrated with 10% gelatin/30% sucrose/PBS for 1 hour at 50°C. Tissue was embedded in 10% gelatin/30% sucrose/PBS and post-fixed in 30% sucrose/4%PFA/PBS before storage in -80°C. Gelatin-embedded serial arm sections were cut at 28-50-µm thickness on a freezing microtome (Leica SM2000R) and collected in DEPC-PBS. Sections were mounted and dried on charged, hydrophilic glass slides (TruBond380, Newcomer Supply, Middleton, WI). Slides were stored at -80°C until further processing.

cDNA Synthesis and Cloning

Dissected octopus central brain tissue and arm tissue was flash-frozen on dry ice and stored at -80°C until RNA extraction. Tissue was homogenized with a micropestle and RNA was extracted with Trizol Reagent (Invitrogen) and phasemaker tubes (Invitrogen). RNA was stored at -80°C in RNase-free water (Sigma-Aldrich) until used for cDNA synthesis with SuperScript III 1st-strand cDNA kit (Invitrogen) following manufacturer instructions. cDNA was diluted in RNase-free water and stored at -20°C.

PCR primers were designed with MacVector software (version 12.6.0) or PrimerBlast from NCBI (Table 2.2). PCR reactions were conducted using the T100 thermocycler from BioRad. Reaction solutions were incubated at 95°C for 5 minutes before undergoing 35-40 rounds of amplification cycles: 95°C for 30 seconds, 52-57°C for 45 seconds, and 72°C for 1 minute. A final elongation step was performed at 72°C for 10 minutes. The sequence for *Dpe SYT1* was synthesized by Twist Bioscience (South San Francisco, CA; Table 2.3).

Sequences for *SYT1, VACHT, VIAAT, LHX3* and *NKX6* were previously cloned by Dr. Carrie Albertin and were available in the lab. Natalie Grace Schulz isolated *FMRF*, *PRM*, *PIEZO*, *TTN*, and *Dpe SYT1* cDNAs. Natalie Grace Schulz and I cloned *MYH*, *CPLX1*, and *MUNC18*. I cloned *DRGX*, *MNX*, *SLC5A7*, and *TPM.* Sequences for the neurotransmitter genes *GAD* and *CHAT* were cloned by Dr. Rahul Parnaik using degenerate PCR. The sequence for the *GAD* cDNA matches 18-364 of XM_014922646. That for the *CHAT* matches 1085-2063 of XM_014912671.

PCR products and Twist sequence were studied by gel electrophoresis to confirm that the sizes of products were as expected. PCR reactions were ligated into a pGEM T-Easy plasmid (Promega). Closed inserts were Sanger sequenced by the UChicago Comprehensive Cancer Center DNA Sequencing Facility. Plasmids were linearized by SacII (New England Biolabs, Cat#: 50812058) or SpeI (New England Biolabs, Cat#: 50811989) restriction enzyme digestion to generate antisense templates. Following phenol-chloroform extraction of the template, antisense digoxigenin (DIG)-labeled riboprobes (Sigma-Aldrich, Cat#: 11277073910) were transcribed with SP6 or T7 RNA polymerase (New England Biolabs). After transcription, residual template was digested with RNase-free DNase I (Sigma-Aldrich) at 37°C for 15

minutes. Riboprobes were ethanol-precipitated and stored in 100µl of DEPC-H_2O at -20°C until use.

In situ hybridization

Slides of sectioned tissue were equilibrated to room temperature and post-fixed in mailers for 15 minutes in 4% PFA/PBS, washed 3x 15 minutes in DEPC-PBS and incubated at 37°C for 15 minutes in proteinase K solution (Sigma-Aldrich; 1.45 µg proteinase K per milliliter of 100 mM Tris-HCl [pH 8.0], 50 mM EDTA [pH 8.0]). Slides were post-fixed for 15 minutes in 4% PFA/PBS, washed 3x 15 minutes in DEPC-PBS, and acclimated to 72°C for one hour in hybridization solution (50% formamide, 5x SSC, 1% SDS, 200 µg/ml heparin, 500 µg /ml yeast RNA). Slides were transferred to mailers with 1-2 mg antisense riboprobe in 15 mL hybridization solution and incubated overnight at 72°C. The next day, slides were treated 3x 45 minutes in preheated Solution X (50% formamide, 5x SSC, 1% SDS) at 72°C. Slides were washed 3x 15 minutes in room temperature TBST (Tris-buffered saline with 1% Tween 20) and blocked at room temperature for one hour in 10% DIG buffer (Roche) in TBST.

Anti-DIG Fab fragments conjugated to alkaline phosphatase (Sigma-Aldrich, Cat#: 11093274910; RRID: AB_514497) were preabsorbed with octopus embryo powder in 1% DIG buffer in TBST for at least one hour. Slides were then incubated on a rocker overnight at 4°C in preabsorbed antibody diluted to a final concentration of 1:5000 in 10% DIG buffer in TBST.

The next day, slides were rinsed once, washed 3x 15 minutes, then 2x 1 hour in TBST. Slides were washed for 10 minutes in freshly prepared NTMT (100 mM Tris-HCl [pH 9.5], 100 mM NaCl, 50 mM MgCl2, 1% Tween 20). For the color reaction, slides were incubated in nitro blue tetrazolium (NBT, 100mg/mL in 70% dimethyl formamide/30% DEPC-H20, Gold

Biotechnology, St. Louis, MO) and 5-bromo-4-chloro-3-indolyl phosphate (BCIP, 50mg/mL in 100% dimethyl formamide, Gold Biotechnology, St. Louis, MO) in NTMT. Color development proceeded at room temperature and was monitored for a maximum of 5 days. When reaction was complete, slides were washed in TBST overnight and dehydrated through a series of ethanol washes into Histoclear, and coverslipped with Eukitt (Sigma-Aldrich).

Hematoxylin and Eosin (H&E) Staining

Slides were incubated in DEPC-PBS for 4-6 hours at 72°C to melt off gelatin. Then, slides were rehydrated in room temperature deionized water, incubated in Mayer's Hematoxylin (ScyTek, Cat#: HMM500) for 1 minute, and rapidly rinsed in water to prevent overstaining. After a 15-second incubation in a bluing solution (ScyTek, Cat#: BRT500), slices were dehydrated in an ethanol series (70%, 95% and 100%) and placed in Eosin Y (ScyTek, Cat#: EYB500) for 1-minute. Slides were rinsed in 100% EtOH, cleared in Histoclear, and mounted with Eukitt.

Picrosirius Red

The presence of connective tissue was examined with Picrosirius Red (Abcam, Cat#: ab150681). De-gelatinized slides were rinsed 3 times with deionized water, then rehydrated for 1-minute in deionized water. Sections were incubated in Picrosirius Red solution for 5 minutes, de-stained with 2 quick rinses of acetic acid wash, dehydrated in 100% EtOH, and mounted with Eukitt.

Immunohistochemistry

Neuronal processes in octopus arm were labeled with mouse monoclonal antibody 6–11B-1 (1:500 dilution of ascites fluid; Sigma-Aldrich, Cat#: T6793; RRID: AB_477585) and mouse monoclonal antibody SMI-31 (1:500 dilution; BioLegend, Cat# 801601; RRID: AB_2564641). Clone 6–11B-1 was isolated following immunization with sea urchin sperm flagella protein preparations (Piperno and Fuller, 1985). It recognizes an acetylated α-tubulin (acTUBA) epitope found broadly but not universally across microtubules and has been extensively employed to identify axon tracts in vertebrate and invertebrate nervous systems (Chitnis and Kuwada, 1990; LeDizet and Piperno, 1991; Shigeno and Yamamoto, 2002; Baratte and Bonnaud, 2009). Clone SMI-31 reacts with a phosphorylated epitope of neurofilament in mammals and neurofilament 220 in squid (Sternberger and Sternberger, 1983; Grant et al., 1995; Grant and Pant, 2016) .The secondary Alexa Fluor® 488 AffiniPure Goat Anti-Mouse IgG (Cat#: 115-545-003; RRID: AB_2338840) and Cy™3 AffiniPure Donkey Anti-Mouse IgG (Cat#: 715-165-151; RRID: AB_2315777) were purchased from Jackson ImmunoResearch (West Grove, PA) and employed at 1:500 dilutions.

For section immunohistochemistry, slides were rinsed 3x 10 minutes (3 times for 10 minutes each) in DEPC-PBS containing 1% tween 20 (PBST) and incubated for 30 minutes in a proteinase K solution (Sigma-Aldrich, Cat#: 03115828001; 19.4 µg proteinase K per milliliter of PBST). Slides were post-fixed with 4% PFA, washed 3x 30 minutes in PBST, blocked in 10% goat serum/PBST (Fisher Scientific, Cat#: 16210072) for 1 hour and incubated in primary antibody diluted in 1% goat serum/PBST for four days at 4°C. After 3x 30 minutes PBST washes, sections were incubated for two days at 4°C with secondary antibody along with 0.01 mg/ml 4′-6-diamidino-2-phenylindole (DAPI; Sigma-Aldrich, Cat#: D9542) to label cell nuclei fluorescently and either 0.2 µl/ml phalloidin-iFluor 594 (Abcam, Cat#: ab176757) or

phalloidin-iFluor 488 (Abcam, Cat#: ab176753) to label filamentous actin (F-actin). Slides were rinsed and washed 3x 5 minutes with PBST and cover slipped with Fluoromount G (Southern Biotech, Birmingham, AL).

For whole mount immunohistochemistry, the following arm slice explants were prepared: dissected axial nerve cord, dissected sucker musculature, 0.5 cm – 1 cm transverse slices of arm, longitudinally bisected slices, and horizontally bisected slices. Explants were washed 3x15 minutes in PBST, dehydrated in a graded methanol series (25, 50, 75% in PBST, each for 10 minutes), rinsed twice in 100% methanol for 10 minutes, and stored overnight at -20°C. The next day, explants were rehydrated in a graded methanol series (75%, 50%, 25% in PBST, each for 5 minutes) and rinsed twice in PBST for 5 minutes. Then, tissue was incubated for 60 minutes at 37°C in a proteinase K solution (19.4 µg proteinase K per milliliter of PBST), post fixed for 15 minutes in 4% PFA/PBS, washed 3x 15 minutes and 1x 60 minutes in PBST, and blocked for an hour in 10% goat serum/PBST. Slices were then incubated in primary antibody for 7 days at 37°C. Following primary incubation, tissue was rinsed 1x, 3x 15 minutes, 5x 60 minutes and overnight in PBST. Tissue was transferred to secondary antibody for seven days at 4°C. Next, the tissue was rinsed with PBST 1x quickly, 3x 15 minutes, 2x 60 minutes, washed with DEPC-PBS 3x 15 minutes, and post fixed for four days at 4°C. Explants were then rinsed 3x 15 minutes in PBS and cleared in a modified version of FRUIT according to the protocol listed below (Hou et al., 2015). Slices were stored in 100% FRUIT at 4°C until imaged.

Tracing

Adult *O. bimaculoides* (n = 13) were anesthetized in 2% EtOH/ASW, and the distal portion of a single arm was amputated with a razor blade. The amputated arm was placed in

ASW, and the animal was either returned to a bucket of ASW to recover or euthanized in 4% EtOH/ASW and trans-orbitally perfused with 4% PFA/PBS. The amputated arm was cut with a razor blade by hand into 0.5 cm-1 cm transverse slices, with the goal of capturing a distance of 1-2 suckers. Slices were placed into 221 media with NuSerum (36% Leibovitz L15-media, 36% filtered seawater, 18% deionized water, 1% pen-strep, 10% NuSerum) prior to injection. Since the arm was actively moving, cutting by hand proved the most effective method to make reliably cut slices. Even in the smaller 2-sucker long slices, the arm still moved around. Large slices and slices cut along different planes were also employed, though larger slices were harder to inject, and hand-made cuts along different planes were less accurate.

Each slice (n = 83) was injected with CF® 488A Dye Dextran (Biotium, Cat#: 80110; 2% solution, 10kD) using a 25 or 32 gauge Hamilton Syringe (Hamilton, model#: 7000.5), rinsed in filtered seawater, and incubated at room temperature in 221 media with NuSerum. After three hours, the slices were rinsed with filtered ASW and fixed in 4% PFA/PBS. Slices were prepared for gelatin embedding and sectioning as described above, sectioned at 50µm, and counterstained with phalloidin-iFluor 594 (0.2 µl/ml in 1%PBST) and DAPI (0.01 mg/ml in 1% PBST) before imaging. Since dextrans can fill blood vessels and muscle, the counterstain provided markers of other tissue types to determine whether the dextrans were placed in neural tissue. The counterstain also highlighted the general geography of the arm, which was helpful at localizing the tracer injection site (Fig. 2.1a-c).

Using this slice culture preparation, other neural tracers were tested (Fig. 2.1d-g). CF® 488A Dye cholera toxin subunit B (Biotium, Cat#00070; 0.5 µg/µl) and CF® 488A Dye wheat germ agglutinin (Biotium, Cat#29022-1; 0.1mg/µl) demonstrated labeling of processes over muscle, with cholera toxin subunit B labeling a smaller subset of fibers compared to both wheat

germ agglutinin and dextrans (Fig. 2.1d, e). CF® 488A Dye Biotin and Fluoro-Gold (hydroxystilbamidine, Biotium, Cat#80014; 50mg/mL) both demonstrated punctate labeling in the cell body layer of the axial nerve cord (Fig. 2.1f, g). Out of all of these tracers, dextrans was chosen for its reliable and intricate labeling of neuronal cell bodies, small processes in the neuropil, and the larger nerve fibers. Based on observations from many injections with dextrans, it is most likely both an anterograde and retrograde tracer in octopus as it is in other systems. More work is needed to determine whether the other tracers are retrograde or anterograde in octopus.

Initial injections were conducted with a glass pipette and a picospritzer. Because of the toughness of the tissue, however, the glass pipettes often broke, so Hamilto Syringes were used instead. The 25 gauge Hamilton syringe was useful for muscle injections, and the 32 gauge Hamilton syringe was ideal for axial nerve cord injections. The needle of these small gauge syringes is quite flexible, which was a technical challenge in addition to injecting into moving tissue and pressing the plunger to do an injection. To solve this problem, the syringe was anchored to a micromanipulator, and a second person assisted me with the injection. With forceps in one hand, I held the slice of arm down to prevent it from moving and with forceps in the other hand, I grasped the end of the syringe to aim it for the relevant target on the slice. On my say so, the assistant used the micromanipulator to lower the syringe as the experimenter guided the needle into the tissue. The assistant pressed down the plunger to inject the tracer and then raised the syringe out of the tissue, again on my say so. I then moved the injected slice into a dish with FSW, and the assistant completed the rinses and placed the slice in 221 media. Jan Kasal, Amelia Cheng, Ellie Khalil-Felbinger, Aashna Moorjani, Natalie Grace Schulz, and Cliff

Ragsdale all served as assistants in this procedure, with Jan Kasal and Amelia Cheng assisting with the majority of the experiments.

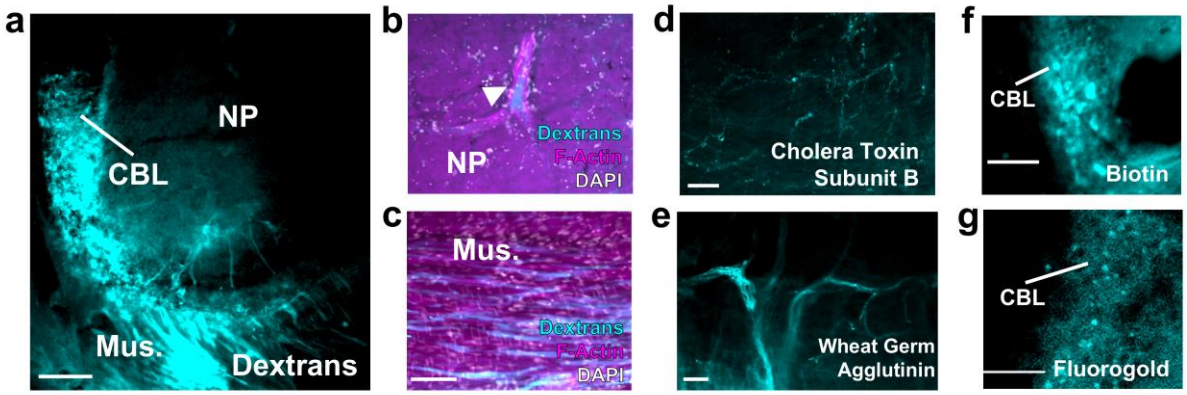

Figure 2.1: Tracers tested.
a, Transverse section of axial nerve cord (ANC) injected with dextrans (cyan). Dextran labels neuronal cell bodies and neuropil. Scale bar: 100 µm **b, c**, Dextrans injections (cyan) will label other tissue types like blood vessels (**b**) and muscle (**c,** Scale bar: 100 µm). Counterstains with phalloidin marking F-actin (magenta) and DAPI (gray) will also label the other tissue types. **d-g,** Injections with other tracers yielded positive labeling of neural processes. Cholera toxin Subunit B (**d**) and wheat germ agglutinin (**e**) both label processes over muscle. Biotin (**f**) and fluorogold (**g**) label neuronal cell bodies. All sections transverse. Scale bars: 50 µm

DiI Labeling

DiI crystals (Biotium, Cat#: 60016) were placed at various targets in 0.5-1cm transverse and longitudinally bisected fixed arm explants. Slices were incubated in 1% PFA/PBS in the dark for 7 days to 6 months. Following DEPC-PBS washes for 3x 15 minutes, explants were cleared in a modified version of FRUIT (Hou et al., 2015).

Tissue Clearing

Two methods for clearing tissue were successfully employed in octopus arm tissue: a modified version of FRUIT (Hou et al., 2015) and a modified version of DEEP-Clear (DEpigmEntation Plus Clearing; Pende et al., 2020) followed by FRUIT. FRUIT is a fructose, urea, and alpha-thioglycerol solution, and the process of clearing involves increasing the

concentration of fructose to its saturation point (100% (w/v) fructose) while decreasing the concentration of urea. In octopus arm tissue, this method does a good job at clearing the musculature and neural tissue, but a poor job at removing the chromatophores, which instead leak a red pigment. DEEP-Clear has previously been shown to remove the pigment of cephalopod chromatophores, and I found it successfully removes the pigment from the chromatophores in the octopus arm. However, DEEP-Clear alone does not do well in clearing the neural tissue and musculature in the arm. DEEP-Clear followed by FRUIT creates the optimal results of removing skin pigment and clearing the musculature and neural tissue, though it then becomes a longer protocol (Fig. 2.2a, b).

Since the skin of the arm was not a primary focus of this study and it is straightforward to remove, the pigmented layers of skin were often dissected off and FRUIT alone was employed for clearing in results reported here. Since this dissection was aimed at simply removing the pigmented layers of the skin, the connective tissue anchoring it and some of the nerves innervating the skin were regularly retained.

The amount of fixation and prior treatment of the tissue created varied levels of clearing. As demonstrated in Figure 2.2, slices that underwent whole mount IHC were cleared most completely.

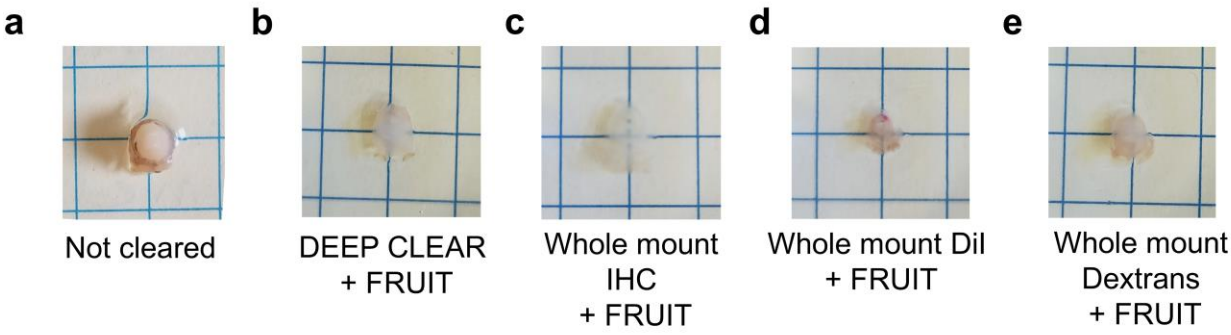

Figure 2.2: Clearing results.
a, Skin-on transverse explant without any clearing. **b,** Skin-on transverse explant cleared with DEEP-CLEAR followed by FRUIT. DEEP-CLEAR removes the chromatophores in the skin and FRUIT clears the musculature. **c-e,** Examples of skin-off transverse explants cleared with FRUIT with different prior treatments. Level of clearing varies based on treatment. Whole mount immunohistochemistry (**c**) yielded the clearest tissue, compared to DiI labeled whole mounts (**d**) or dextran-injected whole mounts (**e**).

FRUIT

Following 3x 15 minute washes in DEPC-PBS, slices were incubated for 24 hours at 37°C in increasing concentrations of FRUIT (35%, 40%, 60% 80%, and 100% FRUIT; see table 2.1). Slices were then stored at 100% FRUIT at 4°C in a 24-well plate sealed with parafilm.

FRUIT can be employed at room temperature, but the best clearing was seen at 37°C. Storage in 100% FRUIT at 4°C is very stable, and cleared slices can still be imaged two-three years later. Table 2.1 depicts the recipes for making 50mL and 100mL of the FRUIT solutions. When making FRUIT, it is recommended to incubate the solutions 37°C to dissolve the solutions fully. Alpha-thioglycerol is included in the solution to prevent browning due to the Maillard reaction. When imaging on the LaVision light sheet microscope, 100% fructose was used to avoid getting alpha-thioglycerol and urea on the microscope instrument.

Table 2.1: FRUIT (in ddH_2O)

FRUIT %	35% FRUIT		40% FRUIT		60% FRUIT		80% FRUIT		100% FRUIT	
mL	50mL	100mL	50mL	100mL	50mL	100mL	50mL	100mL	50mL	100mL
Fructose	17.5g	35g	20g	40g	30g	60g	40g	80g	50g	100g
Urea	24g	48g	24g	48g	17.5g	35g	12.5g	25g	5g	10g
Alpha-TG	1mL	2mL	1mL	2mL	1mL	2mL	1mL	2mL	1mL	2mL

DEEP-Clear and FRUIT

After 3x 15 minute washes in Marine-PBS (5.45g of Na_2HPO_4, 1.55 g of NaH_2PO_4, 29.22 g of NaCl to 1 liter with ddH_2O; Pende et al., 2020), slices were incubated for 2 hours at -20°C in prechilled acetone. Then, slices were washed 3x 15 minutes in Marine-PBS and incubated in

Solution 1.1 (4 mL of THEED, 2.5 mL of TritonX100, 2.5 g of Urea to 50 mL with ddH_2O; Pende et al., 2020) until the pigment was gone. It can take many days for the pigment to disappear fully, and Solution 1.1 was changed daily. Once the pigment was cleared, slices were washed 3x 15 minutes in Marine-PBS and cleared with FRUIT.

Vasculature Injections performed by Natalie Grace Schulz

Lab-raised 6-week-old *O. bimaculoides* (n = 5) were anesthetized in 2% EtOH/ASW. A small incision was made above the right orbital socket to provide access for the pulled glass electrode to enter the white body. Using a picopump, 3-5 μL of a heavy-weight dextran (Invitrogen, Cat#D1818, 70,000 MW, lysine fixable) was injected into each juvenile octopus and allowed to circulate throughout the body for 5 minutes. Animals were then transferred to a 4% EtOH/ASW for five minutes before immersion fixation in 4% PFA/PBS overnight at 4°C. Injected animals were stored in PBS at 4°C before further processing for imaging or immunostaining.

Imaging

The immunolabeled and tracing tissue was studied with a Zeiss Axioskop 50 upright microscope and a Leica MZ FLIII stereomicroscope, both outfitted with the Zeiss AxioCam digital camera and AxioVision 4.5 software system. Selected sections were also studied on a Leica SP5 Tandem Scanner Spectral 2-photon confocal microscope (Leica Microsystems, Inc., Buffalo Grove, IL) or scanned with an Olympus VS200 Research Slide Scanner (Olympus / Evident, Center Valley, PA) with a Hamamatsu ORca-Fusion camera (Hamamatsu Photonics, Skokie, IL). Whole mounts were imaged on a LaVision BioTec UltraMicroscope II (Miltenyi Biotec, Bergish Gladbach, Germany) run by ImSpector Pro v. 7_124 software (LaVision BioTec,

Bielefeld, Germany). Collected images were corrected for contrast and brightness and false colored in FIJI (version 2.1.0/1.53c; National Institutes of Health (NIH)). Whole mount reconstructions were visualized with Arivis Vision4D software v. 3.1 (arivis AG, Rostok, Germany). Diagrams were drawn using GIMP v. 2.10.32.

Segment and sucker ganglion proximal-distal analysis

Two series were created to examine changes along the proximal-distal axis of the arm from the edge of crown webbing to tip. The first series consisted of 3 evenly spaced arm blocks from an arm on the right side (arm R1) of one animal sectioned longitudinally and stained with acTUBA. The second series consisted of 3 evenly spaced blocks from an arm on the left side (arm L3) of a second animal sectioned longitudinally and stained with H&E. For cross sectional area, an arm explant was sectioned horizontally and stained with acTUBA. For segment counts on *D. pealeii*, counts were performed on sections of arm explant stained with ISH for *Dpe SYT1.*

Segment counts: The number of segments were counted along a length of six suckers on the anterior and posterior side of the ANC. The counts for the anterior and posterior sides were averaged together, then divided by six to determine segments/sucker.

Segment Width: Four segments across six suckers on both the anterior and posterior side of the ANC were selected for width measurements and were tagged with either the external side of the ANC (ExA) or internal side of the ANC (InA; Fig. 3.10a, b). Width of each segment along the proximal-distal axis was measured manually using the line tool in FIJI. Measurements on the anterior and posterior side were averaged together to get averages for ExA and InA. Total averages were found by additionally averaging ExA and InA.

Sucker Width: For six suckers in each explant, the width of the acetabulum was measured manually at the widest point using the line tool in FIJI.

Sucker Ganglia Width: The longitudinal width of each sucker ganglion along the proximal-distal axis was manually measured by Aashna Moorjani at the widest point using the line tool in FIJI (Fig. 5.2a, b). The longitudinal widths of the sucker ganglion were then compared to the longitudinal widths of the corresponding suckers (SG width/sucker width).

Cell Density: For each of the segments selected for the width measurements, a rectangle spanning the width of the segment was taken. The number of nuclei, visualized by DAPI, within the rectangle were counted using the analyze particle function in FIJI. The area of the rectangle was also found in FIJI. Density was calculated as the number of nuclei/area. Averages for ExA and InA pooled across both the anterior and posterior side of the ANC as for segment width calculations.

Cross sectional area: Across three suckers, three segments on ExA and three segments on InA were selected for cross sectional area measurements. Visibility of each segment across the oral to aboral extent of the ANC were ensured. The width, defined as the length in the proximal-distal axis, and height, defined as the length perpendicular to the proximal-distal axis, were manually measured in FIJI. Cross sectional area was calculated as width x height.

Cerebrobrachial tract (CBT) proximal-distal analysis

To examine proximal-distal variation in the CBT, four wholemount slices spanning the proximal-distal axis of one arm from two different animals (Arm 1L and 3R) were immunostained for acTUBA. The CBT and whole slice were imaged in the transverse plane.

Maximum projections of the CBT were used to determine subdivisions. Maximum projections of the whole slice were used to determine area.

CBT Subdivisions: Discrete bundles within the CBT across all slices were traced by Aashna Moorjani. Bundles that were consistent across the proximal-distal axis and between arms were demarcated as the main subdivisions. I made this determination, along with verification from Ms. Moorjani.

CBT Area: The area of the CBT and the ANC were calculated by Aashna Moorjani using the polygon tool in FIJI. To ensure the measurement was accurate, adhering the contours of the amorphous octopus anatomy, dots were placed as close to each other as possible. The area for the CBT was then compared to the area of the ANC (CBT/ANC).

Nerve analysis

Large scale nerve analysis was facilitated by segmenting whole mount tissue, immunostained for nerve markers, acTUBA and SMI-31. To examine brachial nerves, two whole mounts of slices stained with acTUBA and one slice whole mount stained with SMI-31 were imaged transversely. To examine the oral nerves, two whole mounts labeled for acTUBA were imaged, one transversely and one longitudinally, and one whole mount with SMI-31 was imaged transversely. To examine the sucker ganglion nerves, 2 whole mount sucker ganglia, immunostained with acTUBA and SMI-31, were imaged transversely and 2 whole mount sucker ganglia, immunostained with acTUBA, were imaged horizontally. Nerve fibers from the axial nerve cord targeting the sucker and brachial musculature were traced using Simple Neurite Tracer (SNT, v. 4.2.0) in FIJI (Arshadi et al., 2021). For nerve fibers targeting the sucker, the major trunks were traced until they began majorly branching at the sphincter of the sucker. Other

branching prior to the sphincter were also excluded. For the brachial nerves, all branch points were followed until they connected with a part of the peripheral nervous system or positive labeling became indistinguishable. Nerves from the sucker ganglion were traced with SNT by Aashna Moorjani with edits from me.

Oral nerve analysis: The traces for the oral nerves were tagged as corresponding to ExA or InA and the 3D spatial coordinates outlining the traces were found using the SNT API (Fig. 3.10a, b , h; Arshadi et al., 2021). The coordinates of tips of the nerve were translated such that the center of all the tips was set as the origin. Subsequently, each tip coordinate was normalized such that the vector from the origin to the tip has a magnitude of 1, creating a circle. To determine percentage of the sucker covered, the angular extent of ExA and InA tips around the circle was computed and divided by 360°. The spatial distribution of tips corresponding to the ExS and the InS were visualized using Matplotlib (v. 3.7.3).

Aboral and central nerve analysis: The traces for the brachial nerves were segregated into the central nerves targeting the oral brachial musculature and the aboral nerves targeting the aboral brachial musculature (Fig. 3.6a). The branching pattern of the nerves were characterized using the SNT Sholl analysis with 10 μm spacing (Fig. 3.6b; Ferreira et al., 2014). The profile was then fit with a 5-degree polynomial and normalized via min-max normalization, where the maximum was set to the radius associated with the longest nerve, the nerve that reaches the skin. The 3D spatial coordinates, root, and tips of the nerves were found using the SNT API (Arshadi et al., 2021). The average trajectory of the nerve was computed by creating a vector from the root of the nerve to the center of the process (Fig. 3.6c). The unit vector for each average trajectory was found and divided by the magnitude of the longest nerve. The distribution of the tips in the aboral-oral and proximal-distal plane were visualized using Matplotlib (Fig. 3.7a). Relation to

the septa were determined using the oral roots as additional markers and used to color code the nerves.

Sucker ganglia nerve fascicle diameters: Using the path fitting feature in SNT, the radii of each node of the paths of the 2 horizontally imaged sucker ganglion were found (Arshadi et al., 2021). Then, using the SNT API and a python script, the radii of the nodes corresponding to the first 300 μm of each path were extracted, smoothed and averaged. The average radius for each path was multiplied by 2 to determine the diameter of the nerve fascicle. The distribution of nerve fascicle diameters was plotted as a histogram using Matplotlib (v. 3. 7.3).

Sucker ganglia nerve root distribution: The SNT API was used to find the 3D coordinates of the roots of the traces from the 2 transversely imaged sucker ganglia and from 1 horizontally imaged sucker ganglion (Arshadi et al., 2021). The coordinates of roots of the nerves were translated and rotated so that the center of all the roots was set as the origin. Subsequently, each root coordinate was normalized so that the vector from the origin to the tip had a magnitude of 1, creating a circle. The spatial distribution of roots from the 3 sucker ganglia was realized in the aboral-oral and external-internal plane with a colormap corresponding to the location of the root in that plane using Matplotlib. The spatial distribution of roots from the horizontally imaged sucker ganglion was also realized with a colormap corresponding to the diameter of the nerve fiber.

Sucker ganglia nerve targets: The 3D spatial coordinates, roots, and tips of the nerves from the horizontally imaged and transversely imaged sucker ganglia, both stained with acTUBA, were found using the SNT API (Arshadi et al., 2021). The average trajectory of each nerve was computed by creating a vector from the root of the nerve to the center of the process

(Fig. 5.8i). The unit vector for each average trajectory was found. The distribution of the average trajectories for the transversely imaged sucker ganglion was realized in the aboral-oral and external-internal planes with a colormap corresponding to nerve root locations using Matplotlib. The distribution of the average trajectories for the horizontally imaged sucker ganglion was realized in the proximal-distal and external-internal planes with a colormap corresponding to nerve target location in that plane.

Statistics

Unless otherwise stated, data are mean +/- standard error of the mean (sem). Using MATLAB (2021b), a two-way ANOVA followed by Tukey's post hoc test was conducted to test for significance along the proximal-distal axis and between the ExS and InS. Data were considered significant if $p < 0.05$. Sample size was not statistically predetermined, and all data were validated by at least two markers and at least two animals.

Table 2.2: Transcripts amplified for in situ hybridization

Gene	NCBI Accession	Forward Primer	Reverse Primer
Obi SYT1	XM_014919324.1	5' CCT GGG ATG GAT ATG TCT GG -3'	5' GTT CGG AAG TCC CAA TAC GA-3'
Obi CPLX1	XM_014919099.1	5' AAA ATG GCG GCA AGT GTA GG 3'	5' AAA GAG GTG AGG GGT TGT GC 3'
Obi MUNC18	XM_052972671.1	5' AGG ATC GGT CTC AGC TGT TG 3'	5' TTT CTT CGC CCT CCA TCT TGA 3'
Obi MNX	XM_014912376.1	5' TGC ATT TGG TCA GGG TCA GC-3'	5' TTT AGG CAA ACA GTT CGC TGG -3'
Obi LHX3	XM_052978610.1	5' GAA TTC GCC CTT CGA TTA CAA 3'	5' ACA GCT AAG CGT TGA AAC AG 3'
Obi NKX6	XM_014926771.2	5' GTC ATA GTT GAT AAA GAC GGC AAA C 3'	5' GTT CTT GTT TCT TTT TAG CTG ATG C 3'
Obi PIEZO	XM_014926525.1	5' CTG GCC AGG CTT TGT CAA TC 3'	5' TCC ATT GGA TCT TCA TTA GTT G 3'
Obi DRGX	XM_014929620.1	5' GGT TAT GGT GCA TGA TGG CG 3'	5' GCA CGT ACG GTC ATT TCT GC 3'
Obi FMRF	XM_014929818.1	5' ACC AGT ATG CAA AGC CAA GC 3'	5' TCT CAT GTT TAT TGA GCA CGT CTG 3'
Obi VACHT	XM_014912673.1	5' TGG ACA ACA TGC TTT ACA TGG -3'	5' ATG AAG CCC ATT TCC CAT TC -3'
Obi SLC5A7	XM_014929182.1	5' ATA TGG GCT GGT CGC AAG TC 3'	5' CTG GTT CCA GTC TGT GGA GG 3'

Obi VIAAT	XM_014931765.1	5' CCG GTA AAA TAT TGG TGG AAT GTC TG - 3'	5' AGT GTT GGT AGA AAT ATT TGT GAG G - 3'
Obi PRM	XM_014927798.1	5' TAG ACT CCG AGA GGG ACA GC 3'	5' ACA CGT TTG CCC AAT GAA GC 3'
Obi TPM	XM_014918517.1	5' CCG ACG AAT TCA GCT TTT GGA 3'	5' ATT TAT TTC AAG GGC AGC TCA AA 3'
Obi TTN	XM_014926173.1	5' AAG GCG AGA ATC ACC CAC TG 3'	5' TGT GTC CAC ACC ATC CAC TG 3'
Obi MYH	HG421291.1	5’ AGG CTG AAT TGG AGA ACG CA 3’	5’ AAG CTC TGC GGA CCT TCT C 3’

Table 2.3: Sequence synthesized for in situ hybridization

Gene	NCBI Accession	Sequence Synthesized
Dpe SYT1 **(Synaptotagmin 1)**	D63797.1	AGGATGGCAAAAAGGGGCTCAAAGGAGCTGT CGACCTCAAAGGTGTACAGTTACTGGGCAACT CTATCAAAGAAAAGGTGCAGCCTGACTTGGAG GAACTGCCAATGAATATGGAAGACAATGAGG ATGCAGAAAGTACAAAATCCGAAGTAAAATT AGGGAAACTTCAATATTCTATGGACTACGATT TTCAGAAAGGCGAGCTAACAGTTAACGTGATA CAGGCTGCCGACCTACCAGGGATGGATATGTC TGGGACATCTGACCCATATGTCAAAGTCTATC TAATGCCCGACAAAAAGAAGAAATTTGAGAC AAAAGTCCATCGGAAAACACTCAACCCAGTAT TTAACGAATCGTTCACTTTTAAGAACGTTCCCT ATGCTGATATTACGGGTAAGACACTTGTGTTT GCGATCTATGATTTTGATCGCTTTTCGAAACAC GACCAAATTGGTCAAGTCCAAGTGGCAATGAA CTCGATAGATCTTGGATCGGTCATGGAAGAGT GGAGAGATCTAACTAGCCCGGATAATGATGCT GAGAAGGAGAACAAGCTGGGTGACATTTGTTT CTCATTGCGATATGTTCCGACTGCTGGCAAAC TGACCGTTGTCATCCTTGAGGCTAAAAATCTA AAGAAAATGGATGTTGGTGGACTATCAGATCC TTATGTAAAGATATCGTTGATGCTTAACGGCA AGAGAATTAAGAAGAAGAAAACCACTGTCAA GAAGTGCACACTGAATCCATACTATAATGAGT CATTCGCGTTTGAAGTCCCGTTCGAACAAATA CAGAAAGTATCCCTCTATGTCACGGTGGTCGA CTACGATCGCATTGGGACCTCTGAACCAATCG GACGAACCTTCCTG

CHAPTER 3

Neuronal segmentation in cephalopod arms[2]

INTRODUCTION

The octopus has a motor control challenge of enormous complexity (Hochner et al., 2023; Olson and Ragsdale, 2023). Each of its eight arms is a muscular hydrostat, a soft-bodied structure that lacks a rigid skeleton and moves with near infinite degrees of freedom (Kier and Stella, 2007; Kennedy et al., 2020). Moreover, the arms are packed with hundreds of chemotactile suckers which can change shape independently (Grasso, 2008; van Giesen et al., 2020). Even with this complexity, octopuses control behaviors effectively along the length of a single arm, across all eight arms and between suckers (Gutfreund et al., 1996; Hanlon and Messenger, 2018; Bidel et al., 2022). The neural circuits underlying these behaviors have been unexplored with modern molecular and cellular methods.

Embedded in the octopus arm is a massive nervous system, with more neurons found distributed across the eight arms than in the brain (Young, 1963, 1971). Most prominent is an axial nerve cord (ANC) running down the center of every arm (Fig. 3.1a, Fig. 3.2a; Graziadei, 1971; Olson and Ragsdale, 2023). Peripheral to the ANC, there are four smaller intramuscular nerve cords (IMNCs), and a sucker ganglion (SG) for every sucker (Fig. 3.1a, Fig. 3.2a). In the ANC, and following the characteristic invertebrate pattern, neuronal cell bodies are localized to a cell body layer (CBL) wrapping around neuropil (NP). Down the long axis of the arm, the ANC is a medullary cord (Richter et al., 2010) that snakes back and forth, with every bend in the ANC forming an ANC enlargement that overlies a sucker (Fig. 3.2g, h; Rossi and Graziadei, 1954;

[2] Published in Nature Communications (doi.org/10.1038/s41467-024-55475-5). Referred to as Olson et al (2025) in other chapters.

these ANC enlargements are themselves sometimes referred to as ganglia, see Young, 1971; Nixon and Young, 2003; Nödl et al., 2016). In transverse sections on the sucker, or oral, side of the ANC, the CBL forms a horseshoe around the NP (Fig. 3.1b, Fig. 3.2b). On the aboral side, or away from the suckers, there is a massive cerebrobrachial tract (CBT) connecting the arms and the brain (Fig. 3.1b, Fig. 3.2b; Graziadei, 1971; Zullo et al., 2019). The CBL itself can be divided into an aboral, or brachial, territory that is dedicated to the sensorimotor control of the arm, and an oral, or sucker, territory for the sensorimotor control of the suckers (Rowell, 1963; Fig. 3.2 g, h). Beyond this classical segregation, further neural divisions within the ANC and in the ANC nerve trajectories for the brachial musculature and the suckers are unknown.

In this study, we investigated the structure of the ANC and its nerves in *Octopus bimaculoides* using modern molecular and cellular techniques. We found that the ANC is segmented, forming columns of neuronal cell bodies. These neuronal segments underlie a modular organization to the ANC neuropil: neuronal cell bodies within each segment send the bulk of their processes directly into the adjoining neuropil, with some reaching the contralateral side. The septa between each segment are neuron-poor but contain nerve exits, vasculature and abundant collagen. Nerves exiting from neighboring septa differ in their fiber trajectories indicating that multiple adjoining segments must cooperate to innervate the arm musculature fully. The nerves for each sucker also exit through septa, radially tiling the sucker to create a spatial topographic map in the ANC. In the squid *Doryteuthis pealeii*, the arms and the sucker-rich club of the tentacles have segments, but the sucker-poor stalk of the tentacles does not, suggesting a strong link between segmentation and flexible sucker-laden arms. Our findings in squid and octopus constitute a clear demonstration of segmental organization in a mollusc.

RESULTS

Segmentation in the ANC:

We found an unexpected neuronal organization in the ANC along the longitudinal axis of the arm: neuronal cell bodies are constrained to segmental columns separated by septa (Fig. 3.1c, d, e). These segments encompass the full aboral to oral extent of the cell body layer, involving both the brachial and sucker territories (Fig. 3.2 g, h). The pattern persists as the ANC weaves from sucker to sucker (Fig. 3.1f, Fig. 3.2 f, g, h). The arm tapers and suckers become smaller along the proximal-distal axis of the arm, as do the widths of the segments (Fig. 3.1h, Fig. 3.2d, e). The consequence is the number of segments per sucker remains constant (average: ~7.5; Fig. 3.1g)

We investigated the septa between segments. The space between the CBL segments is enriched with connective tissue, labeled by Picrosirius Red staining (Fig. 3.4a). Connective tissue pads the length of the septa, and sometimes lines the interface between the CBL and NP (Fig. 3.3f). Vasculature also lies in the septa. Most prominent is F-actin-positive vasculature that travels along the inner border of the CBL and the NP, strictly following the segmental boundaries (Fig. 3.4b, Fig. 3.3e). To confirm that this F-actin labeling identifies blood vessels (Wollesen et al., 2009), we flooded the vascular system with dextran-TRITC. We found an overlap of the vasculature labeled with the dextran and by the F-actin staining (Fig 3.4c, d, Fig. 3.3b, c, d). Thus, as with other segmental systems, such as in insect developmental compartments or vertebrate somites (Campos-Ortega and Hartenstein, 1997; Hubaud and Pourquié, 2014; Clark et al., 2019), multiple tissue types form in a segmental pattern along the ANC.

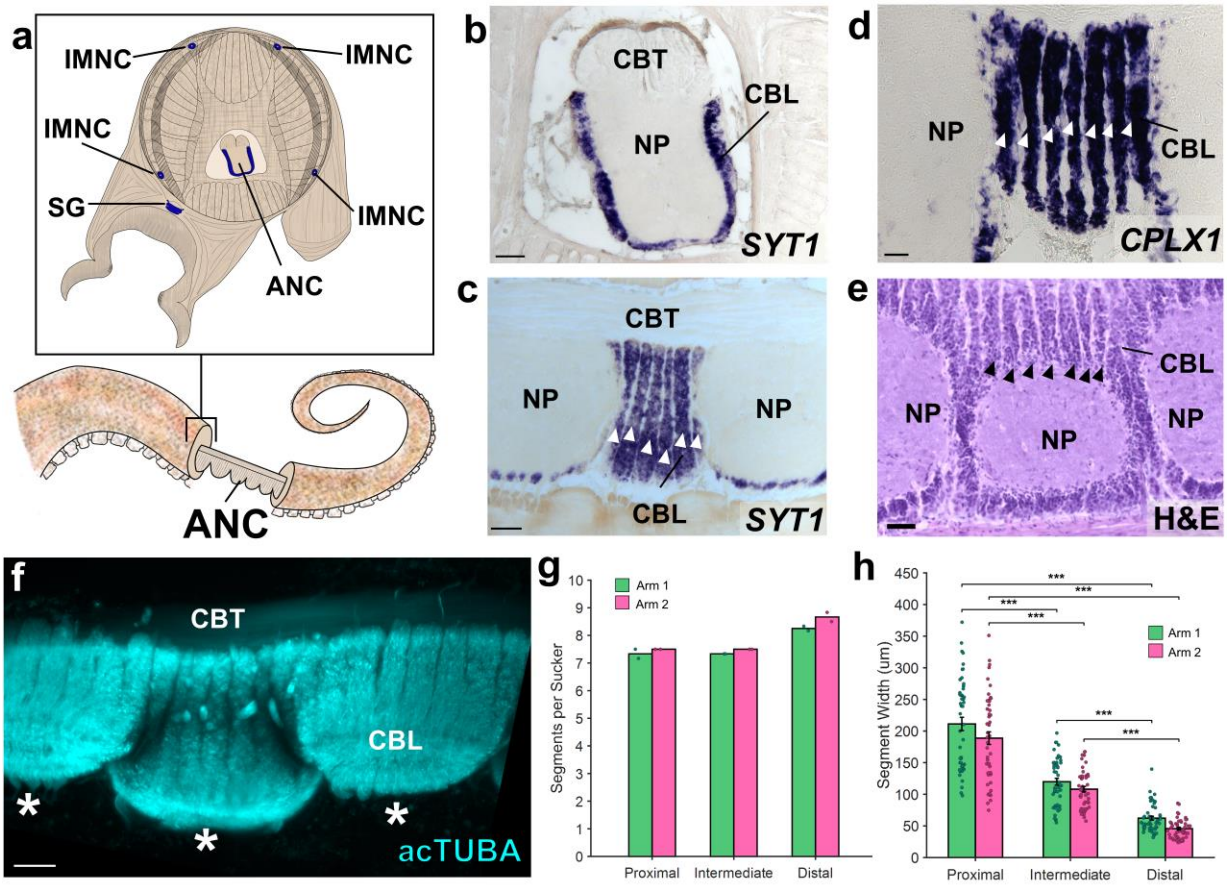

Figure 3.1: The axial nerve cord (ANC) is segmented.
a, Transverse diagram of *O. bimaculoides* arm with the location of neuronal cell bodies outlined in blue. **b,** In situ hybridization (ISH) for synaptotagmin 1 (*SYT1)* in a transverse section of the ANC. Representative sample from 7 explants. Scale bar: 100 µm. **c-e,** Longitudinal sections through the ANC demonstrating segmentation in the cell body layer with (**c**) ISH for *SYT1*, representative sample from 21 explants. Scale bar: 100 µm, (**d**) ISH for complexin (*CPLX1),* representative sample from 7 explants and (**e**) hematoxylin and eosin (H&E), representative sample from 6 explants, scale bars: 50 µm. Arrowheads point to individual segments. **f,** Whole mount immunostaining with acetylated alpha tubulin (acTUBA) of a dissected ANC. Segmentation pattern is continuous as the ANC oscillates from sucker to sucker. Representative sample from 7 explants. * denotes individual suckers. Scale bar: 100 µm. **g,h,** Quantification of segmentation down the proximal-distal axis. Arm 1 (green) was stained with acTUBA and arm 2 (pink), with H&E. (**g**) The number of segments per sucker is maintained along the proximal-distal axis (n = 2 per condition, average Arm 1 = 7.64; average Arm 2 = 7.88). (**h**) Segment width decreases down the proximal distal axis. Data represent mean +/- sem (n = 48 per condition). $P < 0.001$, 2-way ANOVA, with post hoc Tukey's test. CBL, cell body layer; CBT, cerebrobrachial tract; IMNC, intramuscular nerve cord; NP, neuropil; SG, sucker ganglion.

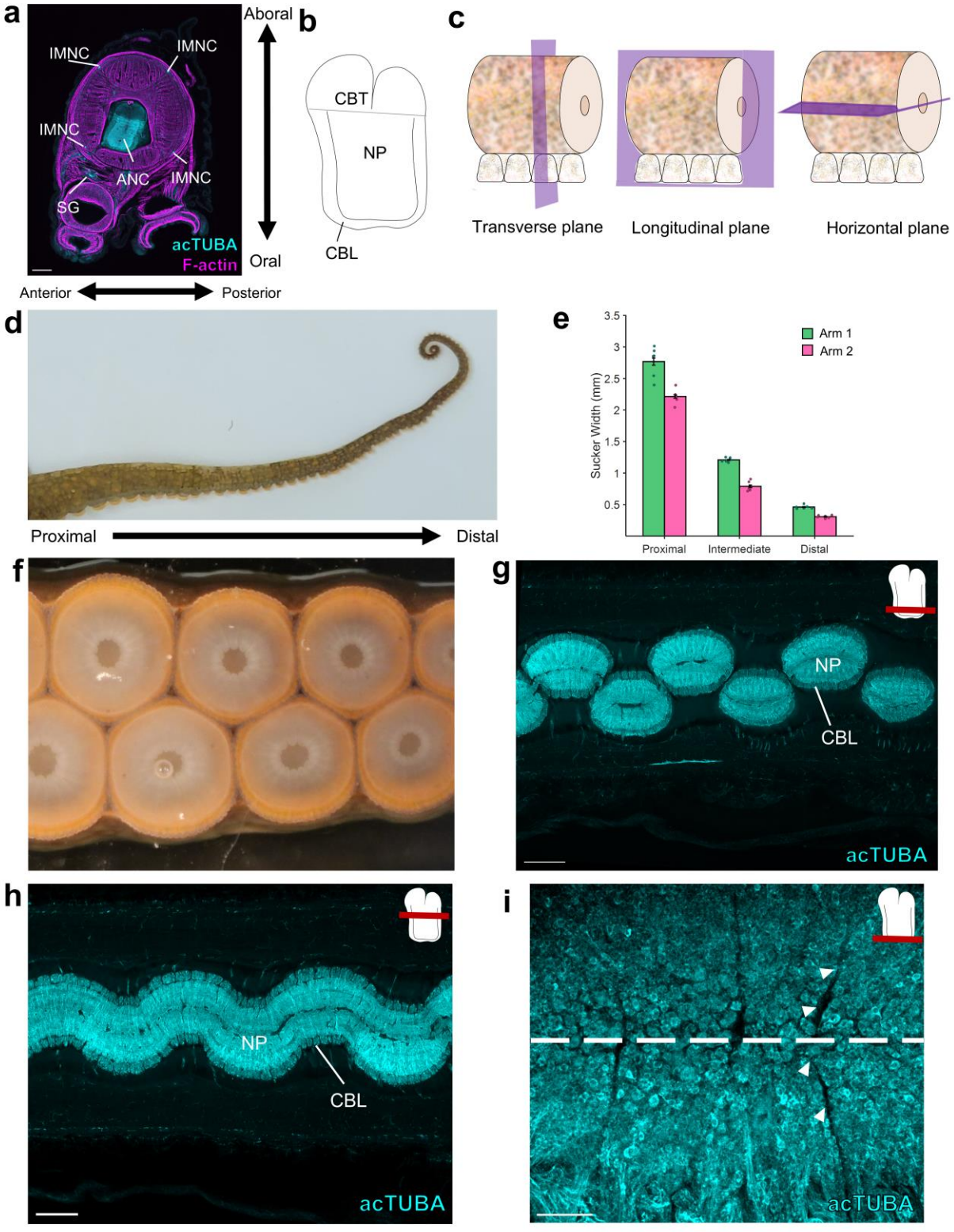
a
IMNC
IMNC
IMNC
ANC
IMNC
SG
acTUBA
F-actin
Aboral
Oral
Anterior
Posterior
b
CBT
NP
CBL
c
Transverse plane
Longitudinal plane
Horizontal plane
d
Proximal
Distal
e
Arm 1
Arm 2
Sucker Width (mm)
3.5
3
2.5
2
1.5
1
0.5
Proximal
Intermediate
Distal
f
g
NP
CBL
acTUBA
h
NP
CBL
acTUBA
i
acTUBA

Figure 3.2: Arm anatomy overview.
a, Transverse section of the arm stained with acTUBA (cyan) and phalloidin (F-Actin, magenta). The main components of the arm nervous system are highlighted. Scale bar: 500 μm. **b,** Cartoon depiction of the ANC. **c,** The three perpendicular planes of sectioning through the arm. The transverse plane is perpendicular to the long axis of the arm. The longitudinal plane is parallel to the long axis of the arm. The horizontal plane is parallel to the long axis of the arm and to the suckers. **d,** Photograph of the arm of *O. bimaculoides.* From proximal to distal, the girth of the arm decreases. **e,** Sucker width decreases from proximal to distal. Arm 1 (green) and Arm 2 (pink). n = 6 suckers per condition, error bars +/- sem. **f,** An en face photograph of the suckers shows that the suckers are arranged in two offset rows. **g,** Horizontal section of the ANC through the sucker territory labeled with acTUBA (cyan). The ANC oscillates to the side overlying the sucker. Scale bar: 500 μm. **h,** Horizontal section of the ANC through the brachial territory labeled with acTUBA (cyan). Scale bar: 500 μm. **i,** Maximum projection of a horizontal slice whole mount immunolabeled with acTUBA (cyan) through the oral CBL. Segments extend across the midline (denoted with the dashed line, arrowheads indicate septum crossing the midline). Scale bar: 100 μm. ANC, axial nerve cord; IMNC, intramuscular nerve cord; SG, sucker ganglion; CBT, cerebrobrachial tract; CBL, cell body layer; NP, neuropil.

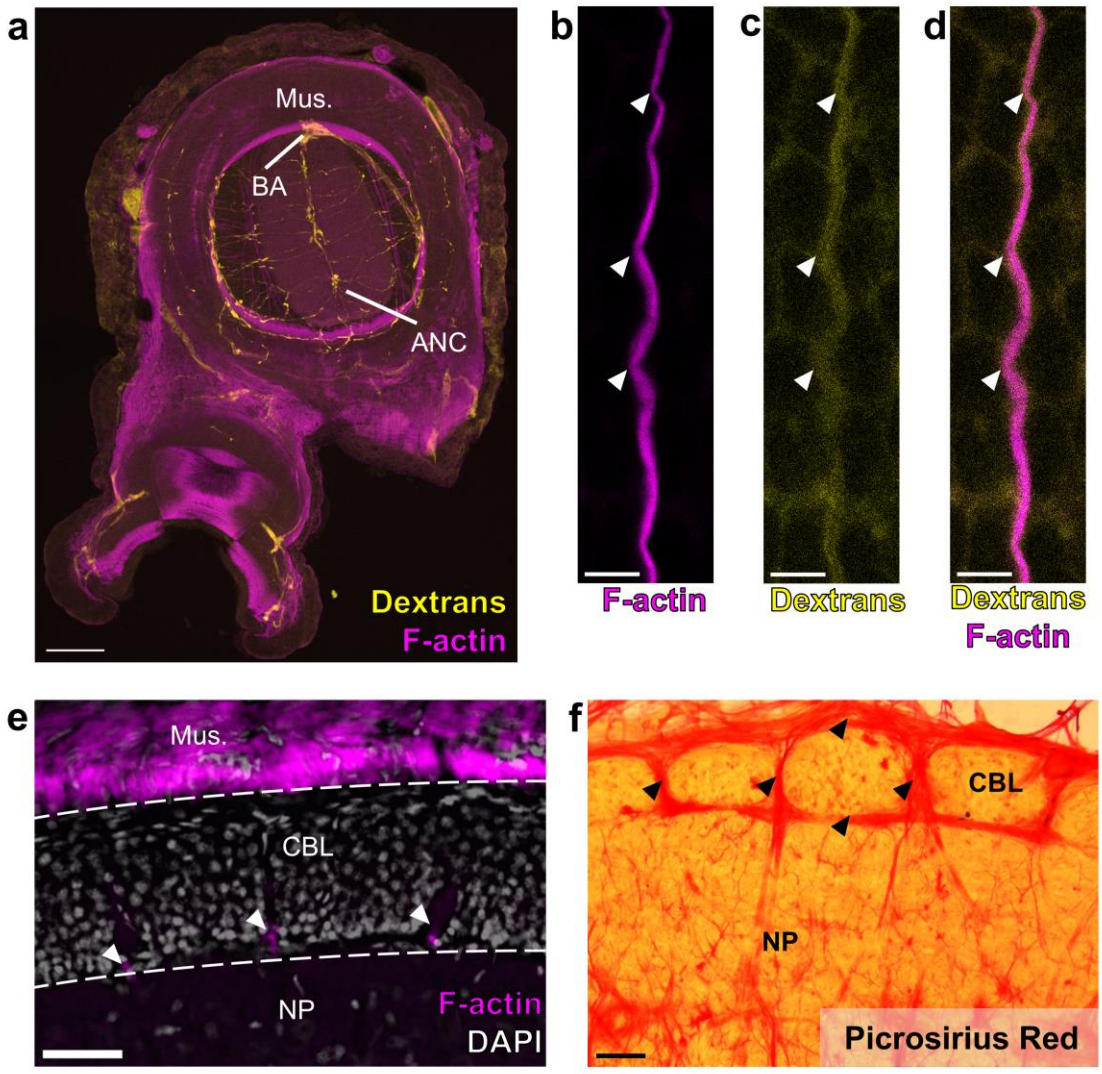

Figure 3.3: Septal localization of vasculature and collagen.
a, Transverse section of arm with dextran labeling (yellow) of the vasculature. F-actin and dextran delivery clearly identify the large brachial artery (BA). Scale bar: 100µm. **b-d,** Maximum projection of a single blood vessel. **(b)** F-actin (magenta) and **(c)** dextrans (yellow) **(d)** colocalize. Arrowheads point to bumps in the blood vessel that are highlighted in both labelings. Scale bar: 5 µm. **e.** Horizontal section through the axial nerve cord (ANC) labeled with F-actin (magenta) and DAPI (gray). The vessels are located in the cell body layer (CBL) at the interface between the CBL and the neuropil (NP), indicated by arrowheads. Scale bar: 50 µm. **f,** Horizontal section through the ANC labeled with Picrosirius Red. Arrowheads point to collagen, labeled in red, which wraps around the CBL segments and extends within the full length of the septa. Scale bar: 50 µm. Mus., brachial musculature.

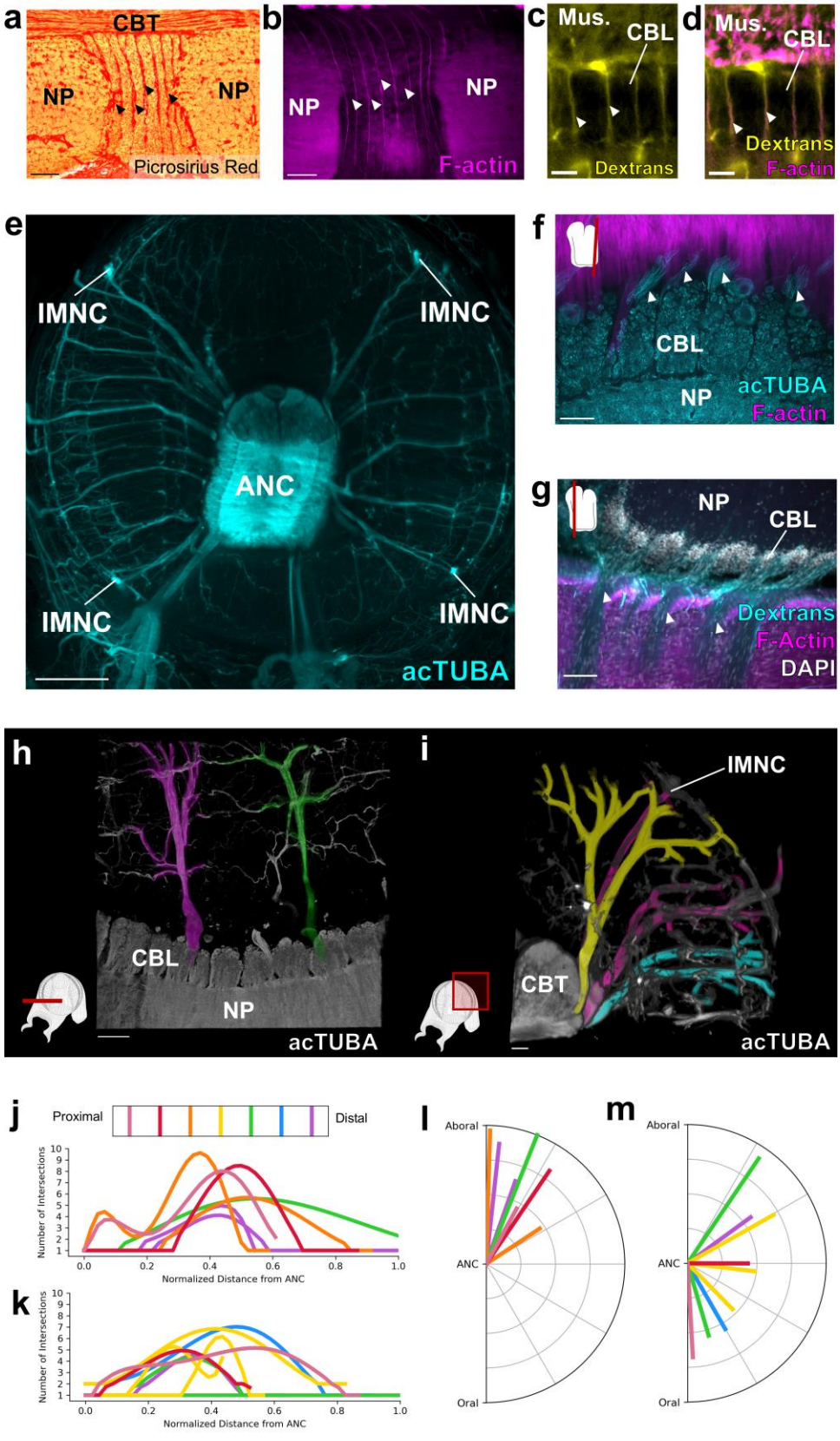
a
CBT
NP
NP
Picrosirius Red
b
NP
NP
F-actin
c
Mus.
CBL
Dextrans
d
Mus.
CBL
Dextrans
F-actin
e
IMNC
IMNC
ANC
IMNC
IMNC
acTUBA
f
CBL
NP
acTUBA
F-actin
g
NP
CBL
Dextrans
F-Actin
DAPI
h
CBL
NP
acTUBA
i
IMNC
CBT
acTUBA
j
Proximal
Distal
Number of Intersections
Normalized Distance from ANC
k
Number of Intersections
Normalized Distance from ANC
l
Aboral
ANC
Oral
m
Aboral
ANC
Oral

Figure 3.4: Organization of the septa and the innervation patterns of the brachial musculature.
a, Picrosirius Red stain of an axial nerve cord (ANC) longitudinal section. Red denotes the presence of collagen. Arrowheads point to collagen rich septa. Representative sample from 3 explants. Scale bar: 100 μm. **b,** F-actin (magenta) labeled by phalloidin is localized to the septa, indicated by arrowheads. Representative sample from 16 explants. Scale bar: 100 μm. **c,** Trans-vascular dextran labeling demonstrates vasculature (yellow) in the septa. Representative sample from 25 explants. Scale bar: 20 μm. **d,** Dextran labeling colocalizes with F-actin staining (magenta). Representative sample from 25 explants. Arrowheads point to septa. Scale bar: 20 μm. **e,** Maximum projection of acetylated alpha-tubulin (acTUBA) whole mount immunostaining of a transverse slice. Nerve fibers exit the ANC at discrete locations. Representative sample from 20 explants. Scale bar: 500 μm. **f, g,** Longitudinal ANC sections of the brachial nerve exits in the septa, indicated by arrowheads. (**f**) acTUBA nerve labeling (cyan), representative sample from 11 explants. (**g**) experimental dextran tracing of oral nerves. Injection site in central NP. Representative sample from 8 explants. Scale bars: 100 μm. **h-m.** Brachial nerves exiting from neighboring septa have different targets. (**h**) Maximum projection of a horizontal whole mount stained with acTUBA. Two nerves (false colored in magenta and green) innervating similar territories of muscle are separated by multiple segments. Representative sample from 10 explants. (**i**) Maximum projection of a transverse whole mount stained with acTUBA. Three nerves (false colored with yellow, magenta, and cyan) exiting from neighboring septa target different brachial territories. Representative sample from 19 explants. Scale bars: 100 μm. (**j-k**) Branching profiles of nerves across multiple septa was characterized by Sholl analysis. Profiles differ from septum to septum. (**j**) Aboral nerves. (**k**) Central nerves. (**l, m**) Nerve fiber average trajectories vary across septa. (**l**) Aboral nerves. (**m**) Central nerves. Mus., brachial musculature.

Relationship to sensorimotor circuits:

Nerve fibers depart at discrete points along the oral to aboral extent of the ANC, utilizing the septa as exit points (Fig. 3.4 e, f, g). Physiological and classic neuroanatomical studies have shown that these nerves carry both sensory and motor information (Rossi and Graziadei, 1958; Rowell, 1966; Gutfreund et al., 2006). Given this result, we used molecular markers to ask whether there might be a segregation of sensory and motor territories within the CBL itself. Markers of motor neurons (*NKX6, MNX, LHX3*) are largely restricted to the lateral sides of the CBL (Fig. 3.5 a, b, c, d). Markers of primary sensory neurons (*DRGX, PIEZO*) are also found distributed throughout this territory (Fig. 3.5 e, f, g). These results indicate that, unlike vertebrate

spinal cord (Jessell, 2000), there is not a clear spatial separation of sensory and motor neurons within the ANC.

Nerves exiting the ANC can be divided into the oral nerves, which innervate the sucker, and aboral and central nerves, which together innervate the brachial musculature (Fig. 3.4f, g, Fig. 3.6a; Graziadei, 1971; Nixon and Young, 2003). We asked how the ANC nerve fibers relate to the segmentation within the ANC by examining the innervation patterns of the aboral and central nerves targeting the brachial muscles. One possibility is that the same pattern of nerves is formed out between every segment. If this were the case, each CBL segment would reflect the same sensorimotor unit, simply spatially shifted down the longitudinal axis of the arm (See Fig. 3.7b). We studied brachial nerve fiber trajectories with whole mount immunohistochemistry for acetylated alpha-tubulin (acTUBA) and in dextran tracer experiments. The average exit trajectory and branching profile, calculated with Sholl analysis, were found to compare nerves exiting between adjoining and more distant septa (Fig. 3.6). For both the central and aboral nerves, nerves exiting between adjoining septa exhibit different branching profiles and exit with different average trajectories (Fig. 3.4i-m). Nerves with similar branching profiles and exit trajectories are separated by multiple septa (Fig. 3.4h, Fig. 3.6). We found, however, that nerve fibers across multiple septa collectively provide full coverage of the brachial musculature (Fig. 3.7). Instead of each segment reflecting identical sensorimotor units, this innervation pattern predicts that adjoining segments collaborate in organizing the brachial muscle activation patterns. Alternating innervation patterns have been documented in other segmented systems, such as that of the rhombomeres in the developing vertebrate hindbrain (Lumsden and Keynes, 1989).

We next interrogated the structure of the NP in the brachial territory of the ANC. Neuronal cell bodies send their projections directly into the NP adjacent to their segments, effectively partitioning the NP (Fig. 3.8a, Fig. 3.9b). Some of these projections extend across the midline, predicting crosstalk from segments on one side of the ANC to those on the other (Fig 3.8a, Fig. 3.9c). In addition, as aboral and central nerve fibers enter the ANC, they branch into segments both proximal and distal to the septum of entry, leading to an overlap of the projections in the NP of nerve fibers from neighboring septa (Fig. 3.8b). Collectively, this circuit structure provides the neural substrate for integration of multiple segments in the control of the brachial musculature (Fig. 3.8c).

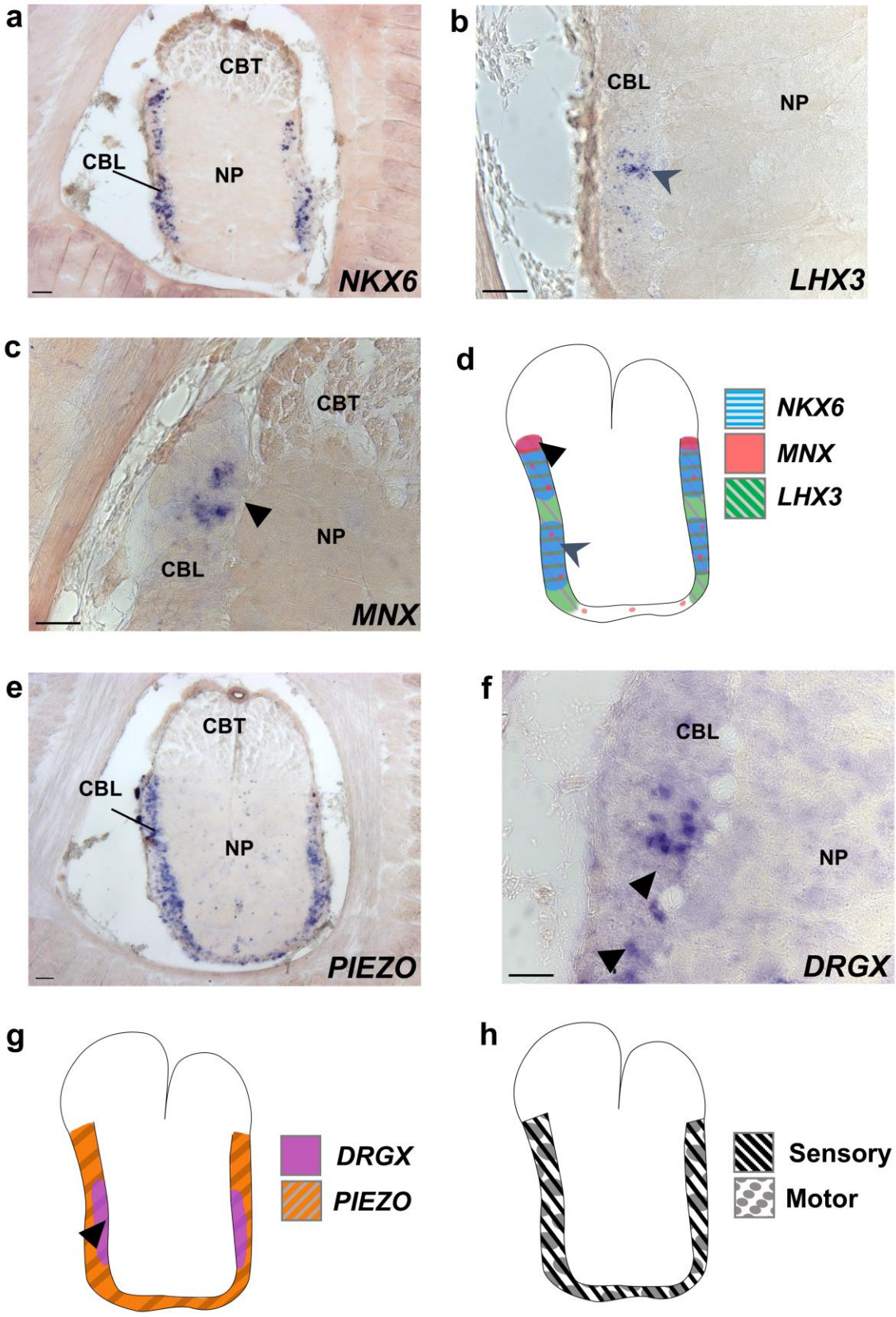
a
CBT
CBL
NP
NKX6
b
CBL
NP
LHX3
c
CBT
NP
CBL
MNX
d
NKX6
MNX
LHX3
e
CBT
CBL
NP
PIEZO
f
CBL
NP
DRGX
g
DRGX
PIEZO
h
Sensory
Motor

Figure 3.5: Markers of sensory and motor neurons label overlapping territories in the ANC.
a-d, ISH for motor neuron markers in ANC transverse sections. **(a)** *NKX6* (NK6 homeobox), **(b)** *LHX3* (LIMB homeobox 3), arrowhead points to expression, **(c)** *MNX* (Motor neuron and pancreas homeobox), arrowhead points to expression **(d)** Cartoon summary of motor neuron marker distributions. Expression is extensive in the lateral walls of the CBL. Arrowheads indicate where expression in **b** and **c** was found. **e-g,** Expression of sensory neuron markers in ANC transverse sections. **(e)** *PIEZO* (Piezo type mechanosensitive ion channel component), **(f)** *DRGX* (Dorsal root ganglia homeobox), arrowhead indicates expression. **(g)** Cartoon summary of sensory neuron marker distribution. Expression is also strong in the CBL lateral walls. Arrowhead indicates where expression in **e** was found. **h,** Diagram of overlapping sensory and motor neuron territories in the CBL. Scale bars: 50 μm. ANC, axial nerve cord; CBL, cell body layer.

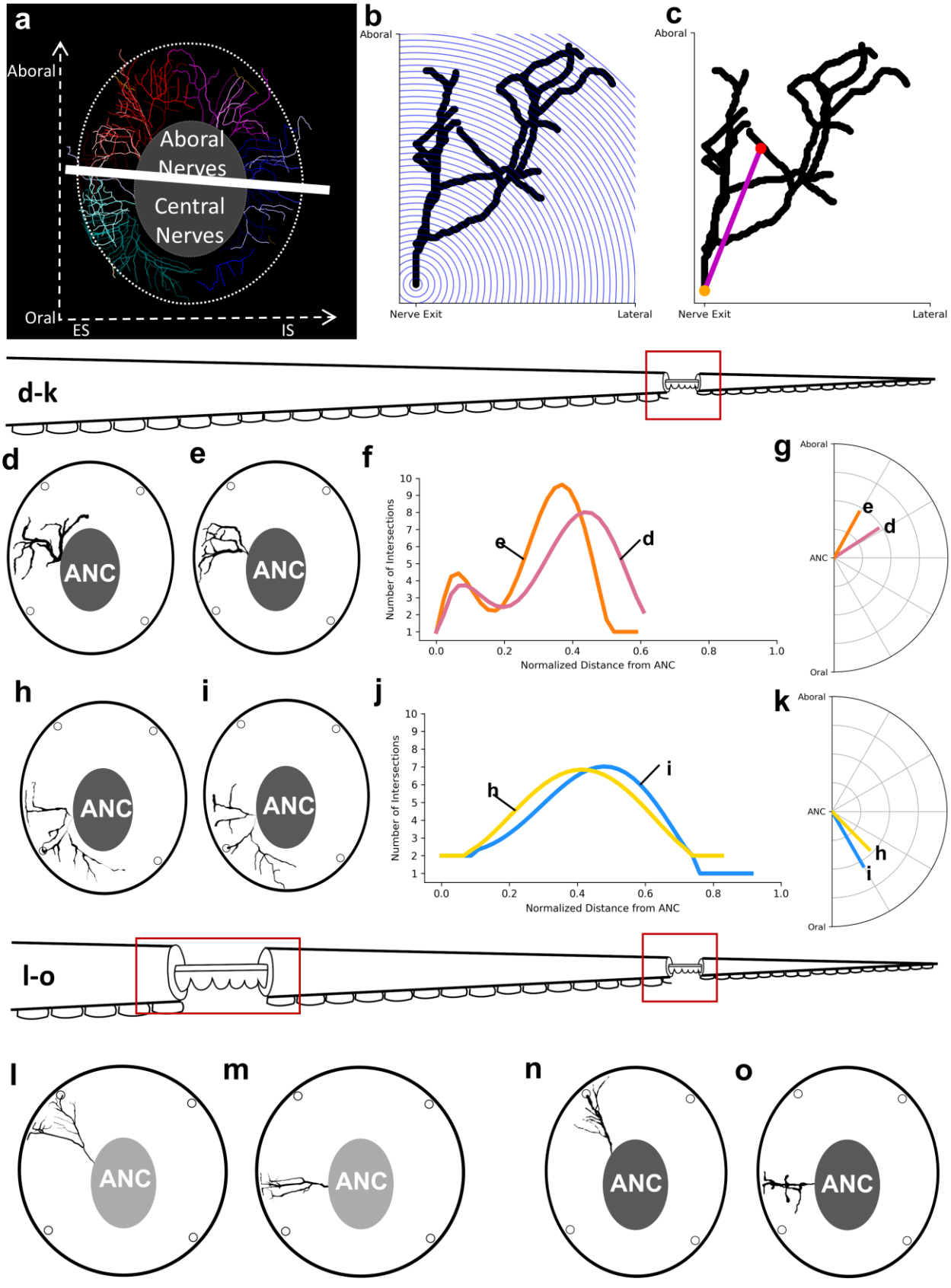
a
Aboral
Aboral Nerves
Central Nerves
Oral
ES
IS
b
Aboral
Nerve Exit
Lateral
c
Aboral
Nerve Exit
Lateral
d-k
d
ANC
e
ANC
f
Number of Intersections
Normalized Distance from ANC
e
d
g
Aboral
ANC
Oral
e
d
h
ANC
i
ANC
j
Number of Intersections
Normalized Distance from ANC
h
i
k
Aboral
ANC
Oral
h
i
l-o
l
ANC
m
ANC
n
ANC
o
ANC

Figure 3.6: Nerve fiber analysis.
a, Brachial nerves segmented out of transverse whole mount slice immunolabeled with acTUBA. Brachial nerve fibers can be split into aboral nerves and central nerves based on ANC exit location. **b,** Diagram depicting Sholl analysis on an example nerve. Branching is characterized as the number of intersections between the nerve fiber and a series of spheres centered at the nerve exit, with an increasing radius of 10 μm. Three-dimensional data were analyzed, with example portrayed here in two-dimensions. **c,** Schematic of the average trajectory, which is a vector created from the nerve exit point to the center of the processes. **d-k**, Within the same slice, similarities in nerve fibers are found separated by more than one segment. **d, e,** Transverse diagrams with two aboral nerves that have similar morphologies. These nerves also have **(f)** similar Sholl profiles and **(g)** average trajectories. **h, i,** Transverse diagrams with two central nerves that have similar morphologies. These nerves also have **(j)** similar Sholl profiles and **(k)** average trajectories. **l-o,** Similarities in nerve fiber morphologies can be found when comparing proximal and distal slices. An aboral nerve from a proximal slice in **(l)** is similar to a selected aboral nerve from a distal slice in **(n).** A central nerve from a proximal slice in **(m)** is similar to a selected central nerve from a distal slice in **(o)**.

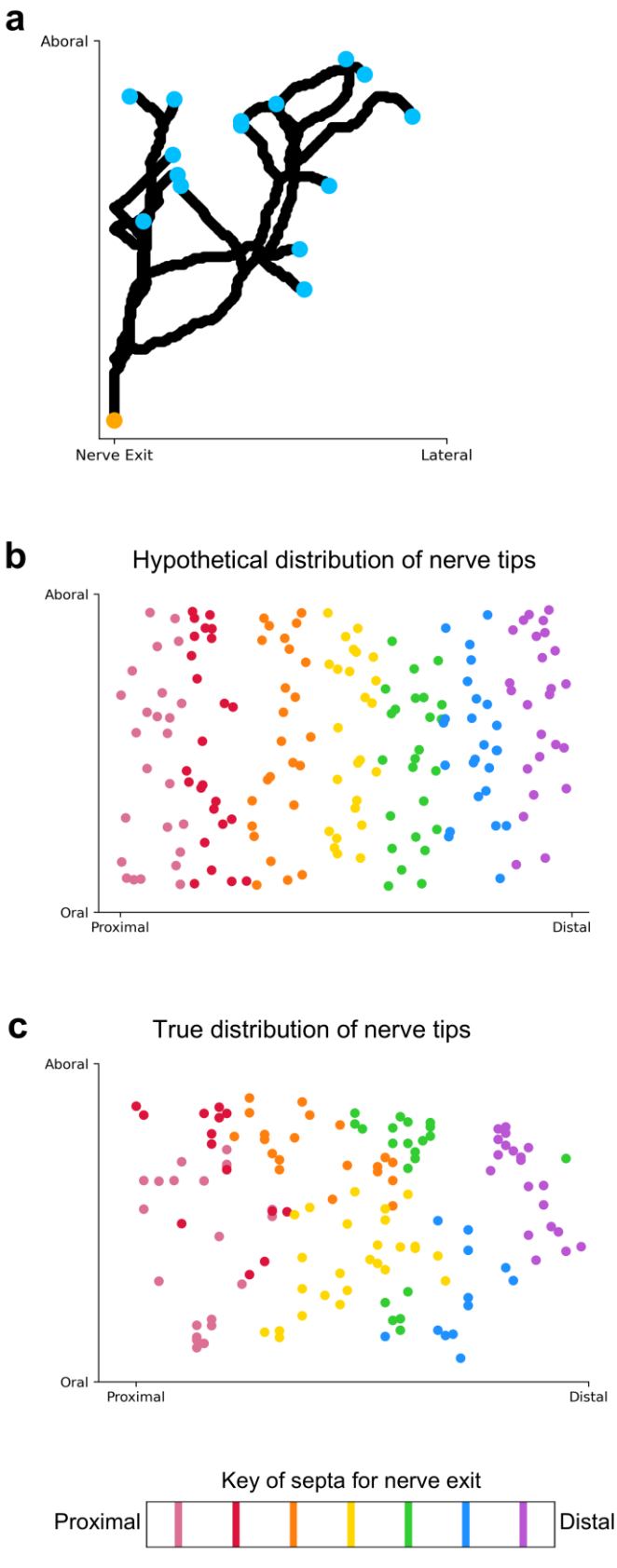
a
Aboral
Nerve Exit
Lateral
b
Hypothetical distribution of nerve tips
Aboral
Oral
Proximal
Distal
c
True distribution of nerve tips
Aboral
Oral
Proximal
Distal
Key of septa for nerve exit
Proximal
Distal

Figure 3.7: Distribution of brachial nerve tips.
a, Example brachial nerve with nerve tips labeled. **b,** Hypothetical distribution of nerve tips across the proximal-distal axis, colored by ANC exit point. Nerves exiting from one septum fully cover the aboral-oral extent of the brachial musculature and do not intercalate with nerves exiting from other septa. **c,** True distribution of nerve tips across the proximal-distal axis, colored by ANC exit point. Only nerve fibers from multiple septa added together cover the aboral-oral extent of the brachial musculature.

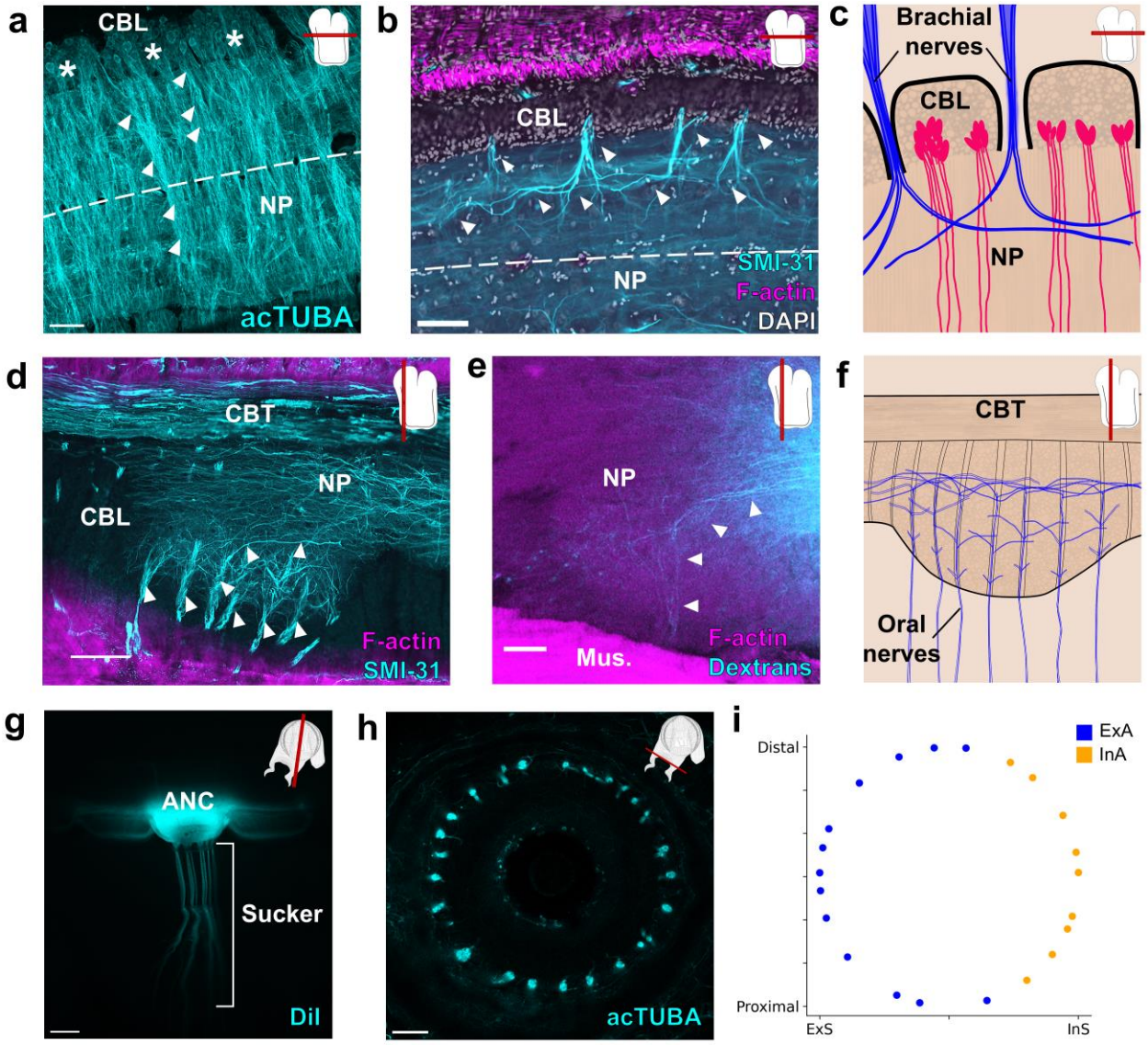

Figure 3.8: Organization of the neuropil (np) and the innervation patterns of the suckers. **a-c,** Aboral, or brachial, NP. (**a**) Maximum projection of a horizontal acTUBA wholemount (cyan), showing that the bulk of each cell body segment extends its processes into the NP of the segment. Some processes cross the midline (dashed line). * denotes individual segments. Arrowheads point to cell body projections. Representative sample from 12 explants. (**b**) Horizontal section immunostained with SMI-31 (cyan), phalloidin (magenta) and DAPI (gray). SMI-31-rich subpopulation of nerve fibers (cyan, denoted with arrowheads) branch proximally and distally upon entering the ANC. Representative sample from 13 explants. (**c**) Diagram of a horizontal section through the brachial NP. Nerve fibers (blue) pool across neurons (magenta) arranged in segments. Scale bars: 100 µm. **d-f**, Oral, or sucker, NP. (**d**) Longitudinal ANC section stained with SMI-31 (cyan) and phalloidin (magenta). NP fibers (cyan) collect into internal fascicles before exiting as oral nerves, indicated with arrowheads. Representative sample from 13 explants. (**e**) Longitudinal section of NP dextran tracer-deposit (cyan) demonstrating NP fibers forming a fascicle, pointed to by arrowheads. Representative sample from 6 explants. (**f**) Diagram of NP fibers in the longitudinal plane. From oral to aboral, oral nerves enter the ANC,

first showing local branching, then more extensive branching. Scale bars: 100 μm. **g-i**, Oral ANC nerves distributed around a sucker. (**g**) Longitudinal whole mount. DiI crystal (cyan) placed in a single ANC sucker enlargement targets a single sucker. Representative sample from 4 explants. Scale bar: 500 μm. (**h**) Horizontal acTUBA-stained section through a sucker demonstrates radially symmetric decoration. Representative sample from 34 explants. Scale bar: 100 μm. (**i**) Distribution of oral nerve fiber tips around a sucker. Nerves from the external ANC side (ExA) are tagged in blue; nerves from the internal side (InA), in orange. Data from a transversely imaged whole mount stained with acTUBA. The ExA covers 68% of the sucker; the InA, 32%.

The sucker is the second major target of the ANC, and we examined the relationship of oral roots innervating the sucker to the ANC segmentation. The expansion of the oral ANC opposite to each sucker was targeted for axon tracing, and, as the example illustrated in Fig. 3.8g demonstrates, the oral nerves arising from each enlargement target a single sucker. This result was confirmed with acTUBA immunostaining (Fig. 3.9j). After exiting the ANC in the septa, the oral roots radially tile the sucker, reaching both the muscles of the sucker and the chemotactile sensory epithelium on the rim of the sucker (Fig 3.8h, Fig. 3.9k, l, m). Nerve fibers from neighboring septa target adjoining territories along the sucker (Fig. 3.9l). This arrangement establishes a spatial topography for the sucker in the ANC ("suckerotopy") based on nerve exits.

We next followed the oral nerves into the ANC neuropil, where they maintain their spatial segregation, establishing an internal ANC suckerotopy (Fig. 3.8d). As demonstrated by DiI crystal placement within a sucker, the oral nerves enter on both sides of the ANC (Fig. 3.10g). Nerve fibers first branch locally, demonstrating short-range projections to ipsilateral nerves entering in adjoining septa (Fig. 3.8d, Fig. 3.9h, i). As the oral roots progress further into the NP, they show projections to NP on the contralateral side (Fig. 3.9g, h). Lastly, the oral roots branch to engage in mid-range projections to the ANC segments of adjoining suckers (Fig. 3.8d, e, f). This circuitry demonstrates pathways for both intra-sucker and inter-sucker communication.

Because the oral nerves for a single sucker enter on both sides of the ANC, nerves arising from one side of the ANC connect to the internal side of the sucker (InS) and nerves arising from the other side connect to the external side of the sucker (ExS) (Fig. 3.10a, b). We discovered that segments are expanded on the ExS of the ANC (ExA) as compared with the InA (Fig. 3.10d, e). Since segments correspond to spatial territories along the sucker, this arrangement suggests that more neural territory is dedicated to the ExS. Accordingly, we found the oral roots corresponding

to the ExS cover approximately 65% of the sucker, whereas the roots issued to the InS cover the remaining 35% (Fig. 3.8i, Fig. 3.9h-j). The sucker sensory epithelium is evenly innervated, with no obvious bias to the ExS side over the InS side (Fig. 3.8h, Fig. 3.9m). Consequently, the asymmetry in segment width is accounted for by an asymmetry in the amount of spatial territory covered, indicating an anisotropic sensory-motor topographic map for a sucker in the ANC.

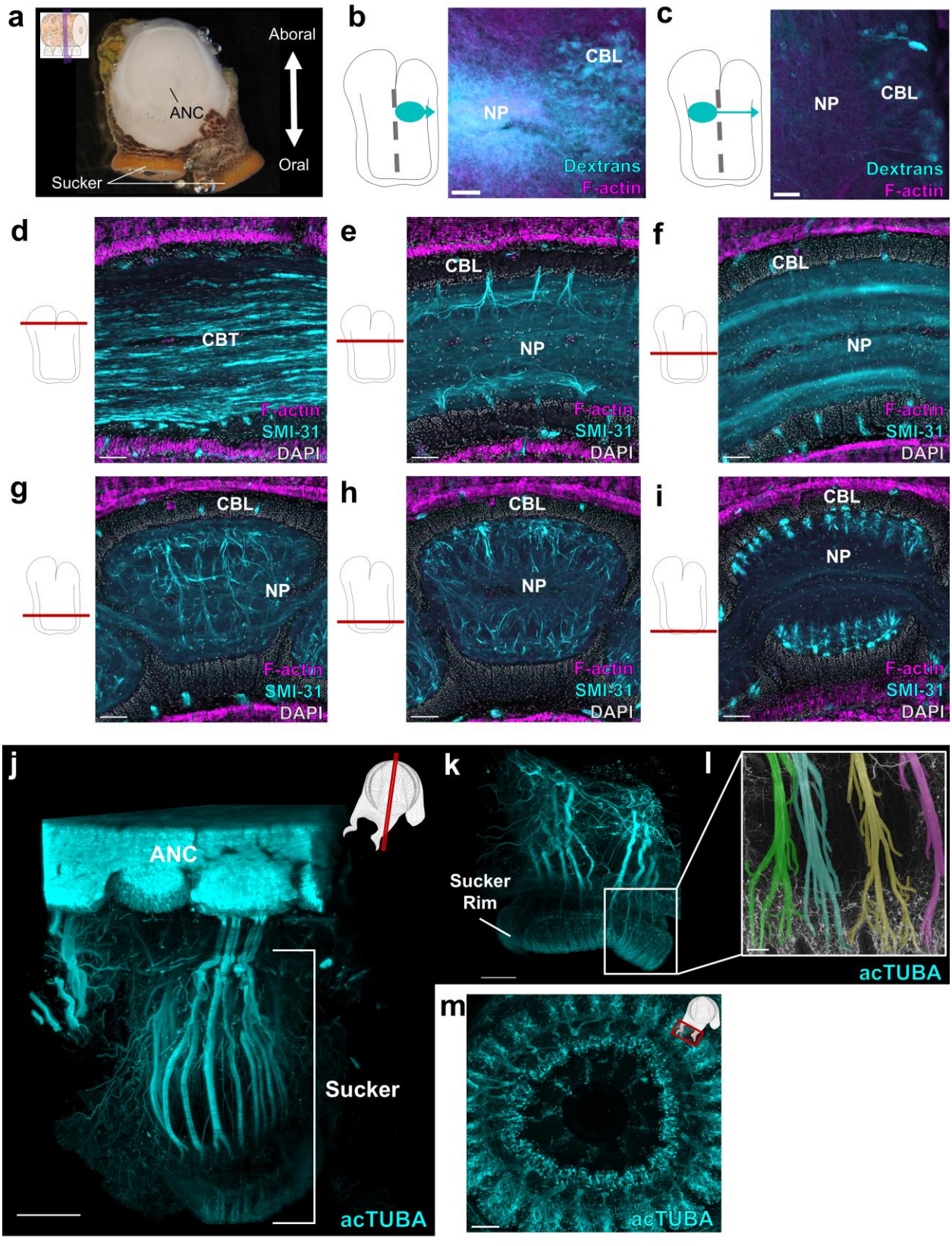
a
Aboral
ANC
Oral
Sucker
b
CBL
NP
Dextrans
F-actin
c
NP
CBL
Dextrans
F-actin
d
CBT
F-actin
SMI-31
DAPI
e
CBL
NP
F-actin
SMI-31
DAPI
f
CBL
NP
F-actin
SMI-31
DAPI
g
CBL
NP
F-actin
SMI-31
DAPI
h
CBL
NP
F-actin
SMI-31
DAPI
i
CBL
NP
F-actin
SMI-31
DAPI
j
ANC
Sucker
acTUBA
k
Sucker
Rim
l
acTUBA
m
acTUBA

Figure 3.9: Neuropil organization.
a, Example transverse slice used for tracer injections. Injections of dextrans were made into the axial nerve cord (ANC). **b,** Transverse section of an injection of dextran (cyan) demonstrating ipsilateral connections to the cell body layer (CBL). Scale bar: 50 μm. **c,** Transverse section of an injection of dextran (cyan) into the neuropil (NP) demonstrating contralateral connections arising from the CBL. Scale bar: 50 μm. **d-i,** Horizontal series stained with SMI-31 (cyan), F-actin (magenta) and DAPI (gray) through the ANC from aboral **(d)** to oral **(i)**. SMI-31 labels a subpopulation of nerve fibers and is useful for illustrating key selected features of fiber architecture. Scale bars: 100 μm**. (d)** Cerebrobrachial tract (CBT) composed of two massive longitudinally running fiber bundles. **(e)** Brachial territory of the ANC. SMI-31 brachial nerves branch in proximal and distal directions, pooling over segments. **(f)** Interface between the brachial territory and the sucker territory of the ANC. This territory is dominated by longitudinally running tracts. **(g-i)** Sucker territory of the ANC, progressively showing **(g)** clear contralateral connections and links to adjoining suckers, **(h)** more restricted intermediate ipsilateral connections, and **(i)** highly local ipsilateral connections. **j,** Maximum projection of a longitudinally cut whole mount labeled with acTUBA (cyan). The oral nerves originate from a sucker enlargement and directly target the corresponding sucker. Scale bar: 500 μm. **k,** Maximum projection of a whole mount of a sucker labeled with acTUBA. The oral nerves can be traced to the sensory epithelium lining the sucker rim. Scale bar: 500 μm. **l,** Oral nerves false colored in their position in the sensory epithelium. Neighboring nerve fibers target adjoining territories along the sucker rim. Scale bar: 100 μm. **m,** Maximum projection of a horizontal slice through a sucker whole mount labeled with acTUBA (cyan). The sensory epithelium is evenly and densely innervated. Scale bar: 100 μm.

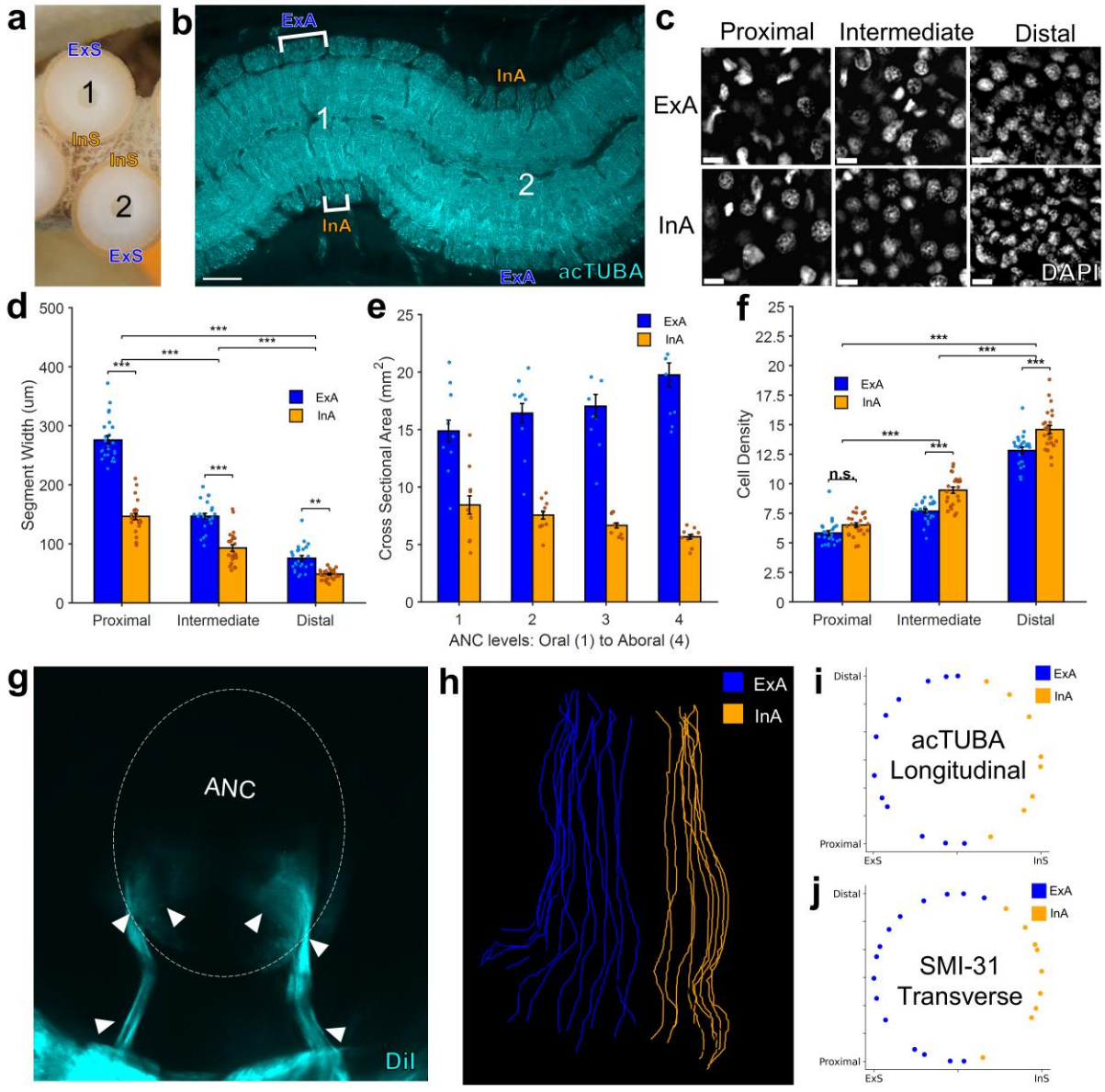

Figure 3.10: External and internal sides of the axial nerve cord (ANC).
a, The sucker can be divided into the internal side (InS), which hugs the midline of the arm, and the external side (ExS). **b,** Horizontal section through the ANC stained with acTUBA (cyan). One side of the ANC (ExA) overlies to sucker's ExS, and the other (InA) corresponds to InS. The numbering in (**b)** corresponds to the numbering in (**a)**. Scale bar: 100 µm. **c,** Example patches of DAPI labeling in the ANC used for cell density calculations. Scale bar: 10 µm. **d,** Width measurements of Arm 1 ANC CBL segments split into ExA (blue) and InA (orange). Segments on ExA were significantly wider than segments on InA. n = 24 per condition, error bars +/- sem, **p<0.01, ***p<0.001, 2-way ANOVA, with post hoc Tukey's test. **e,** Cross-sectional area of segments taken from four horizontal sections stained with acTUBA and spanning the oral to aboral extent of the ANC. Segments corresponding to ExA (blue) had larger

cross-sectional areas compared to InA segments (orange). n = 9 per condition, error bars +/- sem. **f,** Cell density calculations. Cell density significantly increases from proximal to distal and is significantly larger for InA segments in the intermediate and distal slices. n = 24 per condition, error bars +/- sem; n.s., not significant, ***p<0.001, 2-way ANOVA, with post hoc Tukey's test. **g,** Transverse wholemount with DiI (cyan) crystal placed in a single sucker. The oral nerves enter the ANC on both the InA and ExA. Arrowheads follow DiI positive nerve fibers as the enter the ANC. **h,** Traced oral nerve fibers from a transverse whole mount labeled with acTUBA, and tagged for ExA (blue) and InA (orange) targeting. **i,** Distribution of oral nerve tips traces from a longitudinal whole mount stained with acTUBA. ExA covered 63%; InA, 37%. **j,** Distribution of oral nerve tips traces from a transverse whole mount stained with SMI-31. ExA covered 64.5%; InA, 35.5%.

Comparative analysis:

We carried out a comparative analysis to clarify the relationship between ANC segmentation and function by examining the organization of the ANC of the longfin inshore squid, *Doryteuthis pealeii*. Squids, which diverged from octopuses 270 million years ago, have two tentacles in addition to eight sucker-lined arms (Albertin et al., 2022; Fig. 3.11a, e, i). Like octopuses, these limbs are muscular hydrostats, yet they differ in gross morphology and function (Kier and Smith, 1985; Kier, 2016). Where *O. bimaculoides* is benthic, with arms suited for exploration and movement on the seafloor, *D. pealeii* is a pelagic animal and primarily uses its arms and tentacles for prey capture in open water (Hanlon and Messenger, 2018). The tentacle stalks, which are devoid of suckers, rapidly elongate to grab prey with tentacle clubs, the sucker-rich ends of the tentacles. The arms enclose the prey in a coordinated movement as the prey is brought back to the mouth. Morphological differences between squid arm and tentacle muscle composition underlying this functional difference have been described (Kier, 1985, 2016).

In both the arms, tentacle stalks and clubs of *D. pealeii*, there is an ANC mediating sensorimotor control (Fig. 3.11b, f, j). The ANC in the squid has a notably different arrangement from that of octopus, however. The CBL is restricted to the ANC lateral edges, with large longitudinally running fiber-tracts both orally and aborally (Fig. 3.11b, f, j). In the tentacle, the CBL thins along the stalk but expands in the sucker-rich club (Fig. 3.11f, j). We used gene expression and phalloidin staining to look for segmentation in the squid CBL. The CBL in the arm of the squid is segmented, with approximately 4.5 segments per sucker (Fig. 3.11c, d). As in *O. bimaculoides*, F-actin is localized to the ANC septa (Fig. 3.12a). In the tentacle stalk, however, CBL segments as identified by synaptotagmin 1 (*SYT1*) gene expression are at best indistinct, and although F-actin marks regularly spaced vasculature, these are not in the CBL

(Fig. 3.11g, h, Fig. 3.12b). In the sucker-rich tentacle club, by contrast, CBL segments marked by *SYT1* and F-actin within the CBL are readily identified (Fig. 3.11k, l, Fig. 3.12c). This comparative anatomy suggests a strong link between ANC segmentation and flexible cephalopod arms lined with suckers.

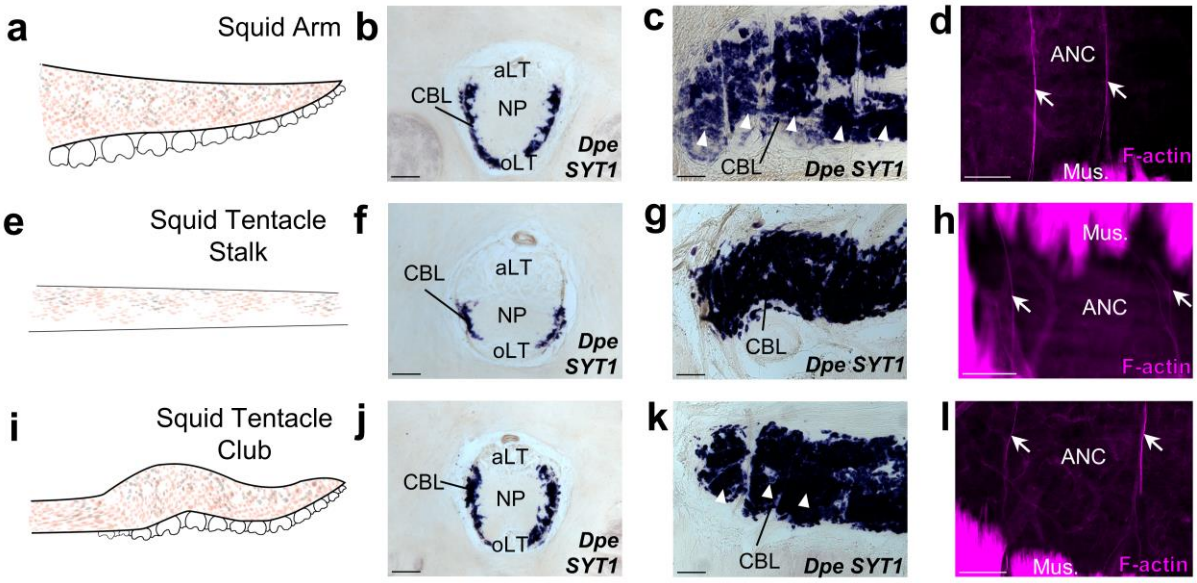

Figure 3.11: Segmentation is a shared feature of flexible, sucker-laden cephalopod appendages.
a-d The axial nerve cord (ANC) of the *D. pealeii* arm is segmented. (**a**) Cartoon depiction of *D. pealeii* arm, which has suckers. (**b**) ISH for *Dpe SYT1* of an ANC transverse section labeling the cell body layer (CBL). Representative sample from 3 explants. (**c**) ISH for *Dpe SYT1* of an arm longitudinal section demonstrates CBL segmentation. Representative sample from 5 explants. (**d**) F-actin (magenta) marks vasculature in the arm ANC septa. Representative sample from 3 explants. **e-h,** The ANC of the tentacle stalk lacks CBL segmentation. (**e**) Cartoon depiction of *D. pealeii* tentacle stalk which is devoid of suckers. (**f**) Transverse ISH section for *Dpe SYT1* demonstrates a clear, although reduced, tentacle CBL. Representative sample from 3 explants. (**g**) *Dpe SYT1* ISH of a longitudinal ANC section does not show CBL segmentation in the tentacle stalk. Representative sample from 3 explants. (**h**) F-actin (magenta) demonstrates a regularly arranged vasculature in the tentacle stalk, but these blood vessels do not lie within the CBL. Representative sample from 4 explants. **i-l,** The ANC in the tentacle club has segments. (**i**) Cartoon depiction of *D. pealeii* tentacle club, which is located at the end of the stalk and has suckers. (**j**) Transverse ISH section for *Dpe SYT1* in the tentacle club ANC demonstrates the CBL. Representative sample from 2 explants. (**k**) Longitudinal *Dpe SYT1* section of the tentacle

club CBL shows segmentation. Representative sample from 2 explants. (**l**) F-actin (magenta) identifies regularly in the tentacle club septa. Representative sample from 2 explants. White arrowheads in (**c, k**) point to CBL segments. White arrows in (**d, h, l**) indicate phalloidin-labeled blood vessels. aLT, aboral longitudinal tract; oLT, oral longitudinal tract. Scale bars: 100 μm.

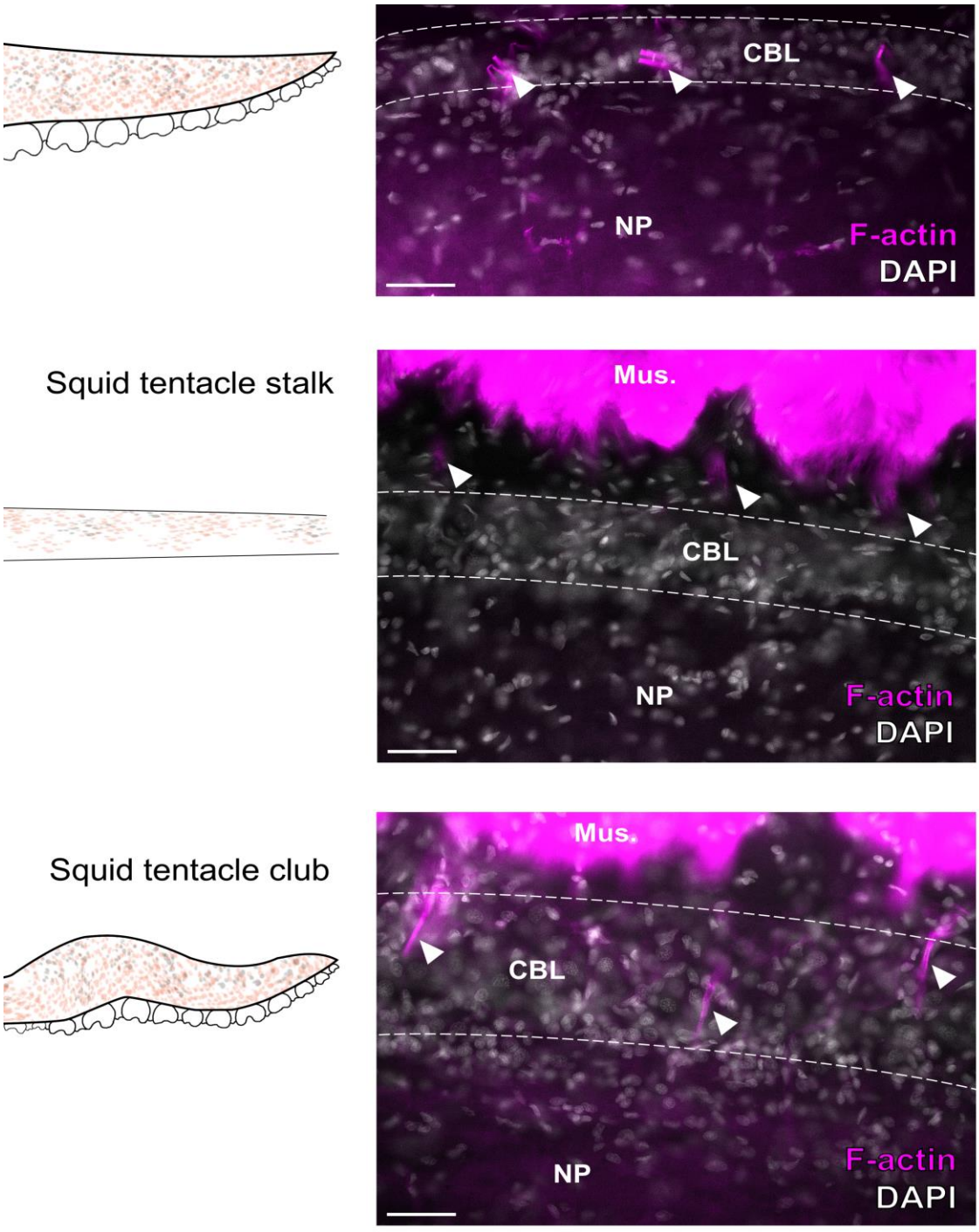

Figure 3.12: Localization of F-Actin in *D. pealeii* axial nerve cord (ANC).
a, Horizonal section through the ANC in *D. pealeii* arm stained for F-actin (magenta) and DAPI (gray). F-actin projections are contained within the CBL, indicated by white arrowheads. **b,** Horizontal section through the ANC in *D. pealeii* tentacle stalk stained for F-actin (magenta) and DAPI (gray). F-actin projections are beyond the CBL, indicated by arrowheads. **c,** Horizontal section through the ANC in *D. pealeii* tentacle club stained for F-actin (magenta) and DAPI (gray). F-actin projections are again within the cell body layer, indicated by arrowheads. Scale bars: 100 μm.

DISCUSSION

The cephalopod arm is a highly redundant structure, with both suckers and the pattern of brachial musculature repeated down its length (Hochner et al., 2023; Olson and Ragsdale, 2023). A parcellation of the ANC into segments is a natural way to relegate motor control of a continuous limb with such a reiterated structure. In fact, many computational models and soft robots inspired by octopus arms divide the arm into repeated segments in their construction or control algorithms (Yekutieli et al., 2005; Rus and Tolley, 2015; Kang et al., 2016; Laschi et al., 2016). Our results, however, demonstrate additional complexities. For the brachial musculature, different sets of nerves exit from adjoining septa, while still providing coverage of the musculature. Instead of a single segment representing the full cylinder of brachial musculature, as is the case in many models, adjoining segments coordinate in parsing control for the muscles. This circuit structure could more effectively smooth continuous movements along the length of the arm, as well as isolate contractions to localized territories in the brachial musculature. The brachial musculature also contains peripheral nervous system elements, such as the intramuscular nerve cords, to which the nerves connect. These peripheral mechanisms could serve as additional pathways for communication between nerves, further linking nerves that are separated by multiple segments.

The ANC contains enlargements corresponding to the location of the suckers (Rossi and Graziadei, 1954; Graziadei, 1971). The neuronal segments described here further subdivide these

swellings into multiple modules. Classic studies have proposed that much of the sensorimotor processing in suckers occurs within the epithelium or in the sucker ganglion, and that by the time the information reaches the ANC, it has been highly downsampled (Graziadei, 1965b; Graziadei and Gagne, 1976). Our investigation of nerve fiber connections illustrates that, at the least, spatial information is preserved within the ANC, creating a suckerotopy. Combined with the projections that interconnect suckers, such a neural architecture would support many behaviors seen in suckers, from passing objects along the suckers to the anisotropic detection of chemical cues (Altman, 1971; Grasso, 2008; Sivitilli et al., 2022; Kang et al., 2023). In particular, deformation of individual suckers has been thought to underlie shape discrimination (Wells, 1964). This spatial mapping could be the basis for ring attractor computations by the axial nerve cord to guide sucker movements in response to sensory cues. Such a mechanism has been described for spatial navigation in the central complex of *Drosophila* (Kim et al., 2017), and recently it has been suggested in biophysical models of directed movements by octopus arms (Wang et al., 2024).

Molluscs are a diverse phylum, and cephalopods in particular exhibit many derived morphologies. Our comparative analysis emphasizes that this segmentation is a derived feature in flexible, sucker-laden arms. Segments are present in the arm and tentacle club in *D. pealeii,* yet they are indistinct in the stalk which is devoid of suckers. Interestingly, there are fewer segments per sucker in the arm of *D. pealeii* compared with that of *O. bimaculoides.* Differences in ecological niche and behavioral repertoire, including prey hunting strategies, could drive this variation (Hanlon and Messenger, 2018; Kang et al., 2023).

There has long been a vigorous discussion in the evolutionary and developmental biology fields about whether segmentation is an ancestral feature of bilateral animals (Chipman, 2019).

In molluscs, segmentation has been proposed as a shared feature of polyplacophorans (chitons) and monoplacophorans (Lemche, 1957; Vagvolgyi, 1967), but the evolutionary interpretations of this similarity has been hotly contested (Wilson et al., 2010; Redl et al., 2014; Wanninger and Wollesen, 2019; Kocot et al., 2020) and, at the least, has not been proposed to encompass the nervous system. A second view of segmentation is that it represents an adaptation useful for generating vermiform movements (Clark, 1964; Vagvolgyi, 1967). Our findings provide a clear example of the second view, that of derived segmentation linked to the control of the motor patterns characteristic of soft-bodied cephalopod (coleoid) arms. This segmentation shares many similarities to segmentation described in other systems: multiple tissue types, reiterated patterning along a longitudinal axis, and utilization for sensorimotor control circuitry (Lumsden and Keynes, 1989; Campos-Ortega and Hartenstein, 1997; Hubaud and Pourquié, 2014; Clark et al., 2019). Whether in development ANC segment generation shares any similarities to segmental patterning mechanisms in other animals (Chipman, 2019) will be important to investigate in future studies. At the adult functional and structural levels, however, the coleoid segmentation appears to reflect one role, that of setting up recurring neuronal modules dedicated to the control of muscles and suckers which are themselves reiterated down the length of the arms.

CHAPTER 4

Longitudinal tracts in the axial nerve cord

INTRODUCTION

Many behaviors, from locomotion to feeding, require the octopus to coordinate motor activity along the length of an arm and between arms (Gutfreund et al., 1998; Sumbre et al., 2006; Kennedy et al., 2020; Bidel et al., 2022). The octopus axial nerve cord (ANC), situated in the center of the brachial musculature, is thought to handle much of the motor control for the arm in coordination with higher motor areas in the octopus brain (Graziadei, 1971; Young, 1971; Hochner et al., 2023; Olson and Ragsdale, 2023). The ANC contains a cell body layer (CBL) that wraps around its neuropil (NP). The CBL is segmented down the long axis of the arm, and the CBL and NP can also be split into an oral sucker territory and an aboral brachial territory (Rowell, 1963; Olson et al., 2025). The oral sucker territory of the ANC forms local enlargements corresponding to each sucker (Rossi and Graziadei, 1954; Olson et al., 2025). While ANC segments in the CBL and the division for brachial and sucker territories provide the structure for parsing the arm into smaller units for local control, they do not account for how movements of the suckers and the arm itself over a distance are controlled and coordinated.

The octopus ANC features a cerebrobrachial tract (CBT) situated aborally to the CBL and NP (Fig. 4.1). The CBT comprises two massive trunks of longitudinally running fibers that interconnect the arms and the brain (Graziadei, 1971; Zullo et al., 2019). Classic studies have noted a parcellation of CBT fibers based on size, though their relative functions are unknown (Graziadei, 1971). These studies also suggested shorter interconnecting systems within the NP. For motor control along the proximal-distal axis of an arm, one possibility is that brain orchestrates the movements by relaying signals through the CBT to activate specific segments.

Recent electrophysiological experiments instead posit that the CBT transmits motor signals *en passant,* allowing for an interplay between signals from the brain and ANC circuitry (Zullo et al., 2019). These studies are, however, few in number, and there is little experimental evidence for how longitudinally running tracts in the CBT are organized.

Similar to octopus, behaviors like prey capture in squid require coordination along the long axis of the arms and tentacles (Kier and Smith, 1985; Kier, 2016; Hanlon and Messenger, 2018). Instead of a single CBT-like structure, the ANC of the squid, *Doryteuthis peallii* has an aboral and oral longitudinal tract (Olson et al., 2025). Beyond this observation, there are no further descriptions of longitudinal fibers tracts in squid.

Here, we explore the organization of the CBT in *Octopus bimaculoides* using modern cellular and molecular methods. We further interrogate the ANC NP for additional longitudinal fiber tracts using tract-tracing methods. We also examine the structure of the longitudinally running tracts in the squid, *D. pealeii.*

RESULTS

Organization of the cerebrobrachial tract:

We confirmed in *O. bimaculoides* that the CBT consists of two trunks of nerves located at the most aboral portion of the ANC (Fig. 4.1a, c). As demonstrated by in situ hybridization with *CPLX1*, the CBT is devoid of neuronal cell bodies (Fig 4.1b). The area of the CBT decreases from proximal to distal, as does the total area of the ANC (Fig. 4.1d, e). Moreover, the proportion of the total ANC area occupied by the CBT does not remain constant, but decreases proximal to distal (Fig. 4.1f). This is reminiscent of spinal cord tracts, which are largest closest to the brain.

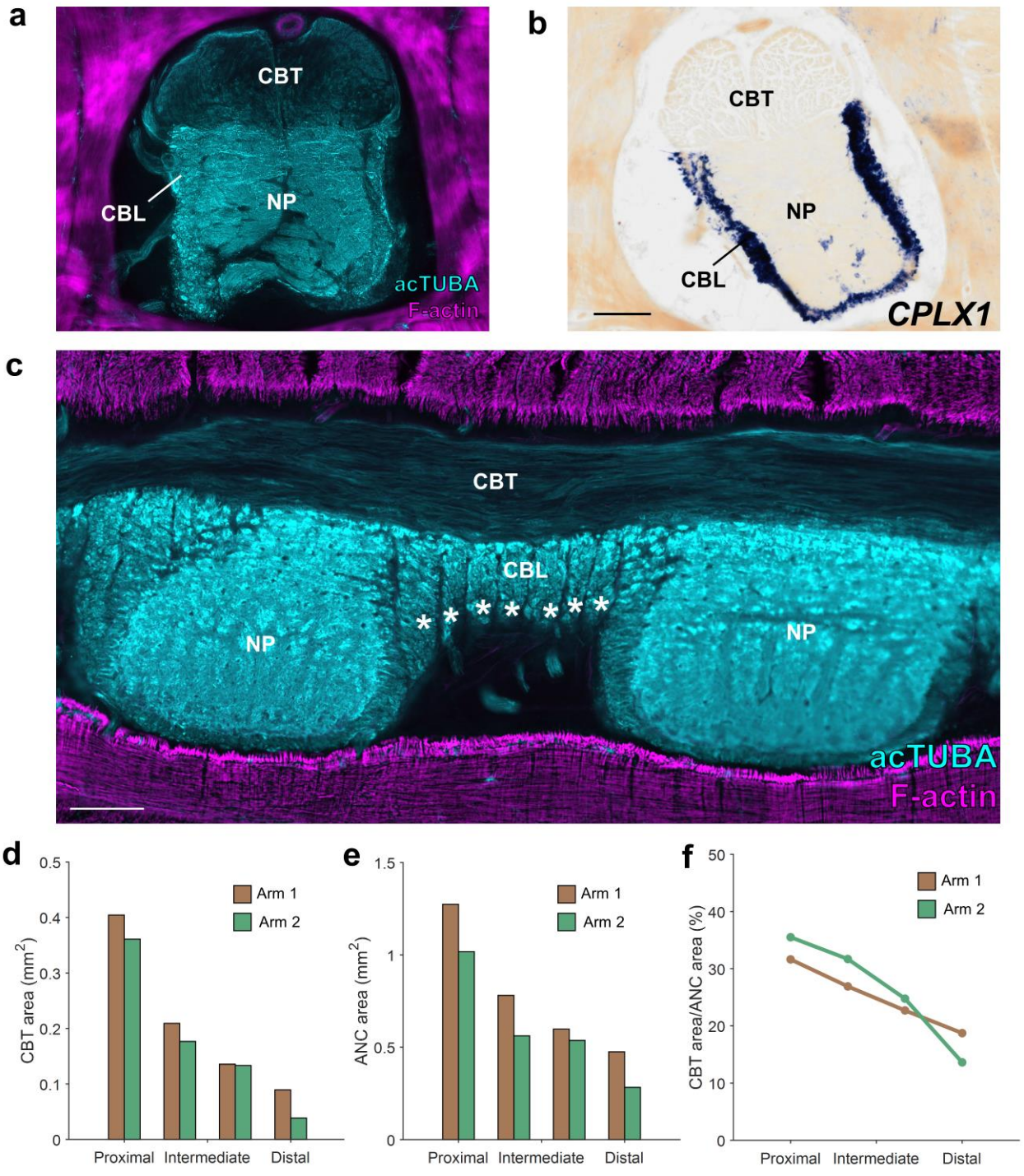

Figure 4.1: Cerebrobrachial tract composition and proximal-distal variation.
a, Transverse section of the axial nerve cord (ANC) stained for acetylated α-tubulin (acTUBA, cyan) and F-actin (magenta). The cerebrobrachial tract (CBT) is aboral to the cell body layer (CBL) and neuropil (NP) and is composed of acTUBA positive fibers. **b,** In situ hybridization (ISH) for complexin 1 (*CPLX1)* in a transverse section of the ANC labels neuronal cell bodies.

Notably, the CBT is devoid of labeling. Scale bar: 250 μm. **c,** Longitudinal section of the ANC stained for acTUBA (cyan) and F-actin (magenta). CBT fibers are oriented longitudinally. CBL segments, denoted by *, are readily apparent in this preparation. Scale bar: 250 μm. **d, e,** Area of the CBT (**d**) decreases from proximal to distal as does the total area of the ANC (**e**). Total ANC area = CBL area + NP area + CBT area. **f**, The proportion of total ANC area occupied by the CBT decreases from proximal to distal. acTUBA, acetylated α-tubulin; ANC, axial nerve cord; CBL, cell body layer; CBT cerebrobrachial tract; NP, neuropil.

We next asked if the CBT has subdivisions by examining the CBT in transverse whole mounts immunostained for acetylated α-tubulin (acTUBA). We found four distinct bundles that could be detected along the proximal-distal axis of a single arm and between two arms: α, β, δ, and γ tracts (Fig. 4.2). These bundles are paired and mirror symmetric across the two CBT trunks. The α tracts are situated aborally and are the most prominent with labeling for acTUBA. The β tracts are oral to the α tracts and hug the midline. The δ and γ tracts are likewise oral to the α tracts, though distributed laterally. The δ tract is positioned closest to the NP, and the γ tract is located aboral to the δ tract. These tracts also demonstrate further sub-compartments, like those seen in the α tract on the distal slice (Fig. 4.2a, b) or the γ tract on the proximal slice (Fig. 4.2g, h). However, we failed to detect these sub-compartments across all slices. This could imply that the fibers in the tracts reorganize along the proximal-distal axis, or it could be an artifact of the method used to determine subdivisions.

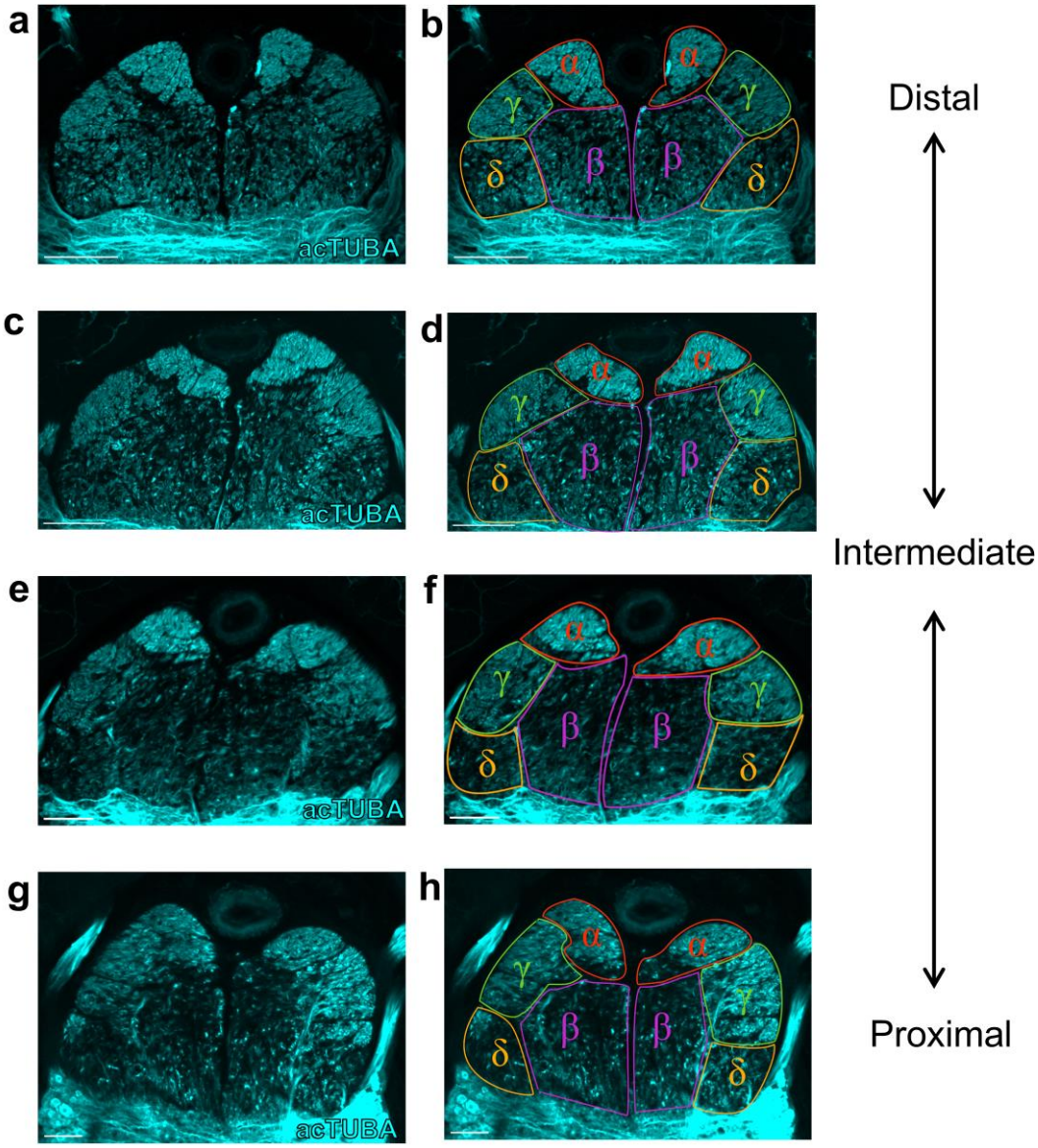

Figure 4.2: Subdivisions of the cerebrobrachial tract.
a-h, Maximum projections of the cerebrobrachial tract (CBT) in transverse whole mount slices from distal (**a, b**) to proximal (**g, h**) stained for acetylated α-tubulin (acTUBA). The CBT can be subdivided into four major tracts: α (red), β (magenta), δ (orange), and γ (green) tracts. Data used to define the tracts is presented in the left column (**a, c, e, g**). Tracts are outlined in the right column (**b, d, f, h**). Scale bars: 100 μm. acTUBA, acetylated α-tubulin.

The CBT demonstrates many connections with the NP, with large processes targeting the aboral α tract and smaller processes targeting more oral bundles (β and δ tracts; Fig. 4.3a). DiI crystal placements in the oral, sucker territory of the ANC NP (Fig. 4.3b) or in the sucker musculature (Fig. 4.3c) elicit extensive labeling of the large connections to the α tract. Once these processes reach the α tract, they split into both proximal and distal branches (Fig. 4.3c). DiI crystal placement into the aboral brachial NP demonstrates labeling in β, δ, and γ tracts, but not the α tract (Fig. 4.3d). Injections of dextrans into the aboral brachial NP label smaller projections innervating the β and δ tracts (Fig. 4.3e). This implies that the β, δ, and γ tracts correspond to connections with the brachial musculature, though connections with the sucker could also be labeled through fibers of passage. Notably, the dextran injections label the ipsilateral CBT trunk, but not the contralateral (Fig. 4.3e). In sum, these results suggest that information for the brachial musculature and the sucker may travel in spatially distinct territories within the CBT.

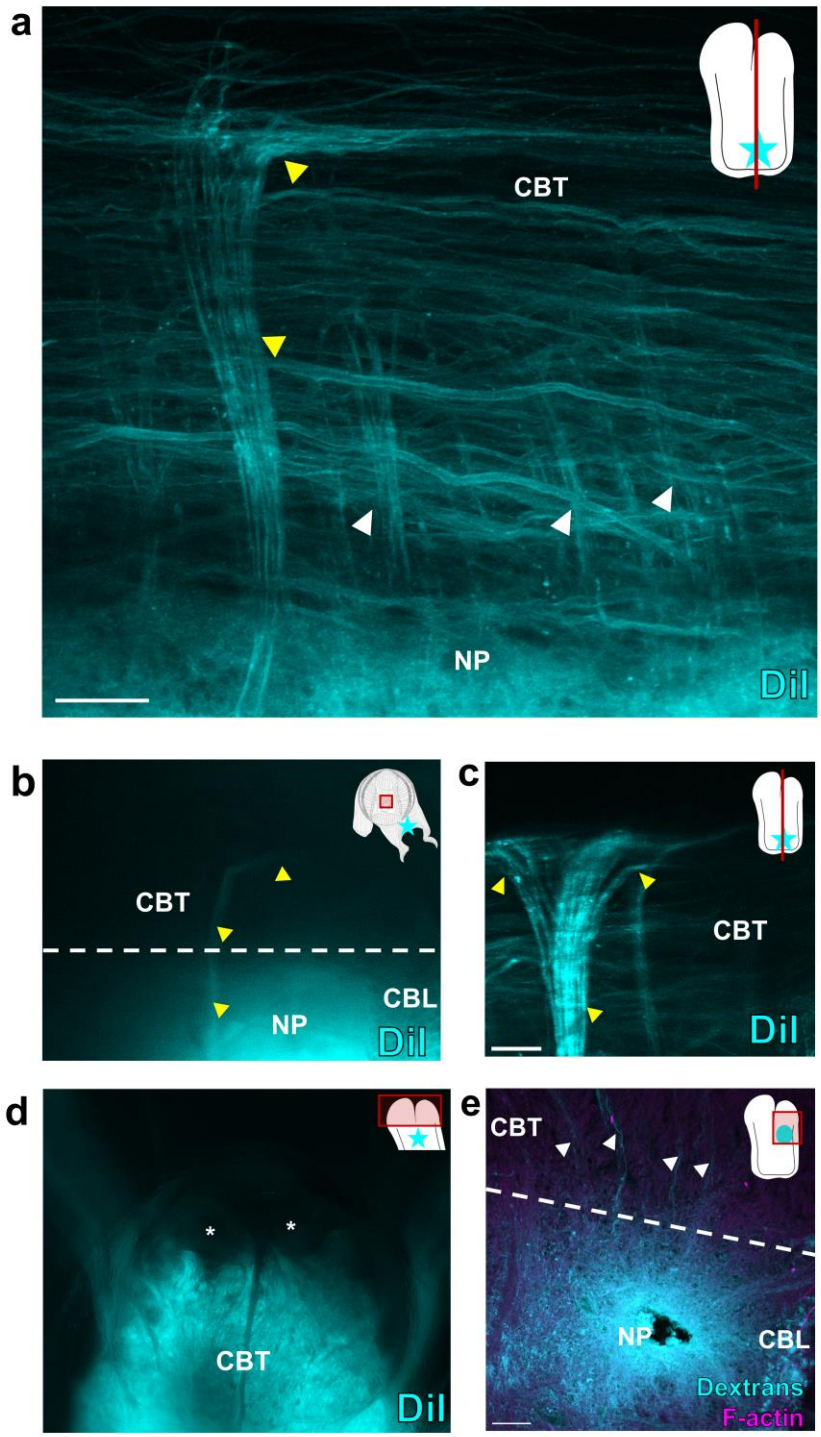

Figure 4.3: Neuropil connections the cerebrobrachial tract.
a, Maximum projection of the cerebrobrachial tract (CBT) in a longitudinal wholemount with DiI (cyan) crystal placed in oral neuropil (NP; star on inset marks crystal placement). The cerebrobrachial tract has many interactions with the NP. Yellow arrowheads point to large

connections. White arrowheads mark small processes. Scale bar: 100 μm. **b,** CBT in a transverse wholemount of with DiI (cyan) crystal placement in sucker musculature (star on inset). Large processes that target α tract are labeled (yellow arrowheads). **c,** Maximum projection of the CBT in a longitudinal wholemount of ANC with DiI (cyan) crystal placed in oral neuropil (NP; star on inset marks crystal placement). Connections to the α tract branch proximal and distal. Yellow arrowheads point to the processes. Scale bar: 100 μm. **d,** Transverse wholemount with DiI (cyan) crystal placement in the aboral neuropil. The β, γ, and δ tracts are labeled, but not the α tract. **e,** Transverse section of an injection of dextran (cyan) into the aboral NP demonstrating connections to the CBT. Scale bar: 100 μm. CBL, cell body layer; CBT cerebrobrachial tract; NP, neuropil.

Longitudinal tracts in *Octopus bimaculoides* NP

We next interrogated the ANC for longitudinally running NP tracts with DiI, dextrans labeling, and immunohistochemistry. We detected an oral longitudinal tract (oLT; Fig. 4.4c, d) and an internal longitudinal tract (iLT; Fig. 4.4e, f) in the oral sucker NP. The trajectories of the oLT and iLT are complex, and Figure 4.4 a and b summarize our conclusions about their shifting relationships. The oLT is situated along the center of the oral sucker NP and as seen in horizontal sections, oscillates through the sucker enlargements (Fig. 4.4b-d). The iLT is found aboral to the oLT (Fig. 4.4a, e). In the horizontal plane, the iLT follows the internal side of the ANC (see Fig. 3.10), switching from one edge to the other to maintain its positioning (Fig. 4.4b, f). In the transverse plane, as the ANC transitions to the next sucker enlargement, the oLT bifurcates into two trunks, and the iLT clearly marks the midline (Fig. 4.4g-j). One of the oLT trunks ascends aborally and loops around the iLT (Fig. 4.4g, h). The other continues orally to connect directly to the oLT in the next enlargement (Fig. 4.4i, j). By projecting aborally, the oLT could receive input from other parts of the arm and mark the transition from one sucker to the next.

The aboral, brachial NP is dominated by longitudinal fibers (Fig. 4.5a, b). Most prominent are two bilateral tracts at the transition between the oral sucker NP and the aboral brachial NP (Fig. 4.5c). These correspond to the most aboral branch point of the oral fascicles,

which feed to the oral roots innervating the sucker (Fig. 4.5d; see also Fig 3.8d-f). By their location at the interface between sucker and brachial territories of the ANC, these tracts could integrate motor control information coordinating the brachial musculature and sucker movements.

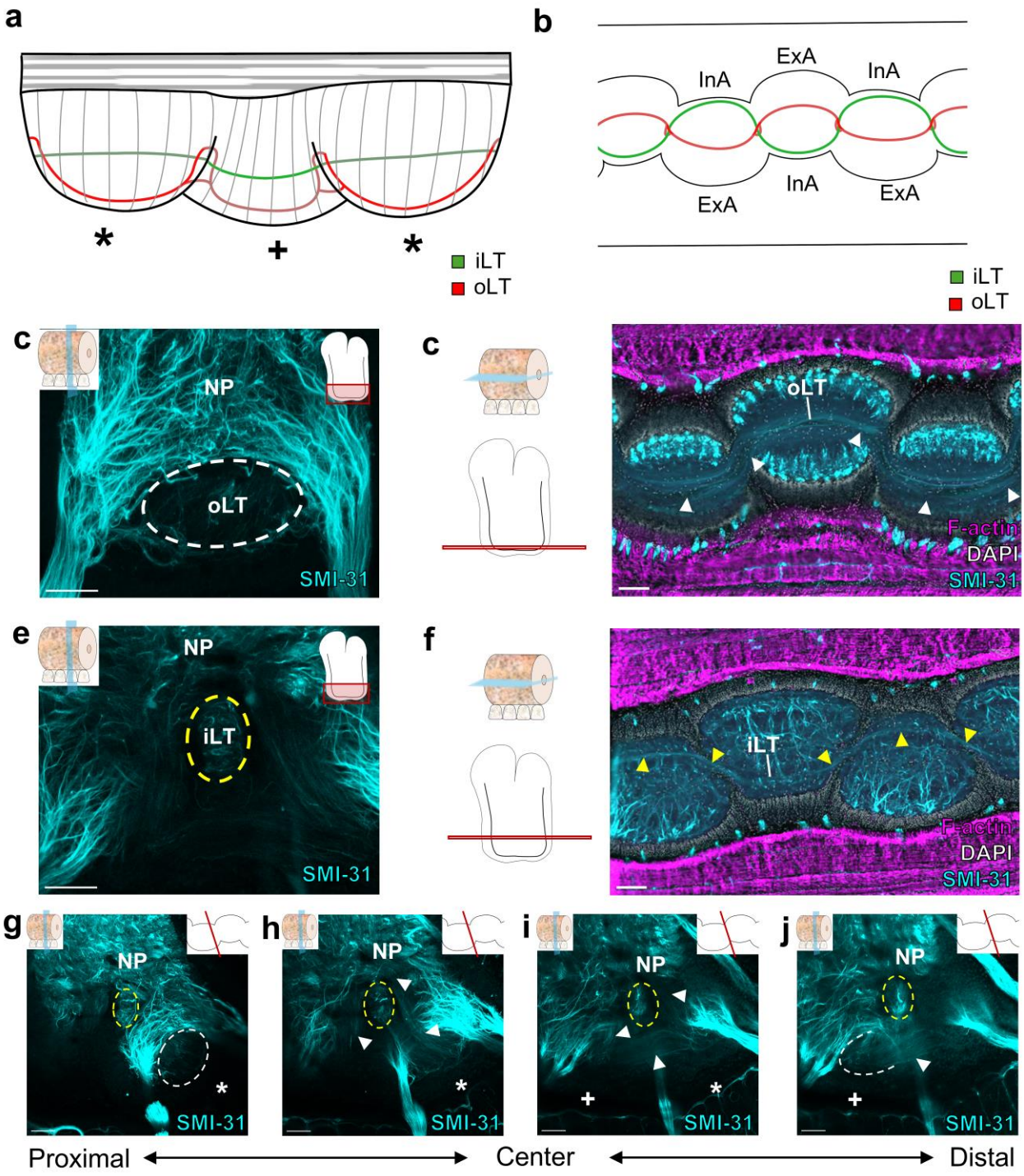

Figure 4.4: Longitudinal tracts in the oral neuropil.
a, Schematic of a longitudinal axial nerve cord (ANC) demonstrating the trajectories of the internal longitudinal tract (iLT, green) and the oral longitudinal tract (oLT, red) as the tracts travel from sucker to sucker. * denotes ANC enlargements for suckers on the same side. + denotes ANC enlargement for suckers on the opposite side. **b,** Diagram of a horizontal section of the

ANC demonstrating the paths of the the oLT (red) and iLT (green) in the oral portion of the ANC. **c,** Maximum projection of a transverse ANC whole mount stained for SMI-31 (cyan). The oLT is outlined with a white dashed line. Key indicates transverse plane of section. Scale bar: 100 μm. **d,** Horizontal section through the oral NP stained for SMI-31 (cyan), F-actin (magenta), and DAPI (gray). The oLT, marked by white arrowheads, is positioned at the midline and oscillates through ANC enlargements. Key indicates horizontal plane of section. Scale bar: 150 μm. **e**, Maximum projection of a transverse ANC whole mount stained for SMI-31 (cyan). The iLT is outlined with a yellow dashed line. Key indicates transverse plane of section. Scale bar: 100 μm. **f**, Horizontal section through the oral NP stained for SMI-31 (cyan), F-actin (magenta), and DAPI (gray). The iLT, marked by yellow arrowheads, follows the internal side of the ANC. **g-j,** Series of maximum projections of transverse ANC wholemount stained SMI-31. Trajectories of the oLT and iLT as the ANC transitions from one enlargement (denoted by *) to the next (denoted by +) are demonstrated. oLT is marked by white dashed line and white arrowheads. iLT is marked by yellow dashed line. Inset in top right depicts plane of section. Scale bars: 100 μm. **g,** Before transitioning to the next enlargement, the iLT is located aboral to the oLT. **h-i,** during the transition to the next enlargement, the iLT marks the midline between the two enlargements and the oLT bifurcates into two trunks. One oLT trunk loops over the iLT (**h**), the other connects directly to the oLT in the next enlargement (**i**). **j**, After the transition, the oLT regains its positioning oral to the iLT. ANC, axial nerve cord; ExA, external side of the axial nerve cord; InA, internal side of the axial nerve cord; iLT, internal longitudinal tract; NP, neuropil; oLT, oral longitudinal tract.

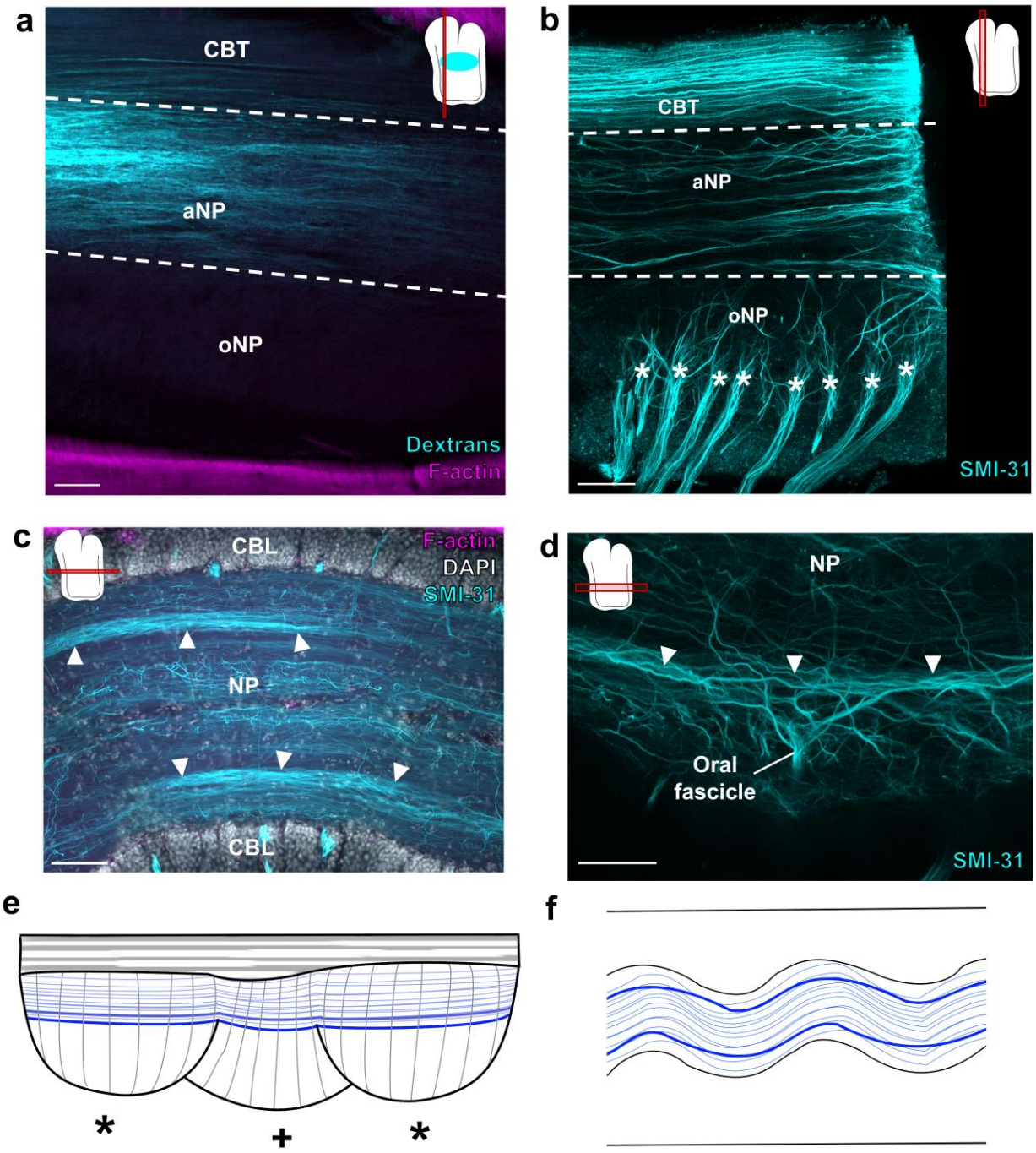

Figure 4.5: Longitudinal tracts in the aboral neuropil.
a-b, The aboral neuropil (NP) is dominated by longitudinal fibers. **a,** Longitudinal section of an injection of dextran (cyan) into the aboral NP demonstrating longitudinal fibers. **b,** Maximum projection of a longitudinal wholemount with SMI-31 immunostaining (cyan) marks the longitudinal fibers in the aboral NP. The oral fascicles (denoted by *) that become the oral roots

targeting the sucker are also readily visible in this preparation. **c,** Horizontal section at the transition from the oral NP to the aboral NP stained for SMI-31 (cyan), F-actin (magenta), and DAPI (gray). There are two prominent bilateral longitudinal tracts, marked by white arrowheads. **d,** Maximum projection of a horizontal wholemount stained for SMI-31 (cyan) displays that these tracts correspond to the most aboral branch point of the oral fascicles. **e-f,** Summary diagrams showcasing the longitudinal tracts (blue) in the aboral NP in a longitudinal ANC cartoon (**e**) and a horizontal ANC cartoon (**f**). The prominent tracts are denoted by thicker lines. * in (**e**) denote ANC enlargements for suckers on the same side, + denote ANC enlargements for suckers on the opposite side. Scale bars: 100 μm. aNP, aboral neuropil; CBL, cell body layer; CBT cerebrobrachial tract; NP, neuropil; oNP, oral neuropil.

Longitudinal tracts in the ANC of *Doryteuthis pealeii*

Like *O. bimaculoides*, *D. pealeii* have an extensive nervous system embedded in the arms and tentacles. In addition to a prominent ANC, the arms and tentacles have 6 intramuscular nerve cords (IMNC) distributed around the lateral edges (Fig. 4.6a-c). The arms and tentacle clubs, which have suckers, also have sucker ganglia that, unlike *O. bimaculoides*, have a canonical ganglionic organization (not shown; see Olson et al., 2025a).

As described in Olson et al. (2025), the ANCs in *D. pealeii* do not have a CBT analogous to the octopus CBT, but rather have major longitudinally running tracts distributed aborally and orally (Fig. 4.6d-f). Fibers in the aboral longitudinal tract (aLT) and the oral longitudinal tract (oLT) show a range of large diameters in transverse cross sections (Fig. 4.6h-k). Those in the tentacle stalk aLT are the largest (Fig. 4.6j). In the arm and tentacle club, where there are suckers, the oLT oscillates around the NP (Fig. 4.6l, n). In the tentacle stalk, the oLT runs straight (Fig. 4.6m). We did not detect clear spatial subdivisions within the oLT or aLT as we did the octopus CBT. Nonetheless, the spatial separation of the oLT and aLT from each other hints at distinct functions. By its location closest to the suckers, the oLT may in part handle long distance sucker communication whereas the aLT may handle long distance brachial musculature communication.

Whether oLT or aLT correspond to the CBT by interconnecting with the brain needs experimental testing with tract-tracing methods.

We identified additional longitudinal fibers in the NP of the squid ANC (Fig. 4.7). In the arm, these longitudinal fibers coalesce into distinct tracts situated at the interface of the CBL and NP (Fig. 4.7a-c). The tentacle stalk ANC NP does not have distinct longitudinal NP tracts (Fig. 4.7d). Instead, the entire border between the CBL and NP is lined with longitudinal fibers (Fig. 4.7e-f). Having distinct bundles in squid arm but not tentacle could pertain to differences in the sensorimotor demands for the suckers or the need to coordinate sucker and arm movements along a distance.

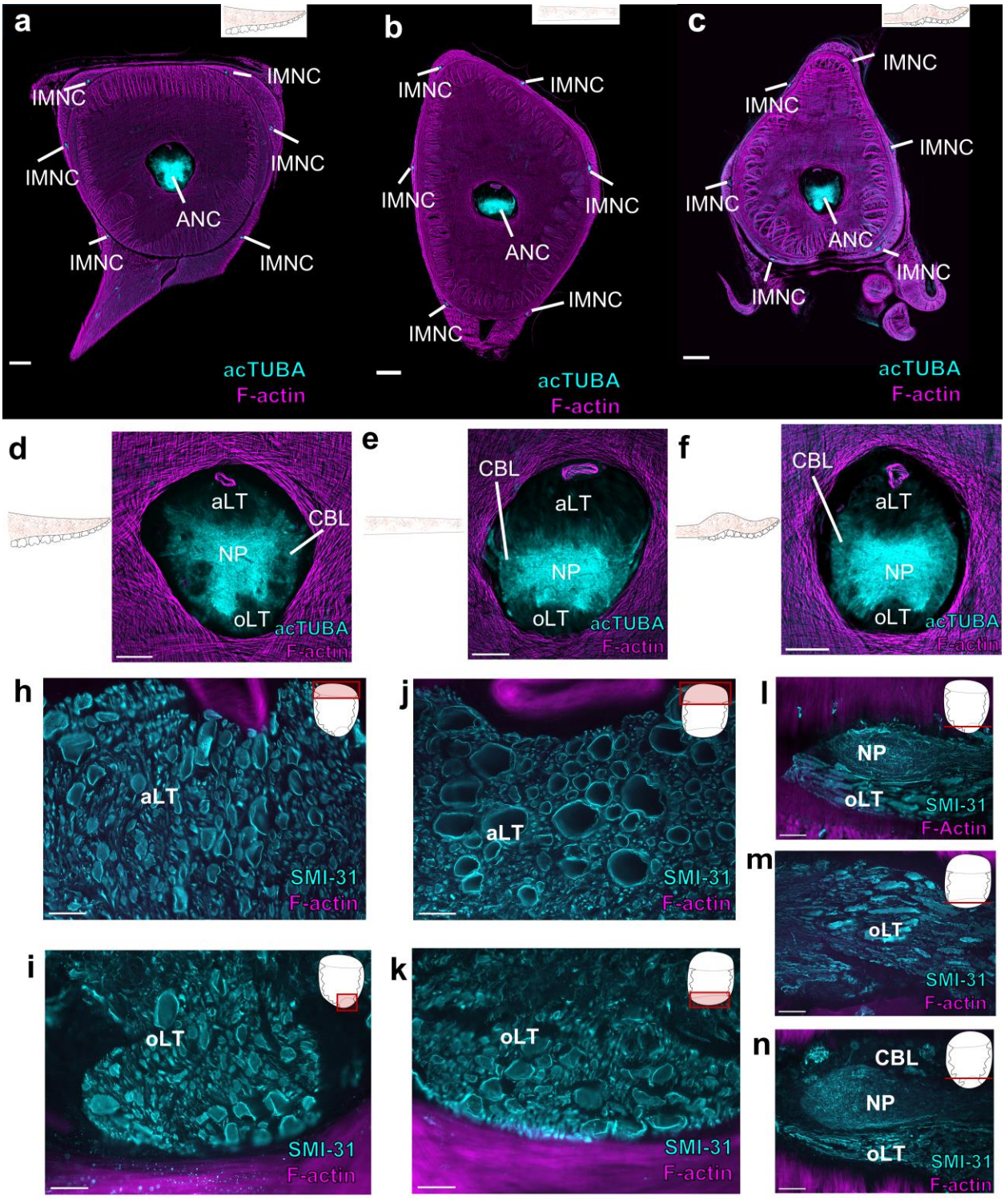
a
IMNC
IMNC
IMNC
IMNC
ANC
IMNC
IMNC
acTUBA
F-actin
b
IMNC
IMNC
IMNC
IMNC
ANC
IMNC
IMNC
acTUBA
F-actin
c
IMNC
IMNC
IMNC
IMNC
ANC
IMNC
IMNC
acTUBA
F-actin
d
aLT
CBL
NP
oLT
acTUBA
F-actin
e
CBL
aLT
NP
oLT
acTUBA
F-actin
f
CBL
aLT
NP
oLT
acTUBA
F-actin
h
aLT
SMI-31
F-actin
j
aLT
SMI-31
F-actin
l
NP
oLT
SMI-31
F-Actin
m
oLT
SMI-31
F-actin
i
oLT
SMI-31
F-actin
k
oLT
SMI-31
F-actin
n
CBL
NP
oLT
SMI-31
F-actin

Figure 4.6: Organization of *D. Pealeii* arm and tentacle nervous system.
a-c, Transverse section of the *D. pealeii* arm (**a**), tentacle stalk (**b**) and tentacle club (**c**) stained for acTUBA (cyan) and F-actin (magenta). The main components of the nervous system are highlighted. Scale bars: 500 µm. **d-f,** Transverse section of the axial nerve cord in the *D. pealeii* arm (**d**), tentacle stalk (**e**) and tentacle club (**f**) stained for acTUBA (cyan) and F-actin (magenta). Each ANC has an aboral longitudinal tract (aLT) and an oral longitudinal tract (oLT). Scale bars: 250 µm. **h-k,** The aLT and oLT are composed of large fibers. **h-i,** Transverse sections through the aLT (**h**) and oLT (**i**) in arm ANC stained for SMI-31 (cyan) and F-actin (magenta). **j-k,** Transverse sections through the aLT (**j**) and oLT (**k**) in the tentacle stalk ANC stained for SMI-31 (cyan) and F-actin (magenta). Scale bars: 50 µm. **l-n**, Horizontal sections through oLT in the arm (**l**), tentacle stalk (**m**) and tentacle club (**n**) stained for SMI-31 (cyan) and F-actin (magenta). In the arm (**l**) and tentacle club (**n**), where there are suckers, the oLT weaves around neuropil (NP). Scale bars: 100 µm. acTUBA, acetylated α-tubulin; aLT, aboral longitudinal tract; ANC, axial nerve cord; CBL, cell body layer; INMC, intramuscular nerve cord; NP, neuropil; oLT, oral longitudinal tract.

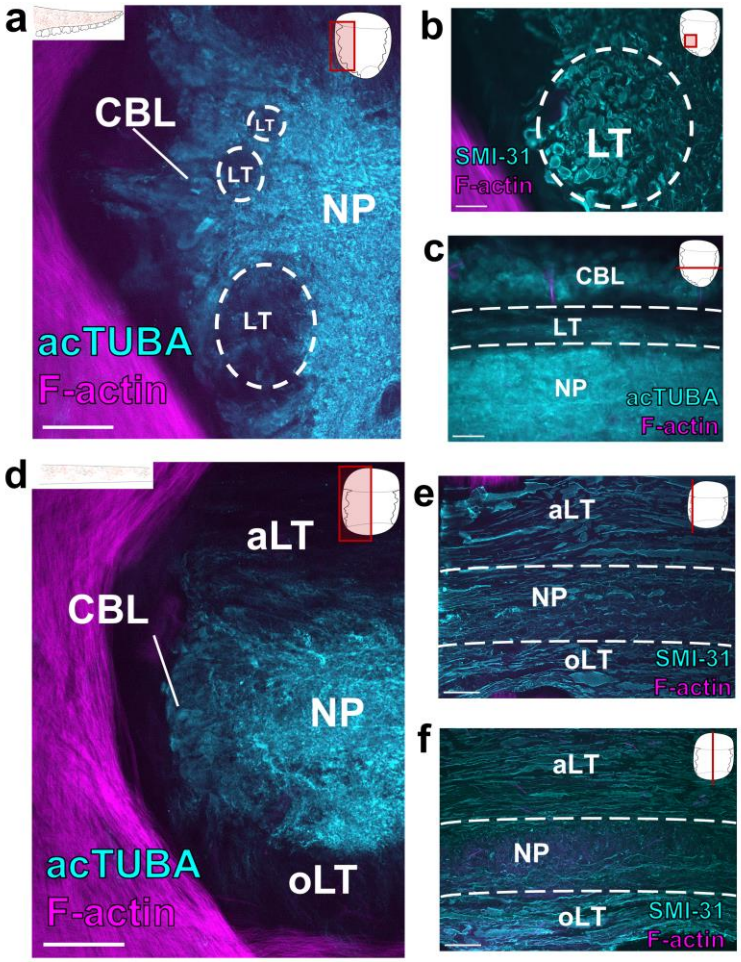

Figure 4.7: Longitudinal tracts in *D. pealeii* neuropil.
a, Transverse section through the axial nerve cord in the squid arm stained for acetylated α-tubulin (acTUBA, cyan) and F-actin (magenta). Defined longitudinal tracts (LT), marked with white dashed line, are apparent by a decrease in acTUBA labeling. Inset depicts field of view. Scale bar: 100 μm. **b,** Transverse section through the squid arm ANC with SMI-31(cyan) immunostaining labels the fibers in the longitudinal tracts. Scale bar: 50 μm. **c,** Horizontal section through the squid arm ANC stained for acTUBA. The longitudinal tracts are located at the border of the cell body layer and neuropil. Scale bar: 50 μm. **d,** Transverse section through the ANC in the tentacle stalk stained for acetylated α-tubulin (acTUBA, cyan) and F-actin (magenta). There are no defined NP tracts. Scale bar: 100 μm. **e-f**, Longitudinal sections through the tentacle stalk ANC stained for SMI-31 (cyan) and F-actin (magenta). Longitudinal fibers are abundant at the interface of the CBL and NP (**e**) but diminish in the center (**f**). Inset displays plane of section. Scale bars: 100 μm. acTUBA, acetylated α-tubulin; aLT, aboral longitudinal tract; ANC, axial nerve cord; CBL, cell body layer; LT, longitudinal tract; NP, neuropil; oLT, oral longitudinal tract.

DISCUSSION

Most behaviors in octopus and squid require the coordination of suckers and arm musculature along the length of the arm (Kier and Smith, 1985; Gutfreund et al., 1998; Sumbre et al., 2006; Kier, 2016; Hanlon and Messenger, 2018; Kennedy et al., 2020; Bidel et al., 2022). Accordingly, the ANC in both *O. bimaculoides* and *D. pealeii* hosts many longitudinal fiber tracts. These can be categorized into intra-neuropil tracts, such as the iLT, and extra-neuropil tracts, like the CBT. Interestingly, both *O. bimaculoides* and *D. pealeii* have an oral longitudinal tract, though the structure is different. The oLT in squid is composed of larger fibers and is situated outside of the NP, whereas the octopus oLT is solidly within NP. In the absence of myelin, large nerve fibers transmit faster signals, so the oLT in squid seems well suited for fast transmission to the brain. Since prey capture in *D. pealeii* requires collective action of two tentacles and eight arms, fast transmission of sensorimotor input for suckers is advantageous (Kier and Smith, 1985; Kier, 2016).

Behaviors involving suckers in octopus are much more expansive (Altman, 1971; Packard, 1988; Grasso, 2008; Hanlon and Messenger, 2018; Bidel et al., 2022; Buresch et al.,

2022). Some of these behaviors involve coordination of suckers along the proximal distal axis, such as passing food along the arm according to its valence (Altman, 1971). The oLT in octopuses may serve as a substrate for sensorimotor communication underlying these behaviors. Sucker movements often result in recruiting the rest of the arm, whether it is to extend an arm to grasp an object or to use the arm to push an object away (Sumbre et al., 2006; Kennedy et al., 2020). The bilateral tracts at the interface between the sucker and brachial NP may serve as pathways for coordinating these behaviors.

Most of the defined tracts within the NP in octopus pertain to the sucker. The brachial NP contains many longitudinal fibers, just not in defined tracts. Given its proximity to CBT, defined tracts within the CBT, such as the β and δ tracts, could be used as intermediate relays for the brachial musculature. Further examination of connections from the brachial NP to these tracts and the regularity of NP-CBT interactions could provide insight into this possibility.

The longitudinal tracts in the ANCs of octopus and squid arms exist in the context of a clear segmental organization of the ANC cell body layer (Olson et al., 2025). Neither the intra-NP nor extra-NP tracts themselves are segmented, but the intra-NP tracts most certainly receive modulation by the segments. The CBT, as an extra-NP tract, may serve as an unmodulated relay of sensorimotor commands. Further descriptions of the inputs to the intra-NP and extra-NP tracts would help clarify the relationship between segments and the longitudinal tracts. Nevertheless, effective motor control for the highly flexible coleoid arm appears to be achieved by segmentation for localized sensorimotor control and longitudinal tracts for coordination over a distance.

CHAPTER 5

Molecular and morphological circuitry of the octopus sucker ganglion[3]

INTRODUCTION

The octopus arm is a remarkable appendage, famously able to contort in near infinite degrees of freedom (Kennedy et al., 2020; Hochner et al., 2023; Olson and Ragsdale, 2023). The hundreds of suckers that line each arm are equally remarkable. These suckers are vital for the survival of the octopus, allowing them to catch prey, distinguish food from other objects, pass food to and from the mouth, manipulate objects, build structures, and tend to their eggs (Altman, 1971; Packard, 1988; Grasso, 2008; Hanlon and Messenger, 2018; Bidel et al., 2022; Buresch et al., 2022). In support of these behaviors, and like the arms themselves, each sucker can be moved independently and in near infinite degrees of freedom (Kier and Smith, 2002; Röckner et al., 2023). The suckers are additionally profound sensory structures, each containing an intricate sensory epithelium enriched with chemotactile and mechanoreceptors, allowing sensory detection of the environment even in the absence of vision (Wells, 1964; Gutnick et al., 2020; van Giesen et al., 2020; Buresch et al., 2022; Kang et al., 2023).

The octopus arm houses a substantial nervous system, much of it dedicated to the control of the suckers (Young, 1963; Graziadei, 1971; Neacsu and Crook, 2024; Olson et al., 2025b). There is a central nerve center: the massive axial nerve cord (ANC), equivalent to a spinal cord, running down the center of each arm. Within the ANC, a neuronal cell body layer (CBL) wraps around the neuropil (NP) forming a horseshoe pattern on the oral, or sucker, side (Graziadei,

[3] Published in Journal of Comparative Neurology (https://doi.org/10.1002/cne.70055). Referred to as Olson et al, 2025a in other chapters.

1971; Olson et al., 2025). On the aboral side, or away from the sucker, there is a cerebrobrachial tract, comprising a pair of fiber tracts connecting the arms and the brain (Graziadei, 1971; Zullo et al., 2019; Olson and Ragsdale, 2023). The CBL and NP of the ANC can be further divided into an aboral brachial territory with connections to the arm, and an oral sucker territory with connections to the sucker (Rowell, 1963; Olson et al., 2025). Down the long axis of the arm, this oral sucker territory of the ANC forms local enlargements over each sucker (Rossi and Graziadei, 1954; Olson et al., 2025; these enlargements are sometimes referred to as ganglia, see: Young, 1971; Nixon and Young, 2003; Nödl et al., 2016; Neacsu and Crook, 2024). From these enlargements, the ANC issues nerves fibers that spatially tile each sucker to create a topographic map (Olson et al., 2025).

The arm also harbors a peripheral nerve center for the sucker: the sucker ganglion (Graziadei, 1971). Given the strong coupling between the ANC and each sucker, what does the sucker ganglion do? Some early authors postulated a primarily motor role, with the sucker ganglion modulating local reflexes for the sucker stalk (Guérin, 1908). Others included a sensory role, with some sucker ganglion cell bodies being primary sensory cells (Rowell, 1963; Graziadei and Gagne, 1976). Lastly, others proposed a dual sensory and motor role (Martoja and May, 1955; Graziadei, 1965a, 1971). Here, we investigated the role of the sucker ganglion by interrogating its molecular composition and circuitry with contemporary molecular and cellular methods.

RESULTS

We confirmed the presence and position of the sucker ganglion in *O. bimaculoides* with in situ hybridization (ISH) for pan-neuronal markers (Fig. 5.1b, c, d, e). As in other species, the sucker ganglion is embedded in the acetabulobrachial muscles (ACBM) comprising the sucker

stalk aboral, or deep, to the acetabulum of each sucker (Fig. 5.1b, f). Because of its position within the sucker musculature, the sucker ganglion is a mobile structure. As reflected in Fig. 5.1f, the sucker ganglion moves with the sucker as the sucker muscles contract.

Suckers decrease in width along the proximal-distal axis of the arm. The sucker ganglion likewise decreases in width, though it maintains its ellipsoid shape down the long axis of the arm (Fig. 5.2c). We asked if this decrease is isometric with the decrease in sucker width. We found instead an allometric relationship: ganglia from the distal region of the arm were larger relative to the width of their respective sucker than ganglia found in the intermediate or proximal regions (Fig. 5.2d). This difference could be due to a developmental constraint on the size of the circuit or underlying functional differences across suckers located at different arm positions.

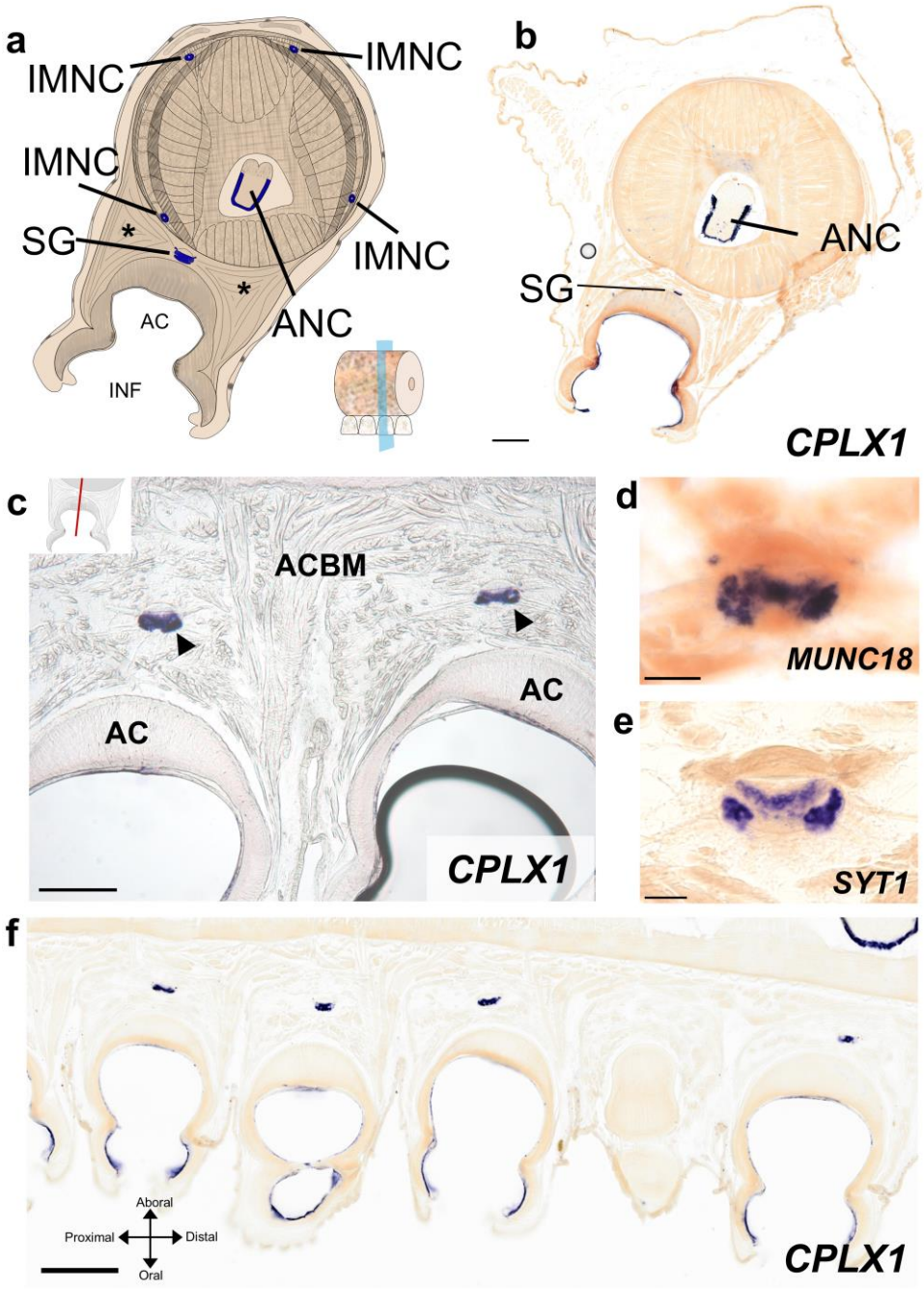

Figure 5.1: Geography of octopus arm and location of sucker ganglion.
a, Diagram of a transverse cross section of octopus arm. The major components of the arm nervous system are highlighted in blue. Key indicates transverse plane of section. *denotes acetabulobrachial muscles (ACBM) **b,** Transverse arm section with in situ hybridization (ISH) for the neuronal gene complexin (*CPLX1*). Neuronal cell bodies in the axial nerve cord (ANC) and sucker ganglion (SG) are labeled. Scale bar: 100 µm **c-f,** Longitudinal sections through the octopus arm, as indicated by inset in c. In the longitudinal plane, the coordinate axes correspond to aboral-oral, proximal-distal, as indicated in f. **c,** ISH of *CPLX1* on a longitudinal section of octopus arm. There is an SG embedded in the ACBM for every sucker. Arrowheads point to the

SG. Scale bar: 250 µm **d-e,** The SG is enriched with other panneuronal markers. **d,** *MUNC18.* **e,** *SYT1.* Octopuses have many isoforms of *SYT*, so *SYT1* may not label all neurons. Scale bars: 50 µm. **f,** ISH of *CPLX1* on a longitudinal section of octopus arm across many suckers. The location of the SG varies based on the location of the sucker. Scale bar: 500 µm. AC, acetabulum; ACBM, acetabulobrachial muscles; ANC, axial nerve cord; IMNC, intramuscular nerve cord; INF, infundibulum; SG, sucker ganglion.

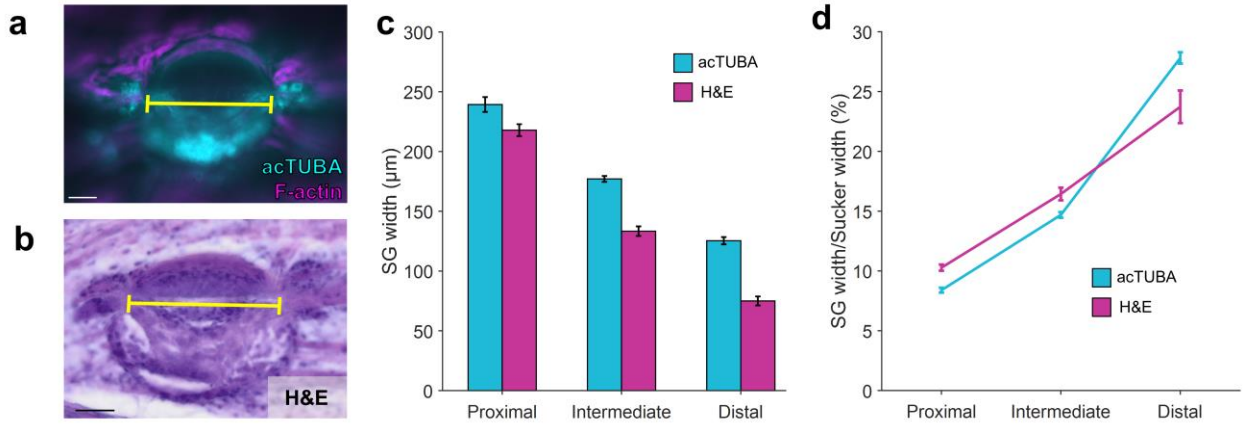

Figure 5.2: Sucker ganglion width changes along the proximal-distal axis.
a-b, Example longitudinal sections through sucker ganglia (SG) used for measurements. Yellow line indicates location of measurement. Scale bars: 50 µm. **a,** SG stained for acetylated α-tubulin (acTUBA, cyan) and F-actin (magenta). **b,** SG stained with hematoxylin and eosin (H&E). **c,** SG width decreases down the proximal (P)- distal (D) axis, error bars +/- sem. **d,** The width of the SG relative to sucker width increases along the P-D axis, error bars +/- sem. acTUBA, acetylated α-tubulin; H&E, hematoxylin and eosin; SG, sucker ganglion.

Internal composition of the sucker ganglion

The octopus sucker ganglion has an unusual structure (Graziadei, 1971). Instead of neuronal cell bodies surrounding a central neuropil (Richter et al., 2010), the sucker ganglion neuropil (NP) is predominantly arranged as a cap on the aboral surface (acTUBA labeling; Fig. 5.3d). A dense cell body region is located just orally to this NP cap, that is, a step closer to the sucker (Fig. 5.3e, f, h-k). This cell body region is composed of small cell bodies situated in a basket of larger cell bodies (Fig. 5.3e, f). At the junction of the NP cap and cell body region is an inner belt (Fig. 5.3d, e). This inner belt is composed of circumferentially running fiber bundles with large cell bodies lining its outer edge (Fig. 5.3d, e, h-k). In addition, connective tissue identified with Picrosirius Red staining forms a distinct plate between the NP cap and cell body region, separating these two territories (Fig. 5.4). On the oral side of the sucker ganglion, that is closest to the sucker, there is a small pocket of neuropil and an additional belt of circumferential fibers (“outer belt”; Fig. 5.3f, g). Unlike the inner belt, however, the outer belt appears devoid of neuronal cell bodies (Fig. 5.3f, g).

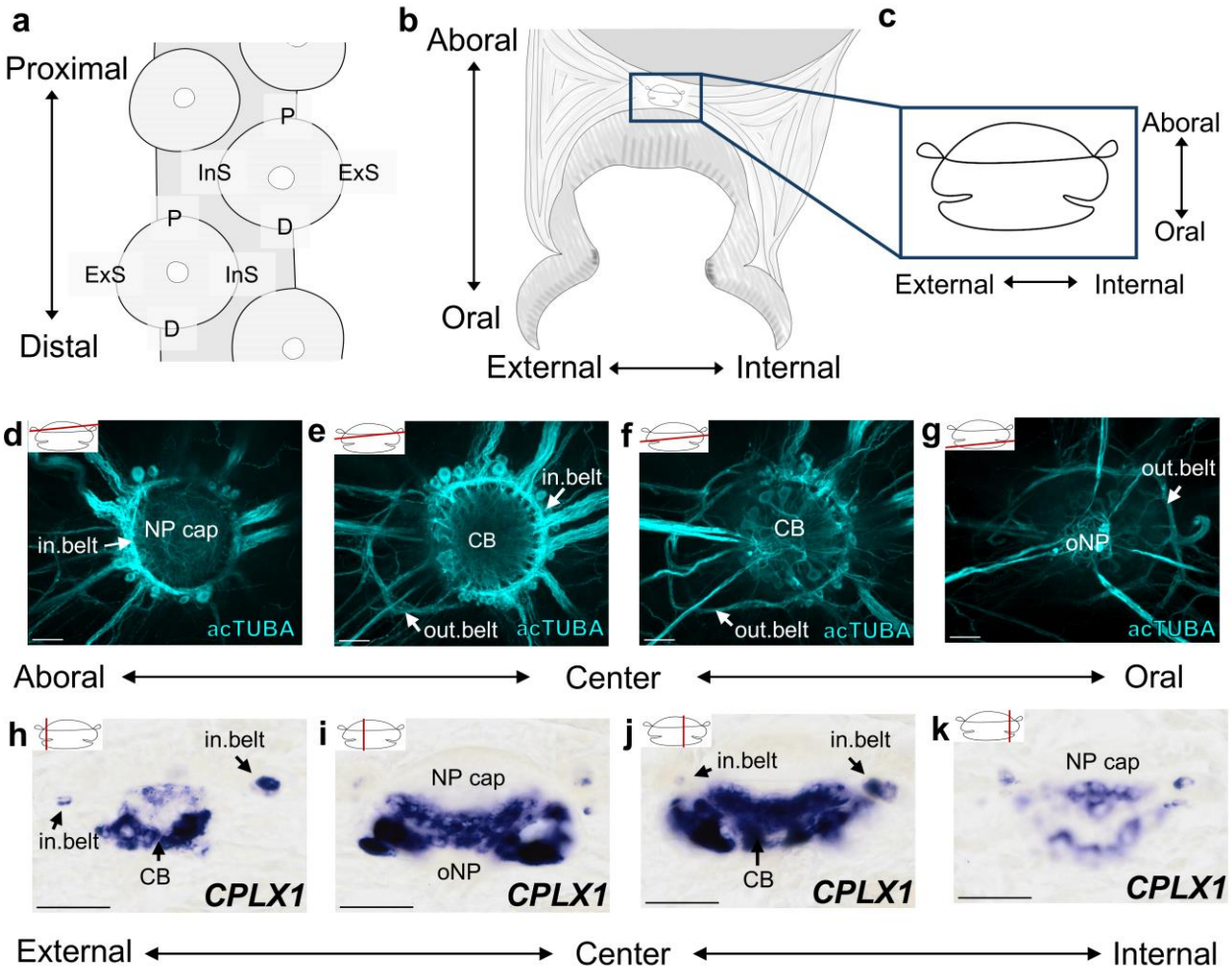

Figure 5.3: Internal neural organization of the sucker ganglion.
a-c, The axes for a sucker: proximal-distal, external-internal, aboral-oral. **a,** An en face, horizontal cartoon of the suckers showing that the suckers are arranged in two offset rows. In the horizontal plane, each sucker has a proximal (P)-distal (D) axis, and an internal side (InS)-external side (ExS) axis. The P-D axis corresponds to the P-D axis for the arm as whole (that is, from head to arm tip). The InS corresponds to the side of the sucker that hugs the midline of the arm. The ExS corresponds to the side of the sucker that is situated on the outer edge of the arm. **b,** A transverse cartoon of a sucker. In the transverse plane, each sucker has an aboral-oral axis and an ExS-InS axis. The aboral side is the side further from the sucker, the oral side is the side closest to the sucker. **c,** A cartoon of a transverse section through the sucker ganglion (SG). Like the whole sucker, the SG has an aboral-oral axis and an ExS-InS axis in the transverse plane. **d-g,** Organization of the SG demonstrated by acetylated α-tubulin (acTUBA, cyan) immunostaining. Horizontal virtual slices produced by fusing multiple 1 µm confocal sections from aboral (d) to oral (g). See Supplemental Video 1 for a 3-D rendering of this dataset. **d,** Most aborally is a neuropil (NP) cap and an internal belt (in.belt) that is composed of circumferential fibers and large cell bodies. **e,** The in.belt is situated aboral to the cell body (CB) region. **f,** Oral to the CB territory is an outer belt (out.belt), composed of circumferentially running fiber bundles. **g,** On the oral side of the SG is a pocket of oral NP (oNP). Inset highlights the slight

asymmetry of the horizontal sections through the SG. **h-k,** Longitudinal sections from external (h) to internal (k) through the SG prepared for in situ hybridization with *CPLX1* demonstrating the location of neuronal cell bodies. Neurons are located in the in.belt and are dense throughout the full extent of CB region. Scale bars: 50 µm. acTUBA, acetylated α-tubulin; CB, cell bodies; D, distal; ExS, external side; in.belt, internal belt; InS, internal side; NP cap, neuropil cap; oNP, oral neuropil; out.belt, outer belt; P, proximal.

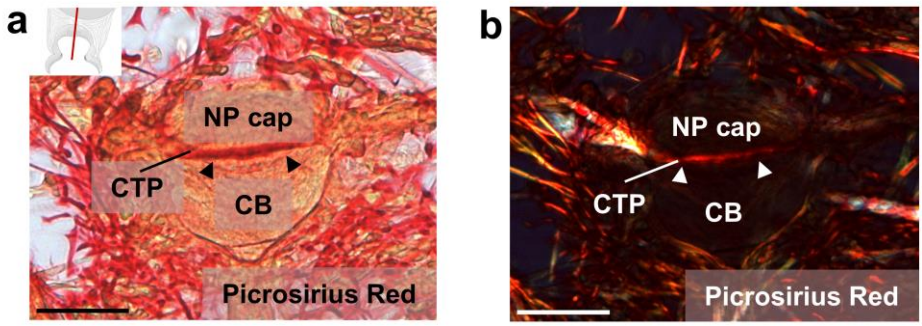

Figure 5.4: Connective tissue splits the sucker ganglion.
a-b, Picrosirius Red staining of a longitudinal section through the sucker ganglion (SG). Red denotes the presence of connective tissue. **a,** Brightfield image depicting the full structure of the SG. Black arrowheads point to connective tissue plate (CTP) between the cell body (CB) region and neuropil (NP) cap. **b,** Polarized light image of the same field, highlighting the red labeling of connective tissue. White arrowheads point to CTP. Scale bars: 50 µm. CB, cell bodies; CTP, connective tissue plate; NP cap, neuropil cap.

Molecular characterization of the sucker ganglion cell bodies

With ISH, we investigated the molecular composition of the cell body region of the sucker ganglion, first examining sensory and motor neuron markers (Jessell, 2000; Coste et al., 2010; Nomaksteinsky et al., 2013). We found positive expression for two motor neuron markers, *MNX* and *LHX3*, and the mechanosensitive ion channel marker *PIEZO* (Fig. 5.5a, b, c). *PIEZO* expression is found in scattered cells throughout the cell body territory, whereas *MNX* and *LHX3* labeling lies at its lateral edges and in its center. *PIEZO* expression was also present in a subset of cells in the inner belt (Fig. 5.5a). Interestingly, we failed to detect clear expression for *DRGX*, the dorsal root ganglion homeobox gene, and *NKX6,* a transcription factor marking motor neurons, despite strong labeling for both of these markers in the ANC and *DRGX* positive cells in the ACBM (Fig. 5.5g, h, i, j; Olson et al., 2025). Hence, while the sucker ganglion contains expression for both sensory and motor markers, its molecular profile differs from that of the ANC.

Graziadei (1965) reported the existence of muscle receptors in the ACBM around the sucker ganglion. With acTUBA immunostaining, we identified many cells embedded in the ACBM which issue processes to nerve fascicles connected to the sucker ganglion (Fig. 5.6). Some of these cells are multipolar with many processes extending into the local musculature (Fig. 5.6b, c). Some cells cluster together in groups (Fig. 5.6d). Others are located close to the sucker ganglion itself (Fig. 5.6e). We also found that the ACBM are enriched with expression of *PIEZO* and *DRGX*, indicating that these cells may be sensory in nature (Fig. 5.5j; *PIEZO* not shown). This suggests the sucker ganglion handles sensory input from cells within the ganglion itself as well as from the local musculature.

We interrogated the sucker ganglion with ISH for other neural subtype markers. The sucker ganglion is enriched for expression of presynaptic cholinergic neuron markers (*VACHT/SLC18A3, SLC5A7*, and *CHAT*). Unlike in the ANC, where we found expression for these cholinergic neuron markers throughout the entirety of the CBL, *VACHT, SLC5A7,* and *CHAT* expression in the sucker ganglion is found at the lateral edges of the ganglion and the center, similar to the labeling pattern of the motor neuron markers (Fig. 5.5d, e, f). Glutamate decarboxylase (*GAD*) and vesicular inhibitory amino acid transporter (*VIAAT*) serve as markers of fast GABAergic inhibitory neurons. We failed to detect expression for either of these inhibitory neuron markers in the sucker ganglion in experiments presenting positive labeling in the ANC or the ACBM (Fig. 5.5k, l, m, n). Rapid ganglionic inhibition therefore would need to be mediated by another neurotransmitter, such as acetylcholine, or by extra-ganglionic input from the ANC or from *VIAAT* positive cells seen scattered within the sucker musculature (Fig. 5.5n).

The expression pattern of *FMRF*, which encodes a neuromodulatory neuropeptide, was striking in the sucker ganglion. In the ANC, it is broadly and abundantly expressed (Fig. 5.7a; see also Winters-Bostwick et al., 2024). In the sucker ganglion, however, it is very restricted (Fig. 5.7b). Moreover, the distribution of labeling is asymmetric within the ganglion, with labelling found only on the external side, or the side that corresponds to the outer edge of the sucker (Fig. 5.7c, see Fig. 5.3a). This asymmetry in molecular identity could underlie an asymmetry in function.

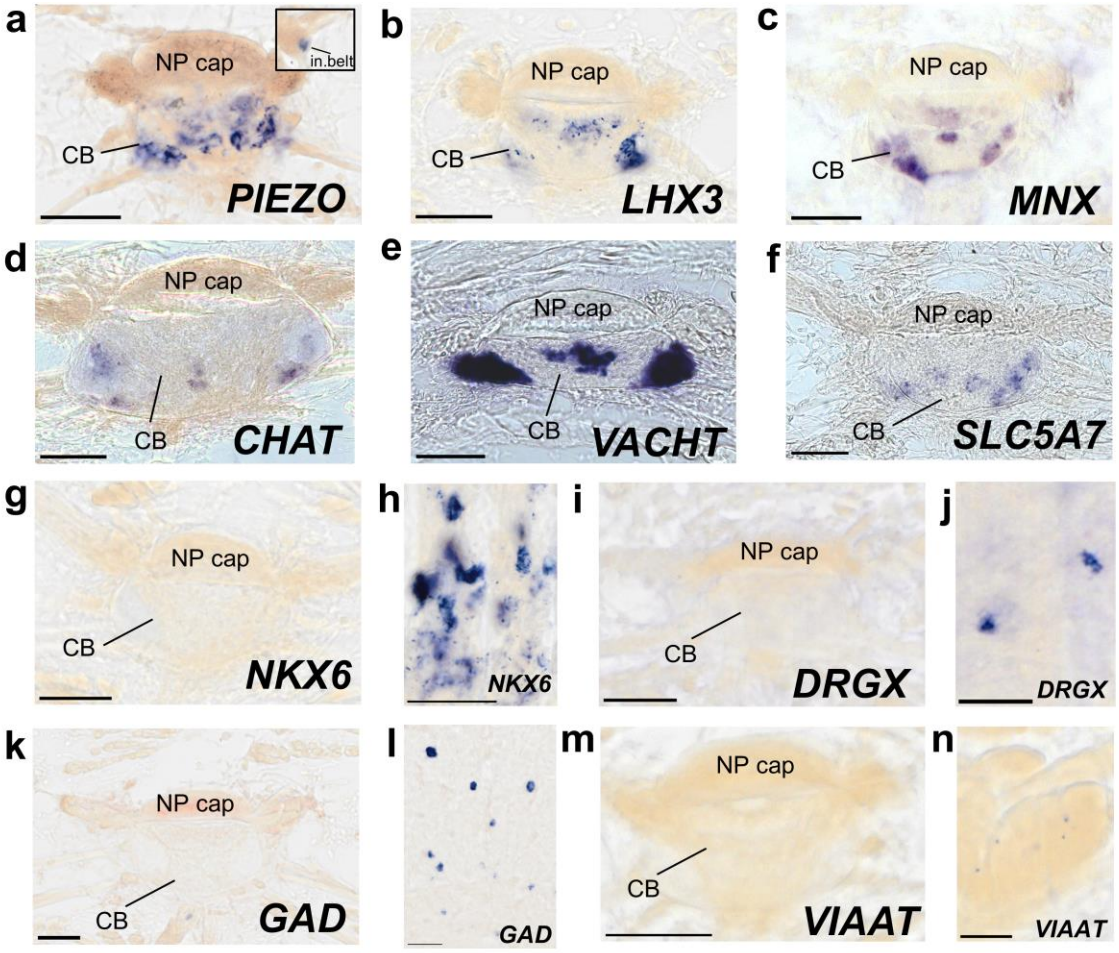

Figure 5.5: Gene expression patterns in the cell body territory of the sucker ganglion. **a-c,** The sucker ganglion (SG) is enriched with the sensory and motor neuron markers, **a,** In situ hybridization (ISH) for the mechanosensory ion channel marker *PIEZO*. Inset demonstrates *PIEZO* labeling in the inner belt (in.belt), **b,** ISH for LIM homeobox 3 transcription factor (*LHX3*), a motor neuron marker, **c,** ISH for motor neuron and pancreas homeobox transcription factor (*MNX*). **d-f,** Presysnaptic markers for cholinergic neurons label a subset of neurons in the cell body region. **d,** ISH for choline acetyl transferase (*CHAT*), **e,** ISH for vesicular acetylcholine transporter (*VACHT*), **f,** ISH for solute carrier family 5 member 7 (*SLC5A7*). Scale bars: 50 µm. **g-j,** The molecular profile of the SG differs from that of the ANC. No positive labeling was detected in the SG for **g,** NK6 homeobox transcription factor (*NXK6*), a motor neuron marker or **i,** Dorsal root ganglion homeobox transcription factor (*DRGX*), despite positive labeling in the ANC (**h,** *NKX6*) or ACBM (**j,** *DRGX*). Scale bars for **g, h, i**: 50 µm. Scale bar for **j**: 20 µm. **k-n,** Markers of inhibitory neurotransmission, **k**, glutamate acid decarboxylase (*GAD*) and **m,** vesicular inhibitory amino acid transported (*VIAAT*), do not show detectable labeling in the SG although the ANC (**l,** *GAD*) and ACBM (**n,** *VIAAT*) demonstrate cellular labeling readily. Scale bars for **k, l, m**: 50 µm. Scale bars for **n:** 20 µm. All sections longitudinal. ACBM, acetabulobrachial muscles, ANC, axial nerve cord, CB, cell bodies; in.belt, inner belt; NP cap, neuropil cap.

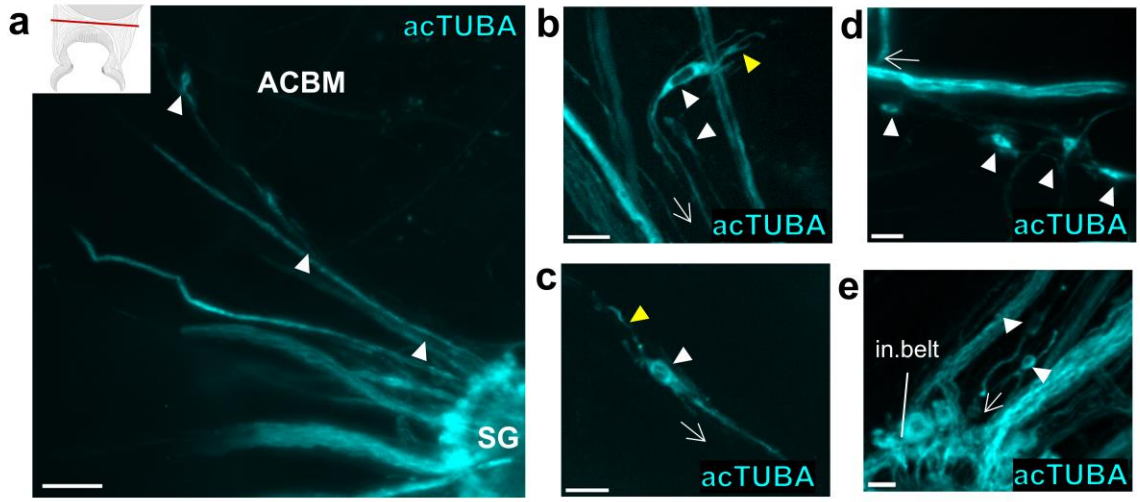

Figure 5.6: Cells in the local musculature feed back to the sucker ganglion.
a, Maximum projection of the sucker ganglion (SG) and surrounding musculature in the horizontal plane stained with acetylated α-tubulin (acTUBA, cyan). Arrowheads point to a cell body in the musculature feeding back to SG. Scale bar: 100 µm. **b-e,** Close-up images of cells in musculature stained with acTUBA. **b-c,** Cells exhibit a complex morphology. Yellow arrowheads point to processes that extend into the musculature, white arrowheads indicate cell bodies. Arrows point in direction of the SG. Scale bars: 25 µm. **d,** Some cells are located in clusters. White arrowheads indicate cell bodies. Arrow points in direction of SG. Scale bar: 50 µm. **e,** Some cells are located close to the SG. White arrowheads indicate cell bodies. Arrow points in direction of the SG. Scale bar: 25 µm. ACBM, acetabulobrachial muscles; acTUBA, acetylated α-tubulin; in.belt, inner belt; SG, sucker ganglion.

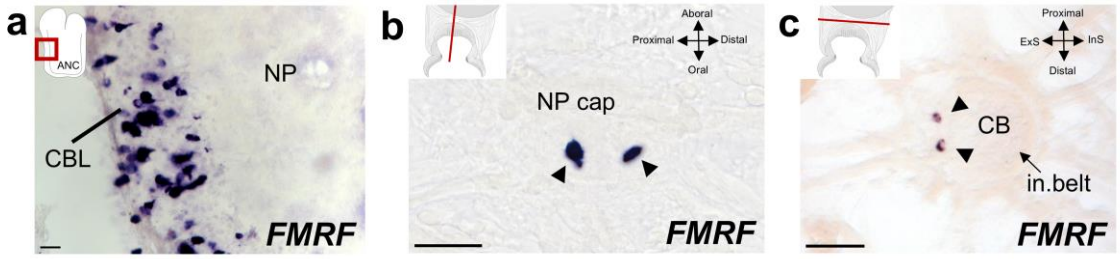

Figure 5.7: Asymmetric gene expression of *FMRF* in the sucker ganglion.
a, Transverse section of the axial nerve cord with in situ hybridization (ISH) for *FMRF*. *FMRF* expression is found abundantly throughout the cell body layer. Inset indicates the location of the panel image **b,** Longitudinal section through the sucker ganglion (SG) with ISH for *FMRF*. Arrowheads point to *FMRF* labeling of a small subset of cells. **c,** Horizontal section through the SG with *FMRF* ISH. *FMRF* labeling is restricted to the external side of the SG, as indicated by arrowheads. ANC, axial nerve cord; CB, cell bodies; CBL, cell body layer; ExS, external side of sucker; InS, internal side of sucker; in.belt, inner belt; NP, neuropil; NP cap, neuropil cap. Scale bars: 50 µm.

Nerve fiber organization

Many fiber fascicles issue from the sucker ganglion (Fig. 5.8a). These bundles vary in diameter from 6 µm to 45 µm, with the bulk falling in the 11-20 µm range (Fig. 5.8b). We examined the location of the fascicles around the perimeter of the sucker ganglion. We found that the roots are primarily distributed along the lateral sides and oral underside, forming a U-shape (Fig. 5.8c, d). There are notable gaps in this pattern, with a prominent gap corresponding to the NP cap, and two bilaterally symmetric gaps corresponding to a bulge in the cell body territory (Fig. 5.8c, d). The largest nerve bundles depart from the aboral portion of the ganglion (Fig 5.8e, f). This territory falls in between the aboral and lateral gaps (Fig. 5.8g). These results suggest a regionalization along the aboral-oral axis within the ganglion based on root location.

We also examined how the trajectories of the nerve fibers vary according to their origin or root location (Fig. 5.8h, i). We found the distribution of trajectories follows the distribution of the roots (Fig. 5.8 d, j). The nerves issuing from the aboral territory between the aboral and lateral gaps extend aborally in the direction of the aboral ACBM and the oral roots leading to the ANC (Fig. 5.8h, j). Those issuing from the oral territory extend laterally and orally in the direction of the lateral ACBM, sucker's acetabulum, and ANC oral roots targeting the sensory epithelium of the sucker (Fig. 5.8h, j). These results establish a spatial regionalization to nerve fiber trajectories along the aboral-oral axis of the sucker ganglion.

In the ANC, there is an asymmetry in nerve fibers targeting the sucker: those issued from the external side of the ANC cover more territory of the sucker compared with those issued from the internal side (Olson et al., 2025b). We asked if such an asymmetric in nerve fiber distribution is present in the sucker ganglion by examining the average trajectories along the external-internal axis (See Fig. 5.3a). We did not detect a similar kind of asymmetry in the sucker ganglion nerve

fibers, with the external and internal sides similarly covered (Fig. 5.8j, k). We found instead a bias away from the proximal-distal axis and towards the external-internal axis, proposing a variation in function between the proximal-distal and external-internal planes (Fig. 5.8k). These results also demonstrate a divergence between sucker ganglion and ANC nerve fiber distributions, signifying that the sucker ganglion has processing roles distinct from those of the ANC.

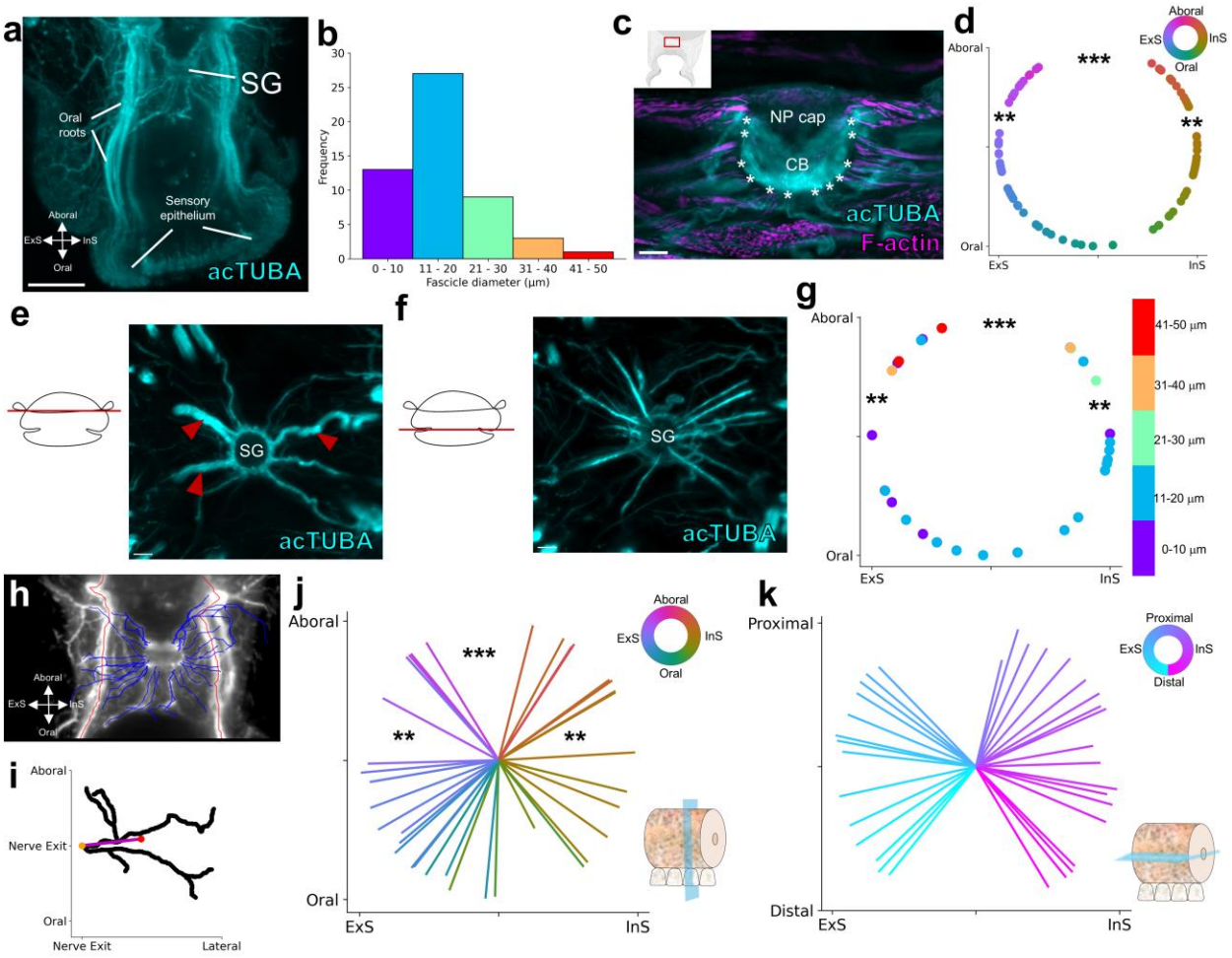

Figure 5.8: Distribution of sucker ganglion nerve fibers.
a, Maximum projection of a whole mount of a sucker stained with acetylated α-tubulin (acTUBA, cyan). Many fascicles enter and exit the sucker ganglion (SG). Scale bar: 250 µm. **b,** Distribution of fascicle diameters. Diameters range from 6-45 µm, with the peak in the 11-20 µm range. **c,** Transverse section through the SG stained with acTUBA (cyan) and F-actin (magenta).

Location of nerve fiber exits are denoted with *. Scale bar: 50 μm. **d,** Distribution of fiber exits around the SG (n = 3 ganglia, 2 stained with acTUBA, 1 stained with SMI-31) plotted in the transverse plane. There is a gap corresponding to the neuropil (NP) cap (***) and two gaps corresponding to a protrusion of the cell body region (**). Color key by location of root in the aboral-oral, external-internal plane. **e-g,** The largest nerve fibers exit aborally. **e,** Horizontal maximum projection of the aboral portion of the SG stained with acTUBA. Red arrow heads indicate large nerve bundles. **f,** Horizontal maximum projection of the oral portion of the sucker ganglion stained with acTUBA. No large nerve bundles are present. Scale bars: 100 μm. **g,** Distribution of fiber exits around the SG (n = 1 ganglion, stained with acTUBA) plotted in the transverse plane. Color key corresponds to size of fascicles. The largest fiber bundles exit aborally, corresponding to the portion between the NP cap (***) and cell body protrusion (**). **h,** Example of SG nerves (blue) segmented out of transverse whole mount slice stained with acTUBA. Red traces depict the axial nerve cord oral roots. **i,** Schematic of the average trajectory, which is a vector created from the nerve exit point to the center of the processes. **j,** Distribution of average trajectories in the transverse plane (n = 1 ganglion, stained with acTUBA). Color key corresponds to nerve root location in the aboral-oral, external-internal plane. Asterisks depict aboral gap (***) and lateral gaps (**) as in d and g. Nerve targets correspond to nerve exit. Key illustrates the transverse orientation. **k,** Distribution of average trajectories in the horizontal plane (n = 1 ganglion, stained with acTUBA). Color key corresponds to nerve target location in the horizontal plane. There is a bias away from the proximal-distal axis. Key illustrates the horizontal orientation. acTUBA, acetylated alpha tubulin; CB, cell bodies; ExS, external side; InS, internal side; NP cap, neuropil cap; SG, sucker ganglion.

DISCUSSION

The sucker ganglia are an exceptional feature of the octopus nervous system. First, across the eight arms of an adult *O. bimaculoides*, there are estimated to be over 1000 ganglia. Second, as noted by Graziadei (1971) and confirmed in the results of this study, they have an inverted structure. Third, as we document here, they have a rich internal complexity, an aboral inner belt with neuronal cell bodies, an oral outer belt devoid of neurons, and a connective tissue plate subdividing the ganglion as a whole (Fig. 5.9a).

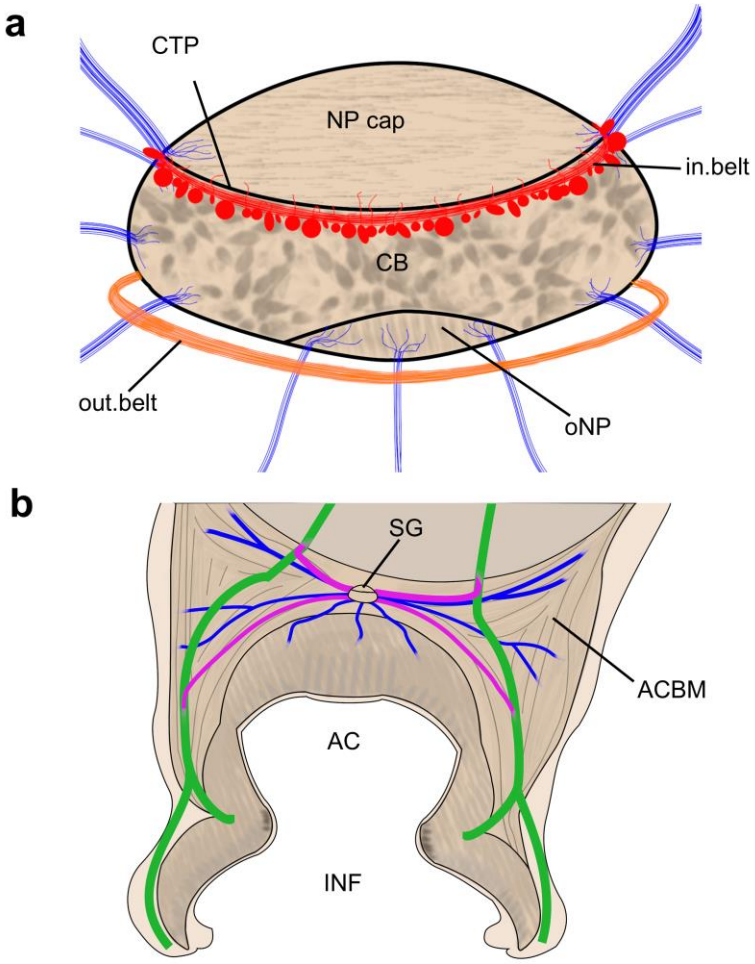

Figure 5.9: Summary of sucker ganglion internal complexity and nerve fiber connections **a,** Cartoon depicting internal organization of the sucker ganglion (SG). The inner belt (red; in.belt), outer belt (orange; out.belt) and nerves (blue) connecting to the SG are highlighted. **b,** Schematic depicting nerve connections. Oral nerves from the axial nerve cord are green. Nerves

from the SG that target the oral nerves are pink. Nerves from the SG that target local musculature are blue. AC, acetabulum; ACBM, acetabular brachial muscles; CB, cell bodies; CTP, connective tissue plate; in.belt, inner belt; INF, infundibulum; NP cap, neuropil cap; oNP, oral neuropil; out.belt, outer belt; SG, sucker ganglion.

Our molecular investigations showed positive expression for both motor and sensory neuron markers, indicating a dual sensory and motor role for the sucker ganglion. The molecular profile of the sucker ganglion, however, is less complex than that of the ANC, consistent with a divergence in function between these two structures. We failed to detect positive expression of *DRGX* within the ganglion, although both the CBL of the ANC and the ACBM are enriched with *DRGX*-expressing cells (Olson et al., 2025). Vertebrate mammalian studies suggest that *DRGX* is expressed in nociceptive sensory cells (Chen et al., 2001; Rebelo et al., 2006). Primary nociceptive cell bodies for the sucker, therefore, may be situated within the ANC or the sucker musculature but not in the sucker ganglion. Our positive detection of *PIEZO* within the sucker ganglion and ACBM support Graziadei's (1965) observation of muscle receptors. This molecular evidence suggests that the sucker ganglion carries proprioceptive information for the sucker.

The presence of both sensory and motor cells suggests that the sucker ganglion is well suited to modulate local reflexes for the sucker without input from the ANC. Indeed, the sucker ganglion extends nerve fibers to the local musculature and cells within these muscles feed back to the sucker ganglion. Classic literature has also suggested the presence of sensory-motor cells extending from the sucker ganglion: a single cell body with one sensory projection that might detect muscle stretch and one motor projection that could activate muscle (Martoja and May, 1955). Future work is needed to investigate this interesting possibility.

Our data strongly imply functional differences in sensory-motor processing across the 3 cardinal axes for a sucker: the aboral-oral, external-internal, and proximal-distal axes (see Fig.

5.3). The sucker ganglion sends nerve fibers in both the oral and aboral directions towards the oral roots issued from the ANC to the sucker epithelium. The connections orally suggest that the sucker ganglion may also exchange information with the sensory epithelium. The connections aborally, combined with the presence of large nerve bundles, suggest that the sucker ganglion sends information to and receives information from the ANC. Hence, the sucker ganglion is situated for both local reflexes and relays to the ANC (Fig. 5.9b).

There is also a bias of nerve fibers in the external-internal and proximal-distal axes, with a prejudice towards the external-internal axis and away from the proximal-distal axis. Along with asymmetric *FMRF* gene expression in the external-internal axis, this could underlie preferential sensorimotor activity along the external-internal axis. Further studies of the distribution of specific chemoreceptor subtypes around the sucker's sensory epithelium could elucidate any biases in sensory transduction, and an examination of individual sucker movements along the cardinal axes could uncover biases in motor action. Interestingly, many behaviors utilizing multiple suckers, such as passing food along the arm or grasping an object, require the coordination of the movements of individual suckers along the proximal-distal axis (Wells, 1964; Altman, 1968; Sivitilli et al., 2022). We did not detect any direct connections between adjoining sucker ganglia, so the ANC most certainly handles the connections needed for concerted motor action between suckers (Rowell, 1963; Graziadei, 1971; Olson et al., 2025). The ANC may also rely on its own separate circuits for control of coordinated motor actions between suckers or instead coordinate the activities of the sucker ganglia. Functional studies are needed to assess the relative roles of the ANC and the sucker ganglion for motor control of the suckers.

Structure and function of peripheral ganglia vary greatly across phyla (Tauc, 1967). Vertebrate sympathetic autonomic ganglia, for example, are traditionally thought of as relay

stations for faithful transmission of central nervous system signals to effectors (Tauc, 1967; Nauta and Feirtag, 1986; Karemaker, 2017). Our data suggest that the sucker ganglia do not have an analogous function as either a sensory or motor relay, but rather exhibit substantial internal integrative circuitry. A comparison to other peripheral ganglia in cephalopods is also informative. Cephalopods have a pair of stellate ganglia located in the mantle, most famously known for the giant fiber system in squid (Young, 1936, 1972; Hodgkin and Huxley, 1939; Lund, 1971; Wang and Ragsdale, 2019). These ganglia are implicated in control of mantle contractions for respiration and escape as well as adaptive coloration both through direct relays from the brain and local ganglionic processing (Young, 1938; Wilson, 1960; Lund, 1971; Bühler et al., 1975; Gonzalez-Bellido et al., 2014, 2018). Structurally, the stellate ganglia have a clear regionalization along the dorsal-ventral axis in the size of the cells and the structure of the NP (Lund, 1971; Young, 1972). This is reminiscent of the regionalization we report in the sucker ganglion along the aboral-oral axis. However, unlike the sucker ganglion, the stellate ganglia have a typical ganglionic structure of cell bodies wrapping neuropil in its center (Lund, 1971; Young, 1972). The stellate ganglia also do not have an equivalent outer or inner belt like the sucker ganglia. Thus, even in the context of other cephalopod ganglia, the structure of the octopus sucker ganglion is strikingly unique.

CONCLUSION

The sucker ganglion is embedded in the sucker musculature, strategically situated between the ANC and the acetabulum of the sucker. Previous anatomical studies have proposed, in turn, a sensory, a motor, or a combined sensory and motor role for the ganglion (Guérin, 1908; Martoja and May, 1955; Rowell, 1963; Graziadei, 1965a; Graziadei and Gagne, 1976). Our molecular analysis does point to the sucker ganglion having populations of both sensory and

motor neurons. Having intermixed sensory and motor neurons does not, however, guarantee an integrative role for the ganglion. It is our cellular analysis demonstrating a complex internal organization and a suite of fiber projections independent of those of the ANC to the sucker apparatus (Fig. 5.9) that lead us to conclude that the sucker ganglion has specialized and unique integrative roles in sucker sensory-motor neuronal processing.

CHAPTER 6

Discussion

The octopus has the remarkable ability to control and coordinate its highly flexible arms effectively, both along each arm and across all eight arms. The arms are also lined with hundreds of mobile suckers. These suckers are also chemotactile sensory organs. With this thesis, I examined the extensive nervous system in the arm of the octopus to address the question of how a nervous system can control such a flexible appendage. I found that the fundamental organization of the axial nerve cord (ANC), the octopus equivalent to a spinal cord, is segmentation. This segmentation sets up a suckerotopy for each sucker in the ANC. I also found that the ANC has multiple longitudinal tracts for intermediate and long-distance communication. Finally, I establish that the sucker ganglion, one for each sucker, is well posed to mediate local reflexes for that sucker.

The octopus arm is a reiterated structure, with the pattern of muscles and pairs of suckers repeated down the length. For neural control of this redundant structure, segmentation in the ANC signifies many patterns layered on top of each other. Most strikingly, the segmentation establishes a sensorimotor topographic map for the sucker, both through oral nerves that spatially tile the sucker and an internal neuropil (NP) arrangement that maintains the spatial organization. While processes from the sucker musculature and sensory epithelium are major contributors to the oral nerves, sucker ganglion nerves also join the oral nerves as the pathway to interconnect with the ANC. The sucker ganglion nerves appear to only connect with a subset of the oral nerves. Sucker ganglion connections would then account for a subset of the larger suckerotopy pattern in the oral ANC NP. Notably, there is a section through the oral NP in which only a subset

of fibers project across the midline (Fig. 3.9g). These projections could correspond to sucker ganglion processes.

The ANC segmentation also supports sensorimotor control for the brachial musculature. While aboral and central nerves exiting from neighboring septa have distinct trajectories, the pattern shows evidence of repeating a frequency of 3-4 segments. These nerves target the brachial musculature, skin, and intramuscular nerve cords (IMNCs). Interestingly, nerves connecting to the skin are bilaterally symmetric. If a nerve targeting the skin exited on the anterior side of the ANC, there was a second skin nerve exiting on the posterior side of the ANC. Sometimes, these skin nerves were a single bundle targeting the skin. Other times, a nerve had multiple bundles that separately connected to the skin, IMNC and musculature. Similarly, sometimes nerves targeted only the brachial musculature, or they had two major branches, one targeting the IMNC and one targeting the brachial musculature (see Fig. 3.6 for examples of nerve morphology). This suggests connections to the skin, IMNC and brachial musculature could have independent patterning mechanisms that sometimes coincide to use the same ANC septa as exit points. Within the NP of the ANC, the aboral and central nerves seemingly exhibit the same structure regardless of their target (i.e., skin, IMNC or brachial musculature; see Fig. 3.8b, c). The longitudinal tracts within the ANC neuropil could serve as pathways for unmixing processes from different targets.

Our gene expression experiments revealed that sensory and motor cell bodies occupy overlapping territories in the ANC and sucker ganglion. This is in line with previous research which suggest that ANC nerves carry sensory and motor information (Rossi and Graziadei, 1958; Rowell, 1966; Gutfreund et al., 2006), though is a departure from organization seen in other systems (Jessell, 2000; Nomaksteinsky et al., 2013). The ANC and sucker ganglion must have

alternative strategies for parsing motor output from sensory input. The longitudinal tracts within the ANC, for example, could be subdivided into separate bundles for sensory and motor information. Alternatively, the organizational principle may only be revealed through synaptic connections at the ultrastructural level.

The arm tapers down the long axis, with the brachial musculature and suckers decreasing in size. Many biomechanical features emerge from the proximal to distal decrease in brachial musculature. The length of arm needed for a bend is much longer proximally than distally. The distal portions of arm, with a smaller radius in the transverse dimension, will buckle at much lower forces. Accordingly, the width of the segments scales to reflect these changes. Our results suggest that a 1mm length of arm would encompass 20 segments distally but only 5 segments proximally. A decrease in number of segments for the same length of arm proximally also implies that fewer nerves span the same length of arm. Indeed, nerves from proximal blocks of arm exhibit greater branching and a further spread in the z-direction whereas those in distal blocks seem compressed (see Fig. 3.6). Given an increase in propensity for buckling and a lower radius of curvature for bends, neural control for the brachial musculature in distal portions of arm would benefit from an increased number of segments and a greater density of nerves.

Behavioral studies have demonstrated that *O. bimaculoides* will use the distal portion of the arm to explore objects and hunt for food in crevices (Buresch et al., 2022, 2024). Our results show that the sucker ganglion occupies a higher proportion of territory in the sucker in distal portions of the arm. The number of segments in the ANC per sucker was also slightly higher for the distal portion of arm, with an average of 8.5 segments/sucker. With their decrease in size from proximal to distal, the suckers are packed closer together distally. This suggests an increase in chemotactile sensitivity, which could require an increase in neural territory for processing.

Interestingly, a recent EM study on the organization of the ANC in a much smaller octopus, *Octopus bocki*, found 9 segments/sucker (Neacsu and Crook, 2024). While this could be an interspecies difference, this could suggest that as the arm and suckers continue to decrease in size, the number of segments/sucker will increase. Studies on the organization of the ANC in juvenile and hatchling *O. bimaculoides* could provide further insight in how the structure of the arm nervous system scales based on the size of the arm.

Our findings establish strong anatomical bases for a number of behavioral and physiological studies. Our descriptions demonstrate a sensorimotor topographic map for the sucker in the ANC. How is this functionally utilized? Does sensory stimulation of the sucker cause activation localized to a particular segment? Does electrical stimulation of the ANC segments cause localized motor deflections around the sucker? We also found that sucker ganglion is well situated for sensorimotor reflexes: what kind of sensory input is transmitted to the ANC as opposed to the sucker ganglion? How is sucker ganglion input processed? Recent technological advances have begun to make it possible to examine these questions (Gutnick et al., 2023; Gedela et al., 2025).

The results here are all discussed in terms of centralized nerve centers, the axial nerve cord and sucker ganglion, which each have a defined set of nerves. However, this does not capture the full picture of the arm nervous system. Close interrogation of the musculature after immunostaining for acetylated alpha tubulin or ISH with neuronal subtype markers, including markers of motor neurons, reveals widespread positive labeling. One possibility is that this could indicate how densely the musculature is innervated. While classic studies suggest that innervation of the muscles share features similar to the innervation of vertebrate smooth muscles, we still do not know where the neuromuscular junctions are located (Graziadei, 1966). Some of

this labeling, though, is quite extensive and found at the junction between muscle groups. This could represent distributed neural circuits for extremely localized sensorimotor reactions; that is, circuits where the motor neuron is located within the muscle it contracts in response to a stretch. The octopus arm nervous system therefore could provide an interesting case to examine interplay between distributed circuits and centralized circuits for motor control.

Interplay with the brain

The arm nervous system does not act solely in isolation, but rather it interconnects with intermediate and higher motor areas in the brain. Notably, there is an apparent lack of the somatotopy in higher motor centers of the brain (Boycott, 1961; Zullo et al., 2009): stimulation of the higher motor centers creates coordinated movement across all limbs, not merely one. In contrast, we report a sensorimotor topographic map of the suckers in the ANC, which constitutes the lower motor center. This difference could be due to the nature of the motor control problem in the octopus or due to the complex structure of the neuropil of cephalopod brain lobes. Given that arm musculature exhibits a repeated pattern, the same higher order control signal from the brain could be used to produce the same muscle contraction regardless of arm. What would then be needed is to relay the signal to specific arms. Within the brachial lobes, which are the intermediate motor areas, stimulation near the entry of the brachial nerves elicits movements of single arms (Boycott, 1961; Young, 1971). This “brachiatopy” provides the anatomical pathway to direct input to specific arms. The ANC must then handle the problem of localizing motor commands to particular suckers or parts of the arm. The segmented structure of the ANC is well suited to carry out this task.

While an absence of somatotopy seems like a departure from vertebrate systems, a similar feature has been shown to be present in primates. Through elevated current stimulation of

motor cortex in macaques, Graziano et al. (2002) elicited extensive body behaviors and not just single muscle twitches. A recent fMRI study in primates and pediatric humans further suggests a whole body action system embedded within M1(Gordon et al., 2023). As studies of motor control typically center on limited behavioral paradigms, it is possible that a somatotopic map provides a limited view of the functioning of vertebrate motor cortex. Further studies of animals in freely behaving scenarios and of the octopus motor system could provide further insights into alternative computational architectures.

Interestingly, it does appear that sucker sensory-motor control is processed in part by the inferior frontal system (IFS): lesions to the IFS impair the octopus's ability to detect the valence of food and cause the suckers to become sticky (Wells, 1961; Altman, 1971). We provide evidence brachial and sucker information may travel through different tracts within the CBT, which interconnects with the brain. In particular, the α tracts receive large processes from sucker-related areas of the ANC and musculature. These tracts could be the pathways for relaying sucker information to and from the IFS.

Comparisons across cephalopods

A comparison to squid demonstrates that arm nervous system structure varies based on appendage morphology, environmental context and behavioral needs. *O. bimaculoides* is a benthic animal, with arms suited for exploring the ocean floor (Hanlon and Messenger, 2018; Kang et al., 2023; Buresch et al., 2024). As a pelagic animal, the squid *Doryteuthis pealeii* mostly uses its arms and tentacles for the essential behavior of prey capture (Hanlon and Messenger, 2018). As such, *D. pealeii* is predicted to have a relatively impoverished complexity to its arm nervous system in comparison with *O. bimaculoides* (see also Kang et al., 2023).

Accordingly, I found fewer ANC segments, a less complex sucker ganglion, and expansion of longitudinally running tracts in the ANC in *D. pealeii* arms.

The ANC in the loliginid squid tentacle stalk lacks segmentation in the CBL, demonstrating that ANC segmentation is not the only control architecture that could be used to control a flexible muscular hydrostat. However, even in the absence of CBL segments, nerves still regularly exit the tentacle stalk ANC to innervate the surrounding musculature. After the squid positions its full body towards the prey, the tentacle stalks elongate rapidly to grab prey, reaching the target in 15-35 ms (Kier, 1985). With the speed of this motor act in the context of a full body behavior, the main requirement of the ANC could simply be to propagate a signal from the brain along the length of the stalk, activating the relevant muscles through regularly exiting nerve fibers. Local integration of motor commands across segments would not be needed.

Despite an apparently impoverished ANC, *D. pealeii* tentacles and arms have six intramuscular nerve cords (IMNCs) compared to the four seen in *O. bimaculoides.* The IMNCs have been implicated in proprioception (Graziadei, 1965a; Kuuspalu et al., 2022). By their location on the lateral edges of the arms and tentacles, they may in part serve as a signature of the general shape of the appendage. In transverse cross section, the octopus arm is circular in shape (see Fig. 3.2). This shape is well represented by 4 cords. In contrast, the shape of *D. pealeii* arms and tentacles is irregular in transverse cross section (see Fig. 4.6). Four IMNCS would not sufficiently mark the shape of the appendage, whereas six IMNCs could. Work examining the composition of the IMNCs and their function could provide further insight into what drives this difference between squid and octopus.

Conclusion

The work presented in this thesis has greatly extended current descriptions of the extensive nervous system embedded in the arm of the octopus. I found that the ANC controlling the prehensile arm of the octopus is segmented. This segmental arrangement offers a template for modeling the motor control of soft tissues and provides a compelling example of nervous system segmentation in molluscs. The ANC also hosts intra-NP and extra-NP fiber tracts, posed for coordinating motor acts along the length of the arm. Finally, with its unusual and complex internal organization, I found the sucker ganglion is well situated for control of sucker reflexes and integrative sensorimotor processing.

APPENDIX

Octopus bimaculoides arm musculature

The muscles of the arm are an important backdrop for interrogating the structure and function of the nervous system which controls them. Here, we summarize observations from our investigations into the structure and molecular composition of the arm muscles of *Octopus bimaculoides*. These findings were critical to our understanding of the geography of the arm and thus motor control of it. We additionally provide a muscle atlas composed of serially sectioned, longitudinally sliced arm stained by in situ hybridization with myosin heavy chain (*MYH;* Fig. A.6).

Molecular composition of arm muscles

Using in situ hybridization for *MYH* and phalloidin as a marker for F-actin, we verified labeling throughout both the brachial musculature, comprising the longitudinal, transverse, oblique (inner, middle and outer) and circular muscles, and the sucker musculature, comprising the acetabulum, infundibulum, and acetabulobrachial muscles (Fig. A.1). These data confirm that the muscles in the octopus arm possess the canonical muscle contraction units: myosin as a thick filament and actin as a thin filament.

With in situ hybridization, we noticed that the strength of muscle labeling varied based on plane of section. Muscle fibers are most strongly labeled in sections that were cut parallel to the fiber. Sections that were perpendicular to the fiber demonstrated weaker labeling. Thus, labeling of the transverse muscles will be strongest in the transverse plane, and labeling of the longitudinal muscles will be strongest in the longitudinal plane (Fig. A.1a, c). This difference in labeling had its advantages, as the trabeculae of the transverse muscle system were readily apparent in longitudinal sections by decrease in staining intensity (Fig. A.1c). Stains with

phalloidin do not demonstrate this difference in labeling intensity based on plane of section (Fig. A.1b, d). Nonetheless, the trabeculae could still be detected threading through longitudinal muscle following close interrogation of the longitudinal muscles in longitudinal sections (Fig A.1d).

In addition to labeling throughout the brachial and sucker musculature, we detected labeling for both *MYH* and F-actin in the skin (Fig A.1e, f). There are two parallel, longitudinal muscle fibers in the skin situated aboral to the brachial musculature. As the skin is a highly elastic material, these muscles may assist in maintaining tone of the skin as the arm elongates, bends, and twists.

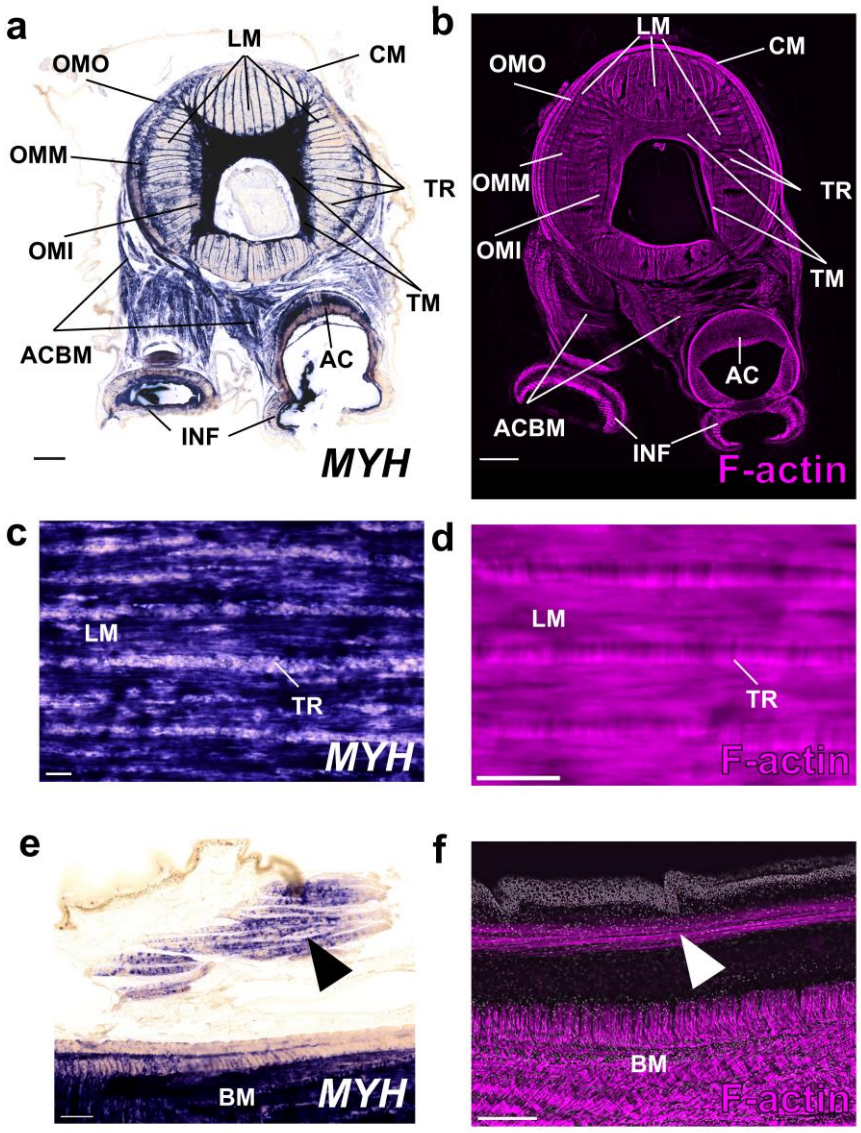

Figure A.1: *MYH* and F-actin labeling throughout the arm.
a, b. Myosin and actin are found throughout all muscle groups in the arms. **a,** Transverse section of arm stained with in situ hybridization (ISH) for *MYH*. **b,** Transverse section of arm stained with phalloidin labeling F-actin. Scale bars: 500 µm **c,** Longitudinal section of the longitudinal muscles (LM) stained with ISH for *MYH.* Note that labeling of the LM is stronger in longitudinal sections. Trabeculae (TR) of the transverse muscle system are detectable by a decrease in stain intensity. **d,** F-actin labeling of LM in the longitudinal plane demonstrating that the TR thread through the LM. Scale bars: 50 µm **e, f.** Longitudinal sections through muscle fibers in the skin located aborally to the brachial musculature (BM). **e,** ISH for *MYH*. **f,** F-actin. Scale bars: 250 µm. BM, brachial musculature; AC, acetabulum; ACBM, acetabulobrachial muscles; CM, circular muscles; INF, infundibulum; LM, longitudinal muscles; OMI, inner oblique muscle; OMM, middle oblique muscle; OMO, outer oblique muscle; TM, transverse muscles; TR, trabeculae.

We next interrogated the musculature for markers of other components of musculature: paramyosin (PRM), titin (*TTN*), and tropomyosin (*TPM*). In invertebrates, *PRM* is a component of the thick filament and typically highlights obliquely striated muscles (Yang et al., 2022). *TTN* is a large molecular spring which, in other systems, anchors myosin to the z band (Eckels et al., 2018). Along with troponin, *TPM* regulates the binding of myosin and actin (Lees-Miller and Helfman, 1991). We found positive expression of each of these markers throughout all muscle groups in the brachial and sucker musculature. These results indicate that octopus arm muscles contain molecular components that exist in other invertebrates. Further interrogation of the distribution of ion channel subtypes across muscle groups could reveal complexities in the function of these muscles (Gilly et al., 2020).

Interestingly, *TPM* and *TTN* both demonstrated labeling in the cell body layer of the ANC. *TPM* has many isoforms, and in other systems, expression in neural tissue has been documented (Lees-Miller and Helfman, 1991; Schevzov et al., 2012). It is hypothesized that in neural tissue, *TPM* plays a role in cytoskeleton restructuring (Schevzov et al., 2012). Recent research has localized *TTN* to the dense fibrillar component of the nucleolus of neurons, including spinal cord motor neurons (George et al., 2024). Further research is needed to determine the role *TPM* and *TTN* in octopus neurons.

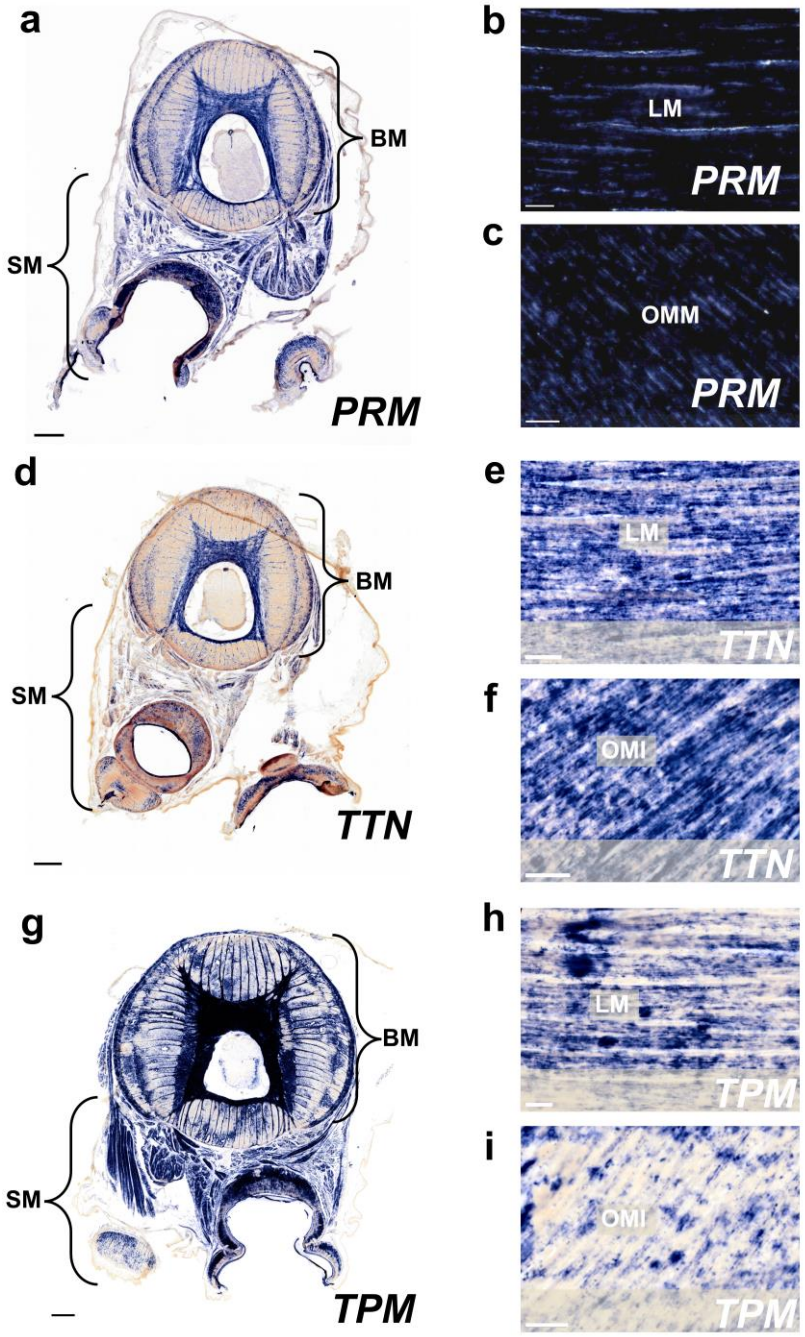

Figure A.2: Distribution of other molecular components of muscle.
Expression for *PRM, TTN,* and *TPM* is detected throughout the brachial musculature (BM) and sucker musculature (SM). Note that labeling is strongest in sections parallel to muscle fibers. **a-c,** in situ hybridization (ISH) of *PRM*. **a,** transverse section of arm depicting labeling for *PRM* in the BM and SM. Scale bar: 500 µm. **b, c** longitudinal sections through the longitudinal muscles (**b**; LM) and middle oblique muscles (**c**; OMM) demonstrating strong labeling for *PRM*. Scale bars: 100 µm. **d-f,** ISH of *TTN*. **d,** transverse section of arm with positive labeling for *TTN* in the BM and SM. Scale bar: 500 µm. **e, f** longitudinal sections through the LM (**e**) and inner oblique

muscle (**f**; OMI) with strong labeling for *TTN*. Scale bars: 100 µm. **g-i,** ISH of *TPM*. **g,** transverse section of arm with positive expression of *TPM* throughout the BM and SM. Scale bar: 500 µm. **h, i** longitudinal sections through the LM (**h**) and OMI (**i**) with clear labeling for *TPM*. Scale bars: 100 µm. BM, brachial musculature; LM, longitudinal muscles; OMI, inner oblique muscles; OMM, middle oblique muscles; SM, sucker musculature.

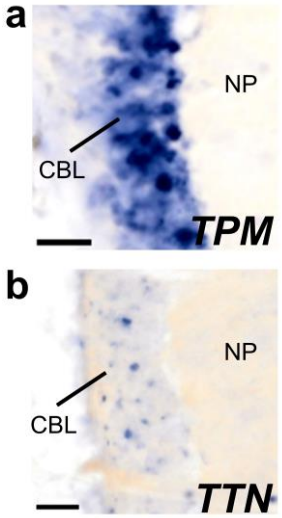

Figure A.3: *TPM* and *TTN* labeling in the ANC.
Positive expression for *TPM* and *TTN* was found in the neuronal cell bodies in the axial nerve cord (ANC). **a,** in situ hybridization (ISH) for *TPM*. **b,** ISH for *TTN*. Scale bars: 50 µm. CBL, cell body layer; NP, neuropil.

Stereotyped structure

To investigate any changes in muscle structure along the proximal-distal axis and across all eight arms, two slices of arm, one proximal and one distal, were taken from each of the arms of an adult octopus. This octopus was reared from hatching in the lab. Because of this, we know the full life history of the octopus and could ensure that no major arm injuries and therefore no major arm regeneration had occurred. Arm blocks were sectioned longitudinally and either stained with phalloidin to label F-actin or with ISH for *MYH*.

The structural pattern based on the striations of the muscles remained consistent along the proximal-distal axis and across the eight arms. The muscle atlas (Fig. A.6) depicts this

stereotyped pattern. Most notably, both sets of outer and inner obliques are angled such that an arrow drawn from oral to aboral would point distally (Fig. A.4a, c). Both sets of middle obliques were oriented such that an arrow from oral to aboral would point proximally (Fig. A.4 b). Given that the obliques are curved, angled muscles thought to mediate torsion (Kier and Stella, 2007), the difference in orientation creates a unique difference in handedness. For arms on the left side of the body, the outer and inner oblique on the anterior side of the arm form a left-handed helix. Those on the posterior side form a right-handed helix. The middle oblique forms a right-handed helix on the anterior side of the arm and a left-handed helix on the posterior side of the arm. The pattern flipped for arms on the right side of the body. Contraction for clockwise twists of the arm could arise from the obliques forming right-handed helices, and contraction for counterclockwise twists of the arm could arise from the obliques forming left-handed helices. Practically speaking, the orientation of the obliques served as a marker for determining the proximal and distal axis when analyzing data presented in Chapter 3, 4, and 5.

Interestingly, we detected variation in the labeling between proximal and distal slices. While labeling for both F-actin and *MYH* was present throughout all muscle groups, labeling on the distal slices was particularly splotchy (Fig. A.4d-k). Since the arm is continuing to grow from the distal tip, this labeling could be associated with less mature muscle fibers. Alternatively, it could indicate differences in state of contraction or muscle activity.

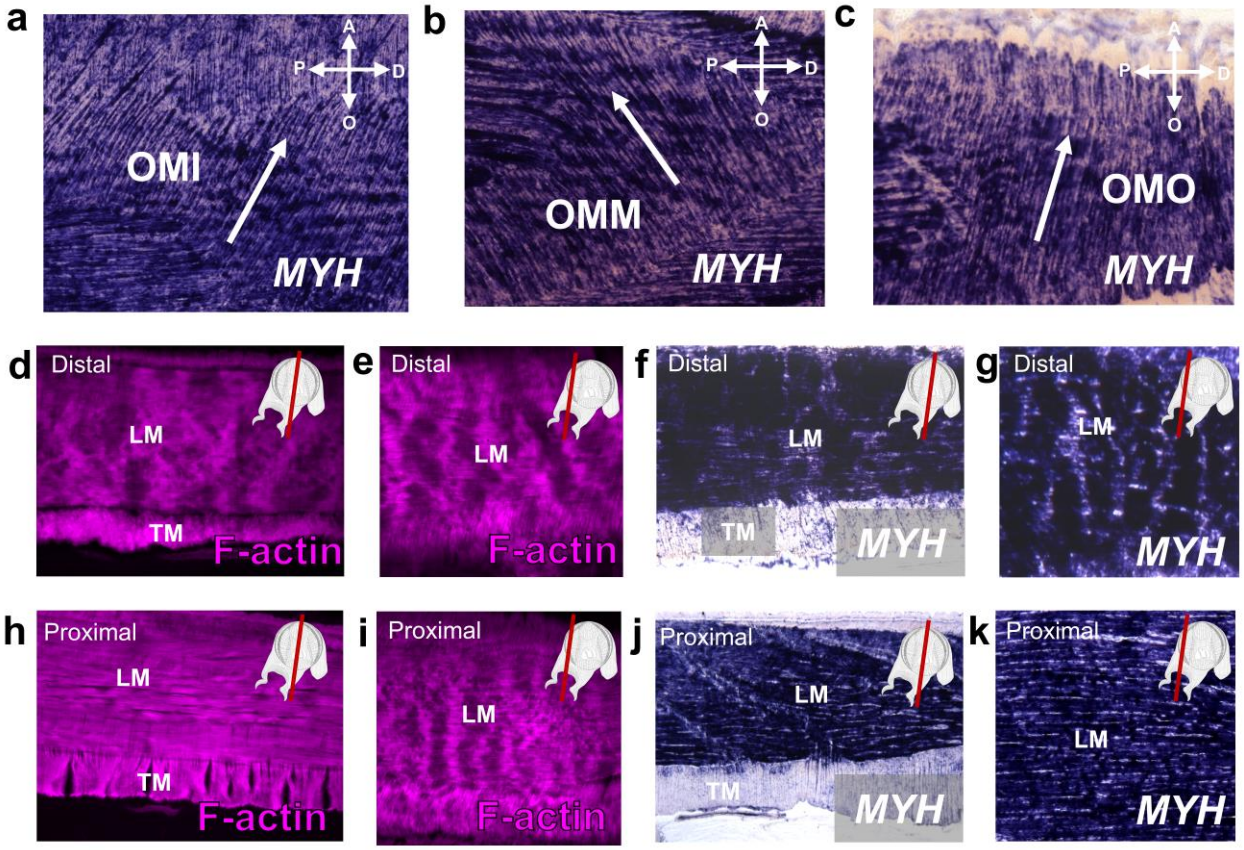

Figure A.4: Orientation of the oblique muscles and proximal-distal variation.
a-c, Longitudinal sections through the oblique muscles stained by in situ hybridization (ISH) for *MYH.* **a,** inner oblique muscle (OMI). Arrow from oral (O) to aboral (A) points distal (D). **b,** middle oblique muscle (OMM). Arrow from O to A points proximal (P). **c,** outer oblique muscle (OMO). Arrow from O to A points D. **d-g**, Longitudinal sections through distal arm blocks. Labeling for F-actin (**d, e**) and *MYH* (**f, g**) was particularly splotchy in both medial (**d, f**) and lateral (**e, g**) sections. Inset depicts plane of section with red line. **h-i,** Labeling for F-actin in longitudinal sections through proximal arm blocks was splotchy in lateral sections (**i**) but not medial sections (**h**). **j-k,** Labeling for *MYH* in longitudinal sections through proximal arm blocks was not splotchy in either medial (**j**) or lateral (**k**) sections. A, aboral; D, distal; LM, longitudinal muscles; O, oral; inner oblique muscle, OMI; middle oblique muscles, OMM; outer oblique muscle, OMO; P, proximal; TM, transverse muscle.

Methods for interrogating the intertwined nature of the muscles

The arm muscle groups are incredibly intertwined. While stains with phalloidin and ISH for markers of muscle components demonstrate this complexity it is challenging to separate

muscle fibers from these methods alone. Injections of dextran into the musculature will fill individual muscle fibers, and this method could be used to disentangle the muscles. For example, in Fig. A.5a, it appears that the transverse muscle mass includes the aboral trabeculae, which flair out upon entering the mass. An injection of dextrans into this aboral musculature validates this point, as individual trabeculae labeled with dextrans weave into the transverse muscles. (Fig. A.5b).

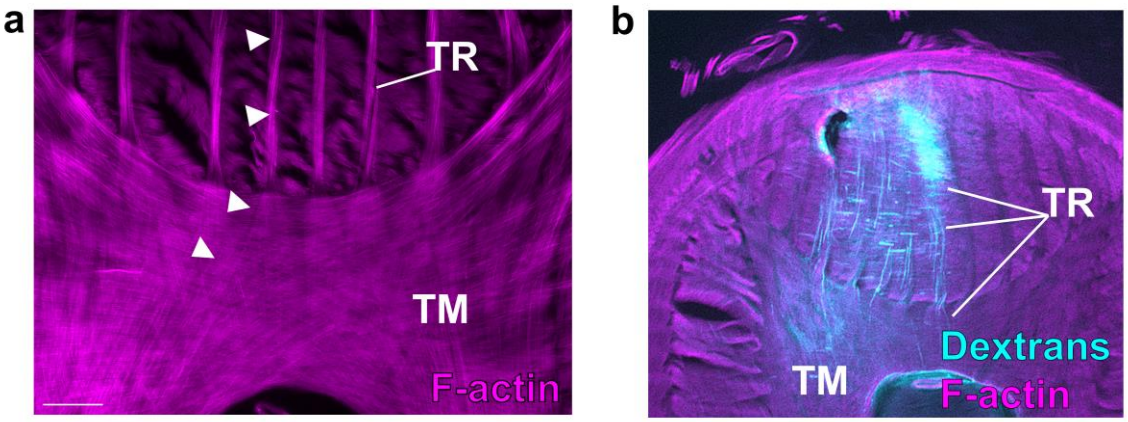

Figure A.5: Interrogating the intertwined nature of octopus arm muscles with dextrans. Evidence that the trabeculae compose the transverse muscle mass. **a,** Transverse section of arm stained with F-actin highlighting the transverse muscles and trabeculae. Arrowheads point to a single trabeculae that appears to flair out in the transverse muscles. Scale bar: 100 µm. **b**, Injection of dextrans into the aboral arm musculature fill individual muscle fibers composing the trabeculae and demonstrate that the trabeculae weave into the transverse muscle mass. TM, transverse muscle; TR, trabeculae.

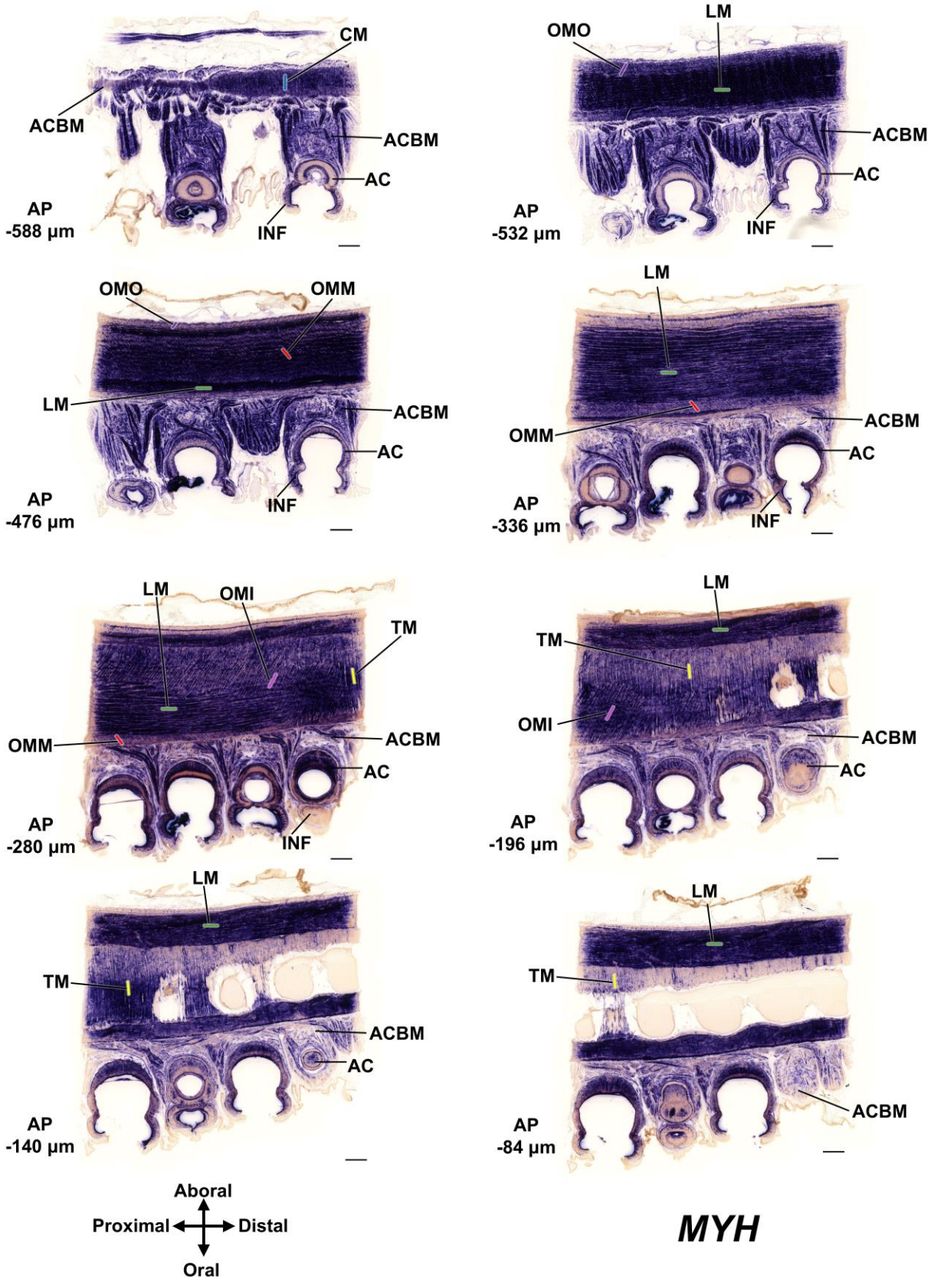
CM
ACBM
ACBM
AC
AP
-588 µm
INF
LM
OMO
ACBM
AC
AP
-532 µm
INF
OMO
OMM
LM
ACBM
AC
AP
-476 µm
INF
LM
OMM
ACBM
AC
AP
-336 µm
INF
LM
OMI
TM
OMM
ACBM
AC
AP
-280 µm
INF
LM
TM
OMI
ACBM
AC
AP
-196 µm
LM
TM
ACBM
AC
AP
-140 µm
LM
TM
ACBM
AP
-84 µm
Aboral
Proximal
Distal
Oral
MYH

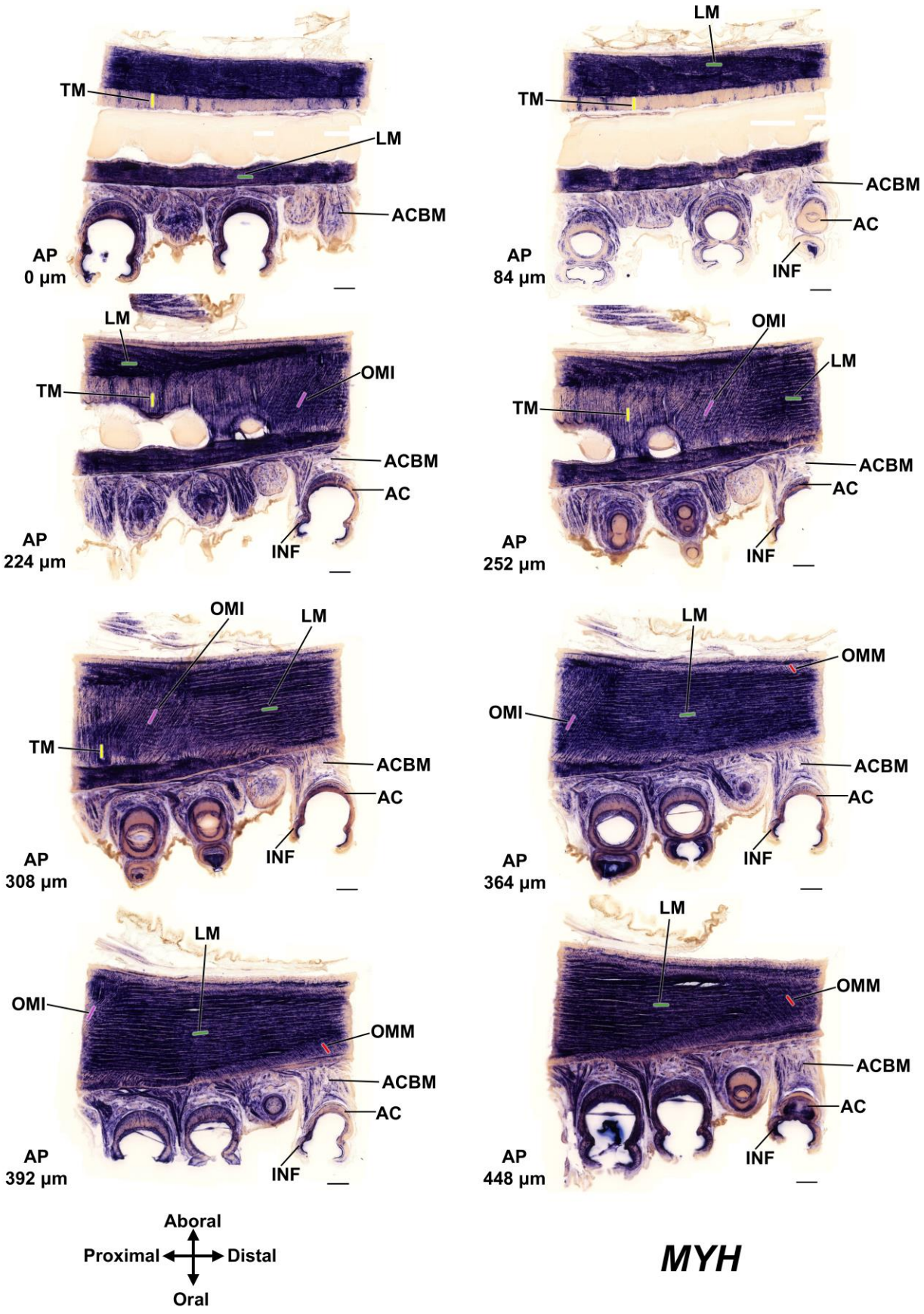
TM
LM
ACBM
AP
0 µm
LM
TM
ACBM
AC
AP
84 µm
INF
LM
TM
OMI
ACBM
AC
AP
224 µm
INF
OMI
LM
TM
ACBM
AC
AP
252 µm
INF
OMI
LM
TM
ACBM
AC
AP
308 µm
INF
LM
OMM
OMI
ACBM
AC
AP
364 µm
INF
LM
OMI
OMM
ACBM
AC
AP
392 µm
INF
LM
OMM
ACBM
AC
AP
448 µm
INF
Aboral
Proximal
Distal
Oral

MYH

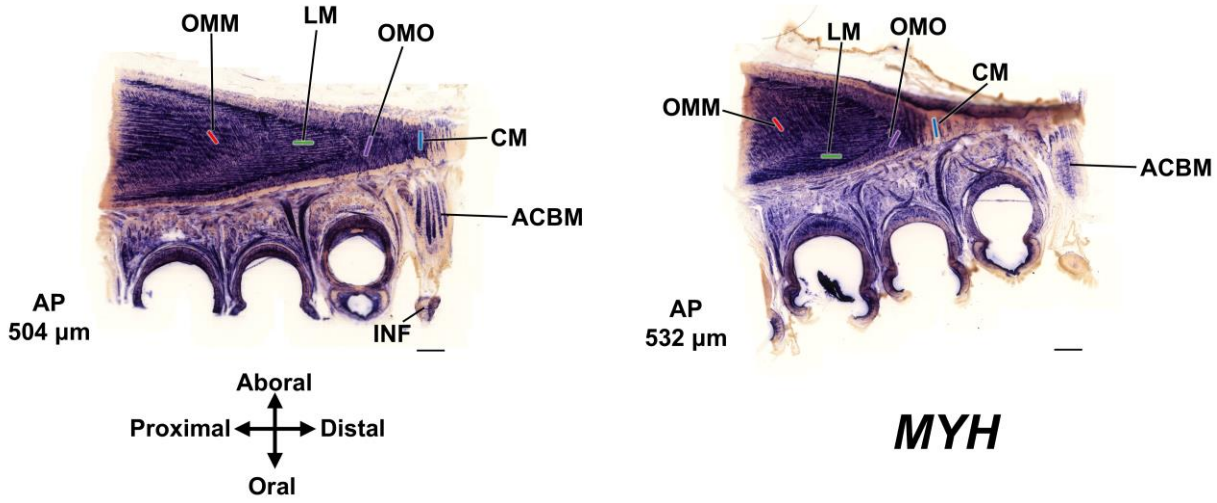

Figure A.6: Muscle atlas.
Serial, longitudinal sections through an intermedial block from arm 1L stained by in situ hybridization for myosin heavy chain (*MYH*). The AP (anterior-posterior) key in the lower left of each section indicates microns from the midline along the anterior-posterior axis. Scale bar: 500 µm. AC, acetabulum. ACBM, acetabulobrachial muscles. CM (blue), circular muscles. INF, infundibulum. LM (green), longitudinal muscles. OMI (pink), inner oblique muscle. OMM (red), middle oblique muscle. OMO (purple), outer oblique muscle. TM (yellow), transverse muscles.

REFERENCES

Albertin CB, Medina-Ruiz S, Mitros T, Schmidbaur H, Sanchez G, Wang ZY, Grimwood J, Rosenthal JJC, Ragsdale CW, Simakov O, Rokhsar DS. 2022. Genome and transcriptome mechanisms driving cephalopod evolution. Nat Commun 13:2427.

Albertin CB, Simakov O, Mitros T, Wang ZY, Pungor JR, Edsinger-Gonzales E, Brenner S, Ragsdale CW, Rokhsar DS. 2015. The octopus genome and the evolution of cephalopod neural and morphological novelties. Nature 524:220–224.

Altman J. 1968. The nervous control of arm and buccal movements in *Octopus vulgaris*. Doctoral Thesis, University College London:1–413.

Altman J. 1971. Control of accept and reject reflexes in the octopus. Nature 229:204–206.

Arshadi C, Günther U, Eddison M, Harrington KIS, Ferreira TA. 2021. SNT: a unifying toolbox for quantification of neuronal anatomy. Nat Methods 18:374–377.

Baratte S, Bonnaud L. 2009. Evidence of early nervous differentiation and early catecholaminergic sensory system during *Sepia officinalis* embryogenesis. J of Comparative Neurology 517:539–549.

Bidel F, Bennett NC, Wardill TJ. 2022. *Octopus bimaculoides*' arm recruitment and use during visually evoked prey capture. Current Biology 32:4727-4733.e3.

Boycott BB. 1961. The functional organization of the brain of the cuttlefish *Sepia officinalis*. Proc R Soc Lond B 153:503–534.

Bühler A, Froesch D, Mangold K, Marthy H-J. 1975. On the motor projection of the stellate ganglion in Octopus vulgaris. Brain Research 88:69–72.

Buresch KC, Huget ND, Brister WC, Zhou EY, Lineaweaver AS, Rifai C, Hu J, Stevenson ZE, Boal JG, Hanlon RT. 2024. Evidence for tactile 3D shape discrimination by octopus. J Comp Physiol A 210:815–823.

Buresch KC, Sklar K, Chen JY, Madden SR, Mongil AS, Wise GV, Boal JG, Hanlon RT. 2022. Contact chemoreception in multi-modal sensing of prey by octopus. J Comp Physiol A 208:435–442.

Byrne RA, Kuba MJ, Meisel DV, Griebel U, Mather JA. 2006. Octopus arm choice is strongly influenced by eye use. Behavioural Brain Research 172:195–201.

Campos-Ortega JA, Hartenstein V. 1997. The Embryonic Development of Drosophila melanogaster. Berlin, Heidelberg: Springer Berlin Heidelberg. Available from: http://link.springer.com/10.1007/978-3-662-22489-2

Chang H-S, Halder U, Shih C-H, Naughton N, Gazzola M, Mehta PG. 2023. Energy-shaping control of a muscular octopus arm moving in three dimensions. Proc R Soc A 479:20220593.

Chen Z-F, Rebelo S, White F, Malmberg AB, Baba H, Lima D, Woolf CJ, Basbaum AI, Anderson DJ. 2001. The paired homeodomain protein DRG11 is required for the projection of cutaneous sensory afferent fibers to the dorsal spinal cord. Neuron 31:59–73.

Chipman A. 2019. Becoming Segmented. In: Fusco G, editor. Perspectives on Evolutionary Developmental Biology. Padova University Press. p 234–244.

Chitnis A, Kuwada J. 1990. Axonogenesis in the brain of zebrafish embryos. J Neurosci 10:1892–1905.

Clark E, Peel AD, Akam M. 2019. Arthropod segmentation. Development 146:dev170480.

Clark MQ, Zarin AA, Carreira-Rosario A, Doe CQ. 2018. Neural circuits driving larval locomotion in *Drosophila*. Neural Dev 13:6.

Clark RB. 1964. Dynamics in Metazoan Evolution: The origin of the coelom and segments. Oxford: Claredon Press.

Clemente AD, Maiole F, Bornia I, Zullo L. 2021. Beyond muscles: role of intramuscular connective tissue elasticity and passive stiffness in the octopus arm muscle function. Journal of Experimental Biology 224.

Coste B, Mathur J, Schmidt M, Earley TJ, Ranade S, Petrus MJ, Dubin AE, Patapoutian A. 2010. Piezo1 and Piezo2 are essential components of distinct mechanically activated cation channels. Science 330:55–60.

Eckels EC, Tapia-Rojo R, Rivas-Pardo JA, Fernández JM. 2018. The Work of Titin Protein Folding as a Major Driver in Muscle Contraction. Annu Rev Physiol 80:327–351.

Ferreira TA, Blackman AV, Oyrer J, Jayabal S, Chung AJ, Watt AJ, Sjöström PJ, Van Meyel DJ. 2014. Neuronal morphometry directly from bitmap images. Nat Methods 11:982–984.

Fiorito G, Affuso A, Basil J, Cole A, De Girolamo P, D'Angelo L, Dickel L, Gestal C, Grasso F, Kuba M, Mark F, Melillo D, Osorio D, Perkins K, Ponte G, Shashar N, Smith D, Smith J, Andrews PL. 2015. Guidelines for the Care and Welfare of Cephalopods in Research –A consensus based on an initiative by CephRes, FELASA and the Boyd Group. Lab Anim 49:1–90.

Gedela NSS, Radawiec RD, Salim S, Richie J, Chestek C, Draelos A, Pelled G. 2025. In vivo electrophysiology recordings and computational modeling can predict octopus arm movement. Bioelectron Med 11:4.

George L, Cameron B, Torres-Hernandez L, Montague V, Lewis K, Smith H, Fox J, Guo X, Kalb RG. 2024. Titin is a nucleolar protein in neurons. Available from: https://www.researchsquare.com/article/rs-4000799/v1

van Giesen L, Kilian PB, Allard CAH, Bellono NW. 2020. Molecular basis of chemotactile sensation in octopus. Cell 183:594-604.e14.

Gilly WF, Renken C, Rosenthal J, Kier WM. 2020. Specialization for rapid excitation in fast squid tentacle muscle involves action potentials absent in slow arm muscle. Journal of Experimental Biology:jeb.218081.

Gonzalez-Bellido PT, Scaros AT, Hanlon RT, Wardill TJ. 2018. Neural control of dynamic 3-dimensional skin papillae for cuttlefish camouflage. iScience 1:24–34.

Gonzalez-Bellido PT, Wardill TJ, Buresch KC, Ulmer KM, Hanlon RT. 2014. Expression of squid iridescence depends on environmental luminance and peripheral ganglion control. Journal of Experimental Biology 217:850–858.

Gordon EM, Chauvin RJ, Van AN, Rajesh A, Nielsen A, Newbold DJ, Lynch CJ, Seider NA, Krimmel SR, Scheidter KM, Monk J, Miller RL, Metoki A, Montez DF, Zheng A, Elbau I, Madison T, Nishino T, Myers MJ, Kaplan S, Badke D'Andrea C, Demeter DV, Feigelis M, Ramirez JSB, Xu T, Barch DM, Smyser CD, Rogers CE, Zimmermann J, Botteron KN, Pruett JR, Willie JT, Brunner P, Shimony JS, Kay BP, Marek S, Norris SA, Gratton C, Sylvester CM, Power JD, Liston C, Greene DJ, Roland JL, Petersen SE, Raichle ME, Laumann TO, Fair DA, Dosenbach NUF. 2023. A somato-cognitive action network alternates with effector regions in motor cortex. Nature 617:351–359.

Grant P, Pant HC. 2016. Compartment-Specific Phosphorylation of Squid Neurofilaments. In: Methods in Enzymology. Vol. 568. Elsevier. p 615–633. Available from: https://linkinghub.elsevier.com/retrieve/pii/S0076687915005510

Grant P, Tseng D, Gould RM, Gainer H, Pant HC. 1995. Expression of neurofilament proteins during development of the nervous system in the squid *Loligo pealei*. J of Comparative Neurology 356:311–326.

Grasso FW. 2008. Octopus sucker-arm coordination in grasping and manipulation. American Malacological Bulletin 24:13–23.

Graziadei P. 1962. Receptors in the suckers of *Octopus*. Nature 195:57–59.

Graziadei P. 1965a. Muscle receptors in cephalopods. Proc Royal Soc B 161:392–402.

Graziadei P. 1965b. Sensory receptor cells and related neurons in cephalopods. Cold Spring Harbor Symposia on Quantitative Biology 30:45–57.

Graziadei P. 1966. The ultrastructure of the motor nerve endings in the muscles of Cephalopods. Journal of Ultrastructure Research 15:1–13.

Graziadei P. 1971. The nervous system of the arms. In: The Anatomy of the Nervous System of *Octopus vulgaris*. Oxford: Claredon Press. p 45–61.

Graziadei PPC, Gagne HT. 1976. Sensory innervation in the rim of the octopus sucker. J Morphol 150:639–679.

Guérin MJ. 1908. Contribution a l'étude des systèmes cutané, musculaire et nerveux de l'appareil tentaculaire des céphalopodes. Archives de zoologie expérimentale et générale 8:1–179.

Gutfreund Y, Flash T, Fiorito G, Hochner B. 1998. Patterns of arm muscle activation involved in octopus reaching movements. J Neurosci 18:5976–5987.

Gutfreund Y, Flash T, Yarom Y, Fiorito G, Segev I, Hochner B. 1996. Organization of octopus arm movements: a model system for studying the control of flexible arms. J Neurosci 16:7297–7307.

Gutfreund Y, Matzner H, Flash T, Hochner B. 2006. Patterns of motor activity in the isolated nerve cord of the octopus arm. The Biological Bulletin 211:212–222.

Gutnick T, Byrne RA, Hochner B, Kuba M. 2011. *Octopus vulgaris* uses visual information to determine the location of its arm. Current Biology 21:460–462.

Gutnick T, Neef A, Cherninskyi A, Ziadi-Künzli F, Di Cosmo A, Lipp H-P, Kuba MJ. 2023. Recording electrical activity from the brain of behaving octopus. Current Biology 33:1171-1178.e4.

Gutnick T, Zullo L, Hochner B, Kuba MJ. 2020. Use of peripheral sensory information for central nervous control of arm movement by *Octopus vulgaris*. Current Biology 30:4322-4327.e3.

Hanlon RT, Messenger JB. 2018. Cephalopod Behavior. 2nd ed. Cambridge University Press.

Herculano-Houzel S, Mota B, Lent R. 2006. Cellular scaling rules for rodent brains. Proc Natl Acad Sci USA 103:12138–12143.

Hochner B, Zullo L, Shomrat T, Levy G, Nesher N. 2023. Embodied mechanisms of motor control in the octopus. Current Biology 33:R1119–R1125.

Hodgkin AL, Huxley AF. 1939. Action potentials recorded from inside a nerve fibre. Nature 144:710–711.

Hou B, Zhang D, Zhao S, Wei M, Yang Z, Wang S, Wang J, Zhang X, Liu B, Fan L, Li Y, Qiu Z, Zhang C, Jiang T. 2015. Scalable and DiI-compatible optical clearance of the mammalian brain. Front Neuroanat 9.

Hubaud A, Pourquié O. 2014. Signalling dynamics in vertebrate segmentation. Nat Rev Mol Cell Biol 15:709–721.

Jessell TM. 2000. Neuronal specification in the spinal cord: inductive signals and transcriptional codes. Nat Rev Genet 1:20–29.

Kang G, Allard CAH, Valencia-Montoya WA, Van Giesen L, Kim JJ, Kilian PB, Bai X, Bellono NW, Hibbs RE. 2023. Sensory specializations drive octopus and squid behaviour. Nature 616:378–383.

Kang R, Guglielmino E, Zullo L, Branson DT, Godage I, Caldwell DG. 2016. Embodiment design of soft continuum robots. Advances in Mechanical Engineering 8:168781401664330.

Karemaker JM. 2017. An introduction into autonomic nervous function. Physiol Meas 38:R89–R118.

Kennedy EBL, Buresch KC, Boinapally P, Hanlon RT. 2020. Octopus arms exhibit exceptional flexibility. Sci Rep 10:20872.

Kier WM. 1985. The musculature of squid arms and tentacles: Ultrastructural evidence for functional differences. J Morphol 185:223–239.

Kier WM. 2012. The diversity of hydrostatic skeletons. Journal of Experimental Biology 215:1247–1257.

Kier WM. 2016. The musculature of coleoid cephalopod arms and tentacles. Front Cell Dev Biol [Internet] 4. Available from: http://journal.frontiersin.org/Article/10.3389/fcell.2016.00010/abstract

Kier WM, Smith AM. 2002. The structure and adhesive mechanism of octopus suckers. Integrative and Comparative Biology 42:1146–1153.

Kier WM, Smith KK. 1985. Tongues, tentacles and trunks: the biomechanics of movement in muscular-hydrostats. Zoological Journal of the Linnean Society 83:307–324.

Kier WM, Stella MP. 2007. The arrangement and function of octopus arm musculature and connective tissue. J Morphol 268:831–843.

Kim SS, Rouault H, Druckmann S, Jayaraman V. 2017. Ring attractor dynamics in the *Drosophila* central brain. Science 356:849–853.

Kocot KM, Poustka AJ, Stöger I, Halanych KM, Schrödl M. 2020. New data from Monoplacophora and a carefully-curated dataset resolve molluscan relationships. Sci Rep 10:101.

Kriellaars DJ, Brownstone RM, Noga BR, Jordan LM. 1994. Mechanical entrainment of fictive locomotion in the decerebrate cat. Journal of Neurophysiology 71:2074–2086.

Kuuspalu A, Cody S, Hale ME. 2022. Multiple nerve cords connect the arms of octopuses, providing alternative paths for inter-arm signaling. Current Biology 32:5415-5421.e3.

Laschi C, Mazzolai B, Cianchetti M. 2016. Soft robotics: Technologies and systems pushing the boundaries of robot abilities. Sci Robot 1:eaah3690.

LeDizet M, Piperno G. 1991. Detection of acetylated α-tubulin by specific antibodies. In: Methods in Enzymology. Vol. 196. Elsevier. p 264–274. Available from: https://linkinghub.elsevier.com/retrieve/pii/007668799196025M

Lees-Miller JP, Helfman DM. 1991. The molecular basis for tropomyosin isoform diversity. BioEssays 13:429–437.

Lemche H. 1957. A New Living Deep-Sea Mollusc of the Cambro-Devonian Class Monoplacophora. Nature 179:413–416.

Lopes VM, Sampaio E, Roumbedakis K, Tanaka NK, Carulla L, Gambús G, Woo T, Martins CPP, Penicaud V, Gibbings C, Eberle J, Tedesco P, Fernández I, Rodríguez-González T, Imperadore P, Ponte G, Fiorito G. 2017. Cephalopod biology and care, a COST FA1301 (CephsInAction) training school: anaesthesia and scientific procedures. Invert Neurosci 17:8, s10158-017-0200–4.

Lumsden A, Keynes R. 1989. Segmental patterns of neuronal development in the chick hindbrain. Nature 337:424–428.

Lund RD. 1971. Stellate ganglion. In: The Anatomy of the Nervous System of *Octopus vulgaris*. Oxford: Claredon Press. p 621–640.

Martoja R, May RM. 1955. Les cellules neuro-sensorieeless et le ganglion sous-acétabulaire dans l'appereil brachial du céphalopode *Octopus vulgaris*. Comptes rendus hedbomadaires des seances de l'Academie des sciences 240:2440–2442.

Matzner H, Gutfreund Y, Hochner B. 2000. Neuromuscular system of the flexible arm of the octopus: physiological characterization. Journal of Neurophysiology 83:1315–1328.

Messenger JB. 1967. The effects on locomotion of lesions to the visuo-motor system in *Octopus*. Proc R Soc Lond B Biol Sci 167:252–281.

Messenger JB. 1971. The optic tract lobes. In: The Anatomy of the Nervous System of *Octopus vulgaris*. Oxford: Claredon Press. p 481–506.

Muntz WRA. 1961. Interocular transfer in octopus: bilaterality of the engram. J Comp Physiol Psychol 54:192–195.

Nauta WJH, Feirtag M. 1986. Fundamental Neuroanatomy. W. H. Freeman and Company.

Neacsu D, Crook RJ. 2024. Repeating ultrastructural motifs provide insight into the organization of the octopus arm nervous system. Current Biology 34:4767-4773.e2.

Nesher N, Maiole F, Shomrat T, Hochner B, Zullo L. 2019. From synaptic input to muscle contraction: arm muscle cells of *Octopus vulgaris* show unique neuromuscular junction and excitation–contraction coupling properties. Proc R Soc B 286:20191278.

Nixon M, Young JZ. 2003. The Brains and Lives of Cephalopods. Oxford University Press.

Nödl M-T, Kerbl A, Walzl MG, Müller GB, De Couet HG. 2016. The cephalopod arm crown: appendage formation and differentiation in the Hawaiian bobtail squid Euprymna scolopes. Front Zool 13:44.

Nomaksteinsky M, Kassabov S, Chettouh Z, Stoeklé H-C, Bonnaud L, Fortin G, Kandel ER, Brunet J-F. 2013. Ancient origin of somatic and visceral neurons. BMC Biol 11:53.

Olson CS, Moorjani A, Ragsdale CW. 2025a. Molecular and Morphological Circuitry of the Octopus Sucker Ganglion. J of Comparative Neurology 533:e70055.

Olson CS, Ragsdale CW. 2023. Toward an understanding of octopus arm motor control. Integrative And Comparative Biology:1–8.

Olson CS, Schulz NG, Ragsdale CW. 2021. Molecular study of the structure and function of the octopus sucker ganglion.

Olson CS, Schulz NG, Ragsdale CW. 2025b. Neuronal segmentation in cephalopod arms. Nat Commun 16:443.

Packard A. 1988. The Skin of Cephalopods (Coleoids): General and Special Adaptations. In: Form and Function. Elsevier. p 37–67. Available from: https://linkinghub.elsevier.com/retrieve/pii/B9780127514116500102

Pende M, Vadiwala K, Schmidbaur H, Stockinger AW, Murawala P, Saghafi S, Dekens MPS, Becker K, Revilla-i-Domingo R, Papadopoulos S-C, Zurl M, Pasierbek P, Simakov O, Tanaka EM, Raible F, Dodt H-U. 2020. A versatile depigmentation, clearing, and labeling method for exploring nervous system diversity. Sci Adv 6:eaba0365.

Piperno G, Fuller MT. 1985. Monoclonal Antibodies Specific for an Acetylated Form of a-Tubulin Recognize the Antigen in Cilia and Flagella from a Variety of Organisms. The Journal of Cell Biology 101:2085–2094.

Rebelo S, Chen Z-F, Anderson DJ, Lima D. 2006. Involvement of DRG11 in the development of the primary afferent nociceptive system. Molecular and Cellular Neuroscience 33:236–246.

Redl E, Scherholz M, Todt C, Wollesen T, Wanninger A. 2014. Development of the nervous system in Solenogastres (Mollusca) reveals putative ancestral spiralian features. EvoDevo 5:48.

Richter S, Loesel R, Purschke G, Schmidt-Rhaesa A, Scholtz G, Stach T, Vogt L, Wanninger A, Brenneis G, Döring C, Faller S, Fritsch M, Grobe P, Heuer CM, Kaul S, Møller OS,

Müller CH, Rieger V, Rothe BH, Stegner ME, Harzsch S. 2010. Invertebrate neurophylogeny: suggested terms and definitions for a neuroanatomical glossary. Front Zool 7:29.

Röckner JL, Arellano MD, Zullo L. 2023. Sucker Attachment and Detachment Patterns in Octopus Vulgaris. In: Meder F, Hunt A, Margheri L, Mura A, Mazzolai B, editors. Biomimetic and Biohybrid Systems. Vol. 14157. Lecture Notes in Computer Science. Cham: Springer Nature Switzerland. p 266–280. Available from: https://link.springer.com/10.1007/978-3-031-38857-6_20

Rossi F, Graziadei P. 1954. Nouvelles recherches sur le systeme nerveux du bras des cephalopodes avec des methodes specifiques pour le tissu nerveux. Acta Anatomica 22:202–215.

Rossi F, Graziadei P. 1958. Nouvelles contributions à la connaissance du système nerveux du tentacule des céphalopodes IV. Le patrimoine nerveux de la ventouse de *I'Octopus vulgaris.* Acta Anatomica: Supplementum 32:1–79.

Rossignol S, Frigon A. 2011. Recovery of locomotion after spinal cord injury: some facts and mechanisms. Annu Rev Neurosci 34:413–440.

Rowell CH. 1963. Excitatory and inhibitory pathways in the arm of *Octopus*. Journal of Experimental Biology 40:257–270.

Rowell CHF. 1966. Activity of interneurones in the arm of the *Octopus* in response to tactile stimulation. J Exp Biol 44:589–605.

Rus D, Tolley MT. 2015. Design, fabrication and control of soft robots. Nature 521:467–475.

Schevzov G, Curthoys NM, Gunning PW, Fath T. 2012. Functional Diversity of Actin Cytoskeleton in Neurons and its Regulation by Tropomyosin. In: International Review of Cell and Molecular Biology. Vol. 298. Elsevier. p 33–94. Available from: https://linkinghub.elsevier.com/retrieve/pii/B978012394309500002X

Shaffer JF, Kier WM. 2016. Tuning of shortening speed in coleoid cephalopod muscle: no evidence for tissue-specific muscle myosin heavy chain isoforms. Invertebr Biol 135:3–12.

Shelud'ko NS, Matusovskaya GG, Permyakova TV, Matusovsky OS. 2004. Twitchin, a thick-filament protein from molluscan catch muscle, interacts with F-actin in a phosphorylation-dependent way. Archives of Biochemistry and Biophysics 432:269–277.

Shigeno S, Yamamoto M. 2002. Organization of the nervous system in the pygmy cuttlefish, *Idiosepius paradoxus* ortmann (Idiosepiidae, cephalopoda). Journal of Morphology 254:65–80.

Sivitilli DM, Smith JR, Gire DH. 2022. Lessons for robotics from the control architecture of the octopus. Front Robot AI 9:862391.

Sternberger NH, Sternberger LA. 1983. Neurotypy: The Heterogeneity of Brain Proteins. Annals of the New York Academy of Sciences 420:90–99.

Sumbre G, Fiorito G, Flash T, Hochner B. 2006. Octopuses use a human-like strategy to control precise point-to-point arm movements. Current Biology 16:767–772.

Sumbre G, Gutfreund Y, Fiorito G, Flash T, Hochner B. 2001. Control of octopus arm extension by a peripheral motor program. Science 293:1845–1848.

Tauc L. 1967. Transmission in invertebrate and vertebrate ganglia. Physiological Reviews 47:521–593.

Vagvolgyi J. 1967. On the Origin of Molluscs, The Coelom, and Coelomic Segmentation. Systematic Zoology 16:153–168.

Wang T, Halder U, Gribkova E, Gillette R, Gazzola M, Mehta PG. 2024. Neural Models and Algorithms for Sensorimotor Control of an Octopus Arm. Available from: https://arxiv.org/abs/2402.01074

Wang ZY, Ragsdale CW. 2019. Cephalopod nervous system organization. In: Oxford Research Encyclopedia of Neuroscience. Oxford University Press. Available from: https://oxfordre.com/neuroscience/view/10.1093/acrefore/9780190264086.001.0001/acrefore-9780190264086-e-181

Wanninger A, Wollesen T. 2019. The evolution of molluscs. Biological Reviews 94:102–115.

Wells MJ. 1959. A touch-learning centre in *Octopus*. Journal of Experimental Biology 36:590–612.

Wells MJ. 1961. Centres for tactile and visual learning in the brain of octopus. Journal of Experimental Biology 38:811–826.

Wells MJ. 1964. Tactile discrimination of surface curvature and shape by the octopus. Journal of Experimental Biology 41:433–445.

Wells MJ. 1978. Octopus: Physiology and Behavior of an Advanced Invertebrate. London: Chapman and Hall Ltd.

Whelan PJ. 2003. Developmental aspects of spinal locomotor function: insights from using the *in vitro* mouse spinal cord preparation. The Journal of Physiology 553:695–706.

Wilson DM. 1960. Nervous Control of Movement in Cephalopods. Journal of Experimental Biology 37:57–72.

Wilson NG, Rouse GW, Giribet G. 2010. Assessing the molluscan hypothesis Serialia (Monoplacophora+Polyplacophora) using novel molecular data. Molecular Phylogenetics and Evolution 54:187–193.

Winters-Bostwick GC, Giancola-Detmering SE, Bostwick CJ, Crook RJ. 2024. Three-dimensional molecular atlas highlights spatial and neurochemical complexity in the axial nerve cord of octopus arms. Current Biology 34:4756-4766.e6.

Wollesen T, Loesel R, Wanninger A. 2009. Pygmy squids and giant brains: Mapping the complex cephalopod CNS by phalloidin staining of vibratome sections and whole-mount preparations. Journal of Neuroscience Methods 179:63–67.

Yang Y, Zhao D, Zhou L, Zhang T, Liu Z, Wu B, Yu T, Zheng Y, Sun X. 2022. Molecular Characterization and Expression Pattern of Paramyosin in Larvae and Adults of Yesso Scallop. Biology 11:453.

Yekutieli Y, Sagiv-Zohar R, Aharonov R, Engel Y, Hochner B, Flash T. 2005. Dynamic Model of the Octopus Arm. I. Biomechanics of the Octopus Reaching Movement. Journal of Neurophysiology 94:1443–1458.

Young JZ. 1936. The giant nerve fibres and epistellar body of cephalopods. Journal of Cell Science S2-78:367–386.

Young JZ. 1938. The functioning of the giant nerve fibres of the squid. Journal of Experimental Biology 15:170–185.

Young JZ. 1963. The number and sizes of nerve cells in *Octopus*. Proceedings of the Zoological Society of London 140:229–254.

Young JZ. 1971. The anatomy of the nervous system of *Octopus vulgaris*. Oxford: Claredon Press.

Young JZ. 1972. The organization of a cephalopod ganglion. Phil Trans R Soc Lond B 263:409–429.

Zullo L, Di Clemente A, Maiole F. 2022. How octopus arm muscle contractile properties and anatomical organization contribute to arm functional specialization. Journal of Experimental Biology 225:jeb243163.

Zullo L, Eichenstein H, Maiole F, Hochner B. 2019. Motor control pathways in the nervous system of Octopus vulgaris arm. J Comp Physiol A 205:271–279.

Zullo L, Sumbre G, Agnisola C, Flash T, Hochner B. 2009. Nonsomatotopic organization of the higher motor centers in octopus. Current Biology 19:1632–1636.